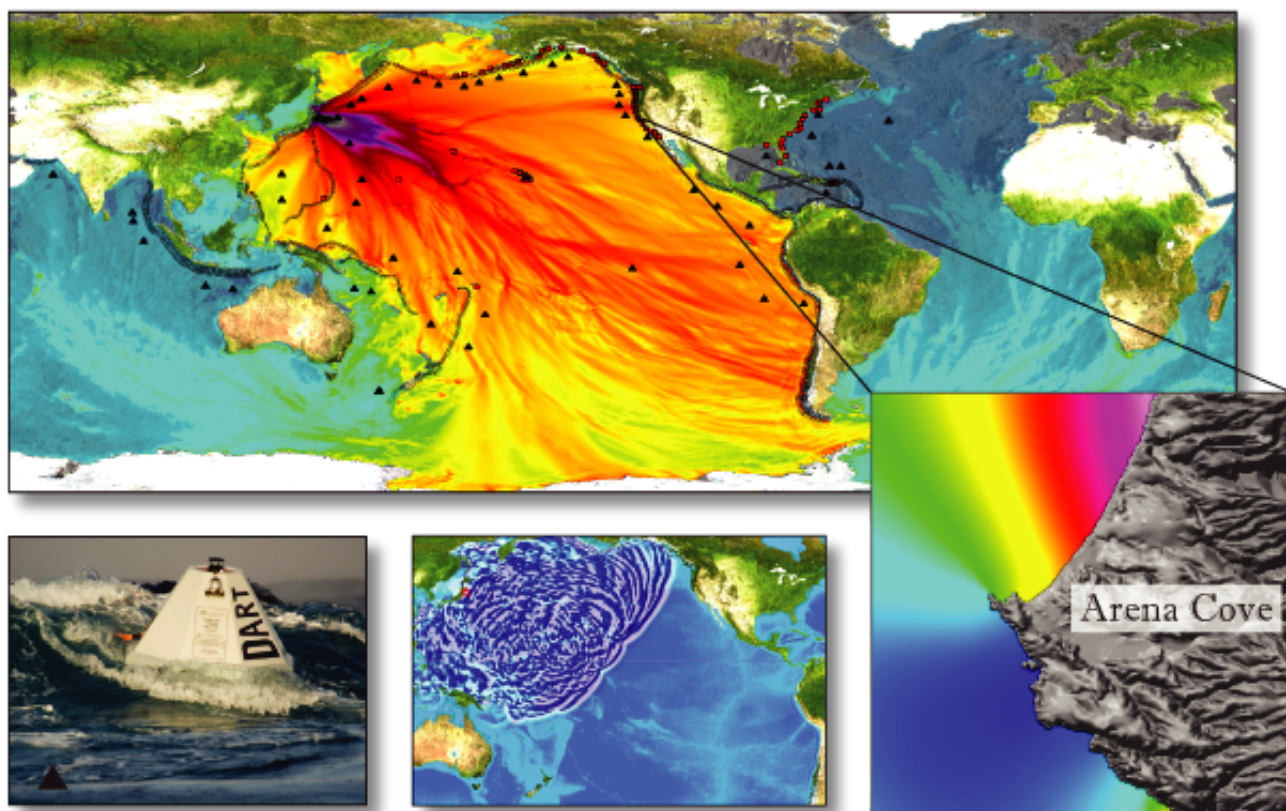


PMEL Tsunami Forecast Series: Vol. 10

A Tsunami Forecast Model for Arena Cove, California

Michael C. Spillane



Front cover image: Overview of NOAA tsunami forecast system. Top frame illustrates components of the tsunami forecast using the 11 March 2011 Tohoku tsunami as an example: DART systems (black triangles), precomputed tsunami source function database (unfilled black rectangles) and high-resolution forecast models in the Pacific, Atlantic, and Indian oceans (red squares). Colors show computed maximum tsunami amplitudes of the offshore forecast. Black contour lines indicate tsunami travel times in hours. Lower panels show the forecast process sequence left to right: tsunami detection with the DART system (third generation DART ETD is shown); model propagation forecast based on DART observations; coastal forecast with high-resolution tsunami inundation model.

PDF versions of the PMEL Tsunami Forecast Series reports are available at
http://nctr.pmel.noaa.gov/forecast_reports

NOAA OAR Special Report

doi:10.7289/V5000020

PMEL Tsunami Forecast Series: Vol. 10 **A Tsunami Forecast Model for Arena Cove, California**

M.C. Spillane^{1,2}

- 1 Joint Institute for the Study of the Atmosphere and Ocean (JISAO), University of Washington, Seattle, WA
- 2 NOAA/Pacific Marine Environmental Laboratory (PMEL), Seattle, WA

April 2015



**UNITED STATES
DEPARTMENT OF COMMERCE**

**Penny Pritzker
Secretary**

NATIONAL OCEANIC AND
ATMOSPHERIC ADMINISTRATION

Kathy Sullivan
Under Secretary for Oceans
and Atmosphere/Administrator

Office of Oceanic and
Atmospheric Research

Craig McLean
Assistant Administrator

NOTICE from NOAA

Mention of a commercial company or product does not constitute an endorsement by NOAA/OAR. Use of information from this publication concerning proprietary products or the tests of such products for publicity or advertising purposes is not authorized. Any opinions, findings, and conclusions or recommendations expressed in this material are those of the authors and do not necessarily reflect the views of the National Oceanic and Atmospheric Administration.

Contribution No. 3390 from NOAA/Pacific Marine Environmental Laboratory

Contribution No. 2087 from Joint Institute for the Study of the Atmosphere and Ocean (JISAO)

Also available from the National Technical Information Service (NTIS)

(<http://www.ntis.gov>)

Contents

Foreword	xi
Abstract	1
1. Background and Objectives	3
1.1 The setting	3
1.2 Natural hazards	4
1.3 Tsunami warning and risk assessment	8
2. Forecast Methodology	9
2.1 The tsunami model	9
2.2 NOAA's tsunami forecast system	9
3. Model Development	11
3.1 Digital elevation models	11
3.2 Tides and sea level variation	12
3.3 The CFL condition and other considerations for grid design	12
3.4 Specifics of the model grids	14
3.5 Model run input and output files	15
4. Results and Discussion	17
4.1 The micro-tsunami tests	17
4.2 The mega-tsunami tests	19
4.3 Model validation with historical events	20
4.4 Further historical simulations	22
4.5 The Mendocino earthquake of 25 April 1992	24
4.6 The Tohoku tsunami of 11 March 2011	25
4.7 Simulation of the remaining synthetic mega-tsunami events	26
5. Conclusions	27
6. Acknowledgments	27
7. References	29
FIGURES	33
Appendix A.	65
A1. Reference model *.in file for Arena Cove, California	65
A2. Forecast model *.in file for Arena Cove, California	66
Appendix B. Propagation Database: Pacific Ocean Unit Sources	67

Appendix C. Synthetic Testing Report: Arena Cove, California	115
C1. Purpose.....	115
C2. Testing procedure.....	115
C3. Results.....	116
Glossary	125

List of Figures

1	The Point Arena area of southern Mendocino County, California.....	35
2	Views of present-day Arena Cove, California, and its appearance in the early 1900s.....	36
3	Extract from the oblique 3-D view of the Arena Cove digital elevation model provided by NGDC, highlighting sites of potential inundation identified by CalEMA.....	37
4	Distribution of the historical tsunami sources employed for the development of the Arena Cove forecast model.	38
5	A sample time interval from the Arena Cove tsunami-capable tide gauge, unrelated to tsunami activity.	39
6	The setting of the Arena Cove model and its nested model grids. Plate boundaries are shown, as are the southernmost unit sources representing Cascadia.....	40
7	Nested grid representation for the Arena Cove reference model.	41
8	Nested grid representation for the Arena Cove forecast model.....	42
9	Comparison of the reference and forecast model time series at the warning point for micro-tsunami scenario EPSZ B19, illustrating the close agreement between the model responses and showing the signature of model instability in the reference model prior to the finalization of its bathymetry.....	43
10	Locations of synthetic tsunami scenarios employed in the development of the Arena Cove model.....	44
11	Comparison of reference and forecast model results for the synthetic ACSZ 56–65 mega-tsunami scenario representing the Cascadia Subduction Zone.....	45
12	Comparison of reference and forecast model results for the synthetic KISZ 01–10 mega-tsunami scenario representing Kamchatka.....	46
13	Comparison of reference and forecast model results for the synthetic NTSZ 30–39 mega-tsunami scenario representing Samoa.	47
14	Comparison of reference and forecast model results for the synthetic moderate event at NTSZ 36 near Samoa.....	48
15	Comparison of reference and forecast model results for the historical 1946 Unimak tsunami (prior to tide gauge installation).....	49
16	Comparison of reference and forecast model response for the historical 1964 Alaska tsunami (prior to tide gauge installation).....	50

17	Comparison of reference and forecast model hindcasts of the 2006 Kuril event with sea level fluctuations, observed by the tsunami-capable Arena Cove tide gauge.....	51
18	Comparison of reference and forecast model hindcasts of the 2009 Samoa event with sea level fluctuations in Arena Cove.....	52
19	Comparison of reference and forecast model hindcasts of the 2010 Chile event with sea level fluctuations in Arena Cove.....	53
20	Simulated model response to the historical 1896 Sanriku, 1952 Kamchatka, 1957 Andreanof, 1960 Chile events. Proxy observations are provided, where available, from other California locations.....	54
21	Forecast model response to the 1994 East Kuril, 1995 Chile, 1995 Kuril, and 1996 Irian Jaya events. Tide gauge data, where available, are from Arena Cove.....	55
22	Forecast model response to the 1996 Andreanof, 2001 Peru, 2003 Hokkaido, and 2003 Rat Island events. Tide gauge data are from Arena Cove.....	56
23	Forecast model response to the 2006 Tonga, 2007 Kuril, 2007 Solomons, and 2007 Peru events. Tide gauge data are from Arena Cove.....	57
24	Forecast model response to the 2007 Chile, 2009 Papua New Guinea, 2009 Kuril, and 2009 Vanuatu events. Tide gauge data are from Arena Cove.....	58
25	Forecast model response to the 2009 Samoa and 2010 Chile events. Tide gauge data are from Arena Cove.....	59
26	Seismicity in the vicinity of Cape Mendocino and the source mechanisms of recent earthquakes.....	60
27	Comparison of real-time forecast and hindcast reference model representations of the 2011 Tohoku (Honshu) event with sea level observations in Arena Cove.....	61
28	Predicted maximum sea level (from the forecast model) at the Arena Cove tide gauge for the mega-tsunami scenarios described in Table 6.....	62
29	Comparison of reference and forecast model predictions for inundation of the Arena Cove/Manchester Beach region for selected mega-tsunami scenarios and the ensemble used in the CalEMA study.....	63
B1	Aleutian–Alaska–Cascadia Subduction Zone unit sources.....	69
B2	Central and South America Subduction Zone unit sources.....	75
B3	Eastern Philippines Subduction Zone unit sources.....	87
B4	Kamchatka–Bering Subduction Zone unit sources.....	89
B5	Kamchatka–Kuril–Japan–Izu–Mariana–Yap Subduction Zone unit sources.....	91

B6	Manus–Oceanic Convergent Boundary Subduction Zone unit sources.....	99
B7	New Guinea Subduction Zone unit sources.....	101
B8	New Zealand–Kermadec–Tonga Subduction Zone unit sources.....	103
B9	New Britain–Solomons–Vanuatu Subduction Zone unit sources.....	107
B10	New Zealand–Puysegur Subduction Zone unit sources.....	111
B11	Ryukyu–Kyushu–Nankai Subduction Zone unit sources.....	113
C1	Response of the Arena Cove forecast model to synthetic scenario KISZ 1–10 ($\alpha=25$). Maximum sea surface elevation for A, B, and C grids, and sea surface elevation time series at the C-grid warning point, which can be compared to the equivalent obtained during model development, as displayed in Figure 12.....	118
C2	Response of the Arena Cove forecast model to synthetic scenario KISZ 22–31 ($\alpha=25$). Maximum sea surface elevation for A, B, and C grids, and sea surface elevation time series at the C-grid warning point. For extrema computed during development, see Table C1.....	119
C3	Response of the Arena Cove forecast model to synthetic scenario ACSZ 56–65 ($\alpha=25$). Maximum sea surface elevation for A, B, and C grids, and sea surface elevation time series at the C-grid warning point, which can be compared to the equivalent obtained during model development, as displayed in Figure 11.....	120
C4	Response of the Arena Cove forecast model to synthetic scenario CSSZ 89–98 ($\alpha=25$). Maximum sea surface elevation for A, B, and C grids, and sea surface elevation time series at the C-grid warning point. For extrema computed during development, see Table C1.....	121
C5	Response of the Arena Cove forecast model to synthetic scenario NTSZ 30–39 ($\alpha=25$). Maximum sea surface elevation for A, B, and C grids, and sea surface elevation time series at the C-grid warning point, which can be compared to the equivalent obtained during model development, as displayed in Figure 13.....	122
C6	Response of the Arena Cove forecast model to the 2011 Tohoku (Honshu) tsunami. Maximum sea surface elevation for A, B, and C grids, and sea surface elevation time series at the C-grid warning point, which can be compared to the equivalent obtained during model development, as displayed in Figure 27.....	123

List of Tables

1	Source characterization for historical tsunami events employed in model testing for Arena Cove, California. (a) The standard set for Pacific Ocean models; (b) supplementary historical tsunami events for forecast model testing.....	6
2	The main features of the Arena Cove digital elevation model, provided by NGDC.....	11
3	Tidal characteristics of the Arena Cove tide gauge (9416841).....	13
4	Specifics of the grids and model parameters employed to model Arena Cove.....	14
5	Grid file names and grid-related parameters for Arena Cove.....	15
6	Synthetic tsunami events employed in Arena Cove model testing.....	18
B1	Earthquake parameters for Aleutian–Alaska–Cascadia Subduction Zone unit sources.....	70
B2	Earthquake parameters for Central and South America Subduction Zone unit sources.....	76
B3	Earthquake parameters for Eastern Philippines Subduction Zone unit sources.....	88
B4	Earthquake parameters for Kamchatka-Bering Subduction Zone unit sources.....	90
B5	Earthquake parameters for Kamchatka-Kuril-Japan-Izu-Mariana-Yap Subduction Zone unit sources.....	92
B6	Earthquake parameters for Manus–Oceanic Convergent Boundary Subduction Zone unit sources.....	100
B7	Earthquake parameters for New Guinea Subduction Zone unit sources.....	102
B8	Earthquake parameters for New Zealand–Kermadec–Tonga Subduction Zone unit sources.....	104
B9	Earthquake parameters for New Britain–Solomons–Vanuatu Subduction Zone unit sources.....	108
B10	Earthquake parameters for New Zealand–Puysegur Subduction Zone unit sources.....	112
B11	Earthquake parameters for Ryukyu–Kyushu–Nankai Subduction Zone unit sources.....	114

C1	Maximum and minimum amplitudes (cm) at the Arena Cove warning point for synthetic and historical events tested using SIFT 3.2 and obtained during development.....	117
----	--	-----

Foreword

Tsunamis have been recognized as a potential hazard to United States coastal communities since the mid-twentieth century, when multiple destructive tsunamis caused damage to the states of Hawaii, Alaska, California, Oregon, and Washington. In response to these events, the United States, under the auspices of the National Oceanic and Atmospheric Administration (NOAA), established the Pacific and National Tsunami Warning Centers, dedicated to protecting United States interests from the threat posed by tsunamis. NOAA also created a tsunami research program at the Pacific Marine Environmental Laboratory (PMEL) to develop improved warning products.

The scale of destruction and unprecedented loss of life following the December 2004 Sumatra tsunami served as the catalyst to refocus efforts in the United States on reducing tsunami vulnerability of coastal communities, and on 20 December 2006, the United States Congress passed the “Tsunami Warning and Education Act” under which education and warning activities were thereafter specified and mandated. A “tsunami forecasting capability based on models and measurements, including tsunami inundation models and maps” is a central component for the protection of United States coastlines from the threat posed by tsunamis. The forecasting capability for each community described in the PMEL Tsunami Forecast Series is the result of collaboration between the National Oceanic and Atmospheric Administration office of Oceanic and Atmospheric Research, National Weather Service, National Ocean Service, National Environmental Satellite, Data, and Information Service, the University of Washington’s Joint Institute for the Study of the Atmosphere and Ocean, National Science Foundation, and United States Geological Survey.

NOAA Center for Tsunami Research

PMEL Tsunami Forecast Series: Vol. 10

A Tsunami Forecast Model for Arena Cove, California

M.C. Spillane^{1,2}

Abstract. Operational tsunami forecasting by NOAA's Tsunami Warning Centers relies on the detection of tsunami wave trains in the open ocean, inversion of these data (telemetered via satellite) to quantify their source characteristics, and real-time modeling of the impact on threatened coastal communities. The latter phase of the process involves, for each such community, a pre-tested forecast model capable of predicting the impact, in terms of inundation and dangerous inshore currents, with sufficient resolution and within the time constraints appropriate to an emergency response. To achieve this goal, considerable advance effort is required to tune each forecast model to the specific bathymetry and topography, both natural and manmade, of the impact area, and to validate the model's performance with a broad set of tsunami sources. Where possible, the validation runs should replicate observed responses to historical events, but the sparse instrumental record of these rare but occasionally devastating occurrences dictates that comprehensive testing also include a suite of scenarios that represent potential future events.

During the forecast model design phase, and in research mode outside the pressures of an emergency situation, more detailed and slower-running models can be investigated. These models, referred to as reference models, represent the most credible numerical representation of tsunami response for a study region, using the most detailed bathymetry available and without the run-time constraint of operational use. Once a reference model has been developed, the process of forecast model design is to determine where efficiencies can be gained, through reducing the grid resolution and increasing the model time step, while still adequately representing the salient features of the full solution.

This report documents the reference and forecast model development for Arena Cove, a small inlet south of the rocky Arena Point headland in southern Mendocino County, California. Both the cove and the headland serve as reference points in coastal reports and are tourist venues but, while several tsunamis have been detected by the tide gauge there, no injury or infrastructure damage have been reported to date. The Manchester Beach area north of Point Arena is low-lying and subject to inundation and has been included in the model domain.

1 Joint Institute for the Study of the Atmosphere and Ocean (JISAO), University of Washington, Seattle, WA

2 NOAA/Pacific Marine Environmental Laboratory (PMEL), Seattle, WA

1. Background and Objectives

1.1 The setting

Arena Cove is a semi-circular indentation some 450 m in diameter flanked by cliffs, lying south of the rocky headland whose northernmost point is the site of the Point Arena lighthouse. The cove appears about one-third of the way above the lower edge of **Figure 1** (based on the 2005 National Agricultural Imagery Program image from the United States Geological Survey (USGS) 7.5 arc min quadrangle: 38123h6, available online at atlas.ca.gov/quads). Apart from a pier (better seen in **Figure 2**), raised high above water level on pilings and the focus of local commercial fishing and tourist activity, the waterfront area of Arena Cove is almost devoid of infrastructure, though it lies within the city limits of Point Arena.

This small city's population of about 450 mainly reside at elevations that place them above the level likely to be impacted by even the most severe tsunamis. Population is sparse both to the south and north of Point Arena, but inundation of Manchester Beach State Park, north of the lighthouse, and the low-lying area near the mouth of the Garcia River (crossed by State Highway 1) needs consideration. A comprehensive study of potential tsunami inundation for the entire California coastline was conducted by the University of Southern California Tsunami Research Center. Funded through the California Emergency Management Agency (CalEMA) by the National Tsunami Hazard Program, the study (Barberopoulou *et al.*, 2011) produced a set of inundation maps for emergency planning purposes, accessible in various forms including an online tool, MyHazards (myhazards.calema.ca.gov), which enables users to acquire information specific to their site of interest. The CalEMA inundation results are available in GIS form, and those specific to the Arena Cove area are used throughout this report. In addition to underpinning the modeling effort, the digital elevation model (DEM) for the region, provided by the National Geophysical Data Center (NGDC), includes a 3-D oblique view that assists greatly in visualizing the study area. In **Figure 3**, the CalEMA inundation information is overlaid together with descriptive labels on an extract from the NGDC image, available in full in the DEM Report (Friday *et al.*, 2009).

Arena Cove, both in appearance (**Figure 2**) and population, has not changed substantially since the nineteenth and early twentieth centuries, when it was one of the “Dog Hole” ports of the Mendocino Coast (Haugan, 2005). So named for their small size, these ports nonetheless served an important role in the provision of lumber in the building of the cities of California and in the rebuilding of San Francisco in the wake of the 1906 earthquake and fire (see the inset to **Figure 2**, reproduced by permission of the Mendocino County Historical Society). The Point Arena lighthouse and its namesake city were seriously damaged by the earthquake, and the San Andreas Fault (SAF) dominates the local topography. The

SAF intersects the coast just north of Point Arena en route to the triple junction near Cape Mendocino, the southern limit of the Cascadia Subduction Zone, which constitutes a major earthquake and tsunami hazard to the U.S. West Coast.

Unlike the other ports of the Mendocino Coast, whose mouths have sand bars, the channeling northward of the Garcia River by the SAF leaves a limited watershed to supply sediment to Arena Cove via Point Arena Creek, entering the cove through a small, steep-sided valley. The current pier, rebuilt in 1986 following the damage to its predecessor by a series of storms in 1983, stands on pilings high above water level. It houses a crane to lower boats to the water and the instrumentation for the tide gauge whose sensor is adjacent to the pier. In earlier days, piers and wire chutes atop the flanking cliffs delivered lumber products to coastal schooners. Today's pier supports local commercial fishing and sightseeing; surfing and pier fishing are popular tourist activities.

Apart from the pier and some riprap, the cove remains in its natural state. A congressional study (US Secretary of War, 1914) considered the possibility of engineering works to make Arena Cove a "harbor of refuge" between San Francisco and Humboldt Bay but concluded that this was neither feasible nor a serious need. Consequently, sea level data from the tide gauge represent coastal conditions, unaffected by infrastructure. Port Road links the pier, the parking area, and some buildings housing fishing and tourist amenities to the city proper. Accommodations in the immediate pier area are confined to an inn that is well elevated from the waves associated with winter storms and, as this report will document, even the most severe tsunami.

South of Arena Cove, as illustrated in a striking series of aerial photographs by the California Coastal Records Project (californiacoastline.org), the source of the main frame of **Figure 2**, high cliffs limit potential impact by tsunamis. To the north of the lighthouse, however, and stretching as far as the Irish Beach community, lies Manchester Beach State Park. Inland from the point of entry to the ocean of the Garcia River is the Manchester-Point Arena Rancheria of the federally recognized Band of Pomo Indians. While the historical record of tsunamis does not include mention of this area, its risk for inundation is evident in the CalEMA chart, and the results of this study indicate that it may be prone to inundation in severe tsunami events. Thus, while the study focuses on Arena Cove, and the validation of the forecast model is provided by the tide gauge there, the analysis of the most severe scenarios will consider potential impacts to the Manchester area. The community of Manchester itself appears to be immune to direct impact, though State Highway 1 (also called the Shoreline Highway) may be inundated where it crosses the Garcia River. Queries to the CalEMA "MyHazards" site for Point Arena and Manchester show flooding and earthquake as other hazards to which they are prone, in addition to tsunami.

1.2 Natural hazards

Several instances of mild tsunami signals are evident in the tide gauge records for Arena Cove, whose name appears several times in the records compiled by Lander and Lockridge (1989) and the NGDC Tsunami Hazard Database (Dunbar, 2007; see www.ngdc.noaa.gov/hazard/). The historical record first mentions Mendocino

County with a 1 m wave height associated with the Sanriku event of 1896. O'Brien (1946) described a 2.4 m wave (4.3 m above mean lower low water, or MLLW) at Arena Cove during the 1946 Unimak tsunami, while Noyo Harbor adjacent to Fort Bragg, the largest coastal community in the county (2010 population: 7273; Census Bureau, 2010), endured "100 fishing boats thrown 1.8 m up beach and some damage to pier." While Arena Cove was not explicitly mentioned in connection with the 1957 Andreanof event, there was a report from Noyo Harbor. Similarly, during the 1960 Chile event, Noyo Harbor reported "6 boats broke mooring... pier damaged" and a height of 0.61 m was observed at Gualala River near the southern boundary of Mendocino County. During the 1964 Alaska tsunami, a runup height of 1.83 m occurred at Arena Cove. Several instances of mild response to tele-tsunamis are available, following the installation of a tide gauge in 1978, with which to validate model predictions.

The Mw 7.2 earthquake north of Cape Mendocino on 25 April 1992 was a very mild foretaste of a Cascadia Subduction Zone (CSZ) event. It produced wave heights of 0.14 m at Arena Cove and 0.50 m at Crescent City. Large-scale events on the CSZ are simulated later in the report, but the weak 1992 event will be examined to see whether the presence of the Point Arena headland provides protection to Arena Cove, which lies in its lee for waves propagating along the coast from the north.

Combining events impacting northern California with those that have occurred since the Arena Cove tide gauge was upgraded to 1 min sampling, a total of 27 historical events are available for study. Nineteen of these, listed in **Table 1a**, are the standards for forecast model testing in the Pacific because their seafloor deformation is reasonably well known, either from the literature or, more recently, derived from direct observation of the wave trains they generated. The remaining eight, listed in **Table 1b**, have source characteristics that are less well known; they are included to expand the geographical coverage or because of their special relevance to Arena Cove. The 1992 Mendocino event (discussed in Section 4.5), for example, was the most recent subduction-type event in Cascadia. Others, due to significant noise in the tide gauge, do not produce a clear signal but shed light on Arena Cove as a reference point for coastal impacts. **Figure 4** illustrates the distribution of the 27 historical sources. Those highlighted in red were employed for intercomparison of the reference and forecast versions of the model.

Direct seismic impact is another natural hazard to which Point Arena area is exposed. Its proximity to the rupture zone of the SAF in the San Francisco earthquake of 1906 resulted in significant damage to the town and the destruction of the lighthouse. While the SAF enters the ocean at Manchester Beach, its strike-slip nature reduces the likelihood of severe tsunami wave generation should ruptures occur in the immediate vicinity. Submarine landslides or collapse of sections of sea cliff are a potential local source for tsunami damage. Landslides triggered by seismic events caused significant loss of life during the 1929 Newfoundland event (Fine *et al.*, 2005) and accentuated the 1996 New Guinea tsunami. Landslide-generated tsunami waves are not currently included in the SIFT (Short-term Inundation Forecasting for Tsunamis) forecast methodology, nor are those generated meteorologically. However, to the extent that the waves they produce are detected by the DART (Deep-ocean Assessment and Reporting of Tsunami) array, some warning of their presence may be available.

Table 1: Source characterization for historical tsunami events employed for Arena Cove, California, model testing. Events in bold text were used to compare the reference and forecast model versions. Sources identified as “preliminary” or “ad hoc” may not be identically defined in other forecast model reports. (a) The standard set for Pacific Ocean models; and (b) supplementary historical tsunami events employed for forecast model testing.

Earthquake / Seismic						Model	
Event	USGS		CMT		Tsunami Magnitude	Subduction Zone	Tsunami Source (Reference/Derivation)
	Date Time (UTC) Epicenter	Date Time (UTC) Centroid	Magnitude Mw				
(a) Standard set for Pacific Ocean models:							
1946 Unimak	01 Apr 12:28:56 52.75°N 163.50°W	Not Available	8.5		8.5	ACSZ	$7.5 \times B23 + 19.7 \times B24 + 3.7 \times B25$ (López and Okal, 2006)
1952 Kamchatka	04 Nov 16:58:26.0 52.76°N 160.06°E	Not Available	9.0		9.0	KISZ	$19.71 \times (A4 + Y4 + Z4 + A5 + Y5 + Z5 + A6 + Y6 + Z6)$ [ad hoc]
1957 Andreanof	09 Mar 14:22:31 51.56°N 175.39°W	Not Available	8.6		8.7	ACSZ	$31.4 \times A15 + 10.6 \times A16 + 12.2 \times A17$ [preliminary]
1960 Chile	22 May 19:11:14 38.29°S 73.05°W	Not Available	9.5		9.5	CSSZ	$125 \times (A93 + B93 + Z93 + A94 + B94 + Z94 + A95 + B95)$ (Kanamori and Cipar, 1974)
1964 Alaska	28 Mar 03:36:00 61.02°N 147.65°W	Not Available	9.2		8.9	ACSZ	$15.4 \times A34 + 18.3 \times B34 + 48.3 \times Z34 + 19.4 \times A35 + 15.1 \times B35$ (Tang <i>et al.</i> , 2006, 2009)
1994 East Kuril	04 Oct 13:22:58 43.73°N 147.321°E	04 Oct 13:23:28.5 43.60°N 147.63°E	8.3		8.1	KISZ	$9.0 \times A20$ [ad hoc]
1996 Andreanof	10 Jun 04:03:35 51.56°N 175.39°W	10 Jun 04:04:03.4 51.10°N 177.410°W	7.9		7.8	ACSZ	$2.40 \times A15 + 0.80 \times B16$ [preliminary]
2001 Peru	23 Jun 20:33:14 16.265°S 73.641°W	23 Jun 20:34:23.3 17.28°S 72.71°W	8.4		8.2	CSSZ	$5.7 \times A15 + 2.9 \times B16 + 1.98 \times A16$ [preliminary]
2003 Hokkaido	25 Sep 19:50:06 41.775°N 143.904°E	25 Sep 19:50:38.2 42.21°N 143.84°E	8.3		8.3	KISZ	$3.95 \times (A22 + B22 + A23 + B23)$ [ad hoc]
2003 Rat Island	17 Nov 06:43:07 51.13°N 178.74°E	17 Nov 06:43:31.0 51.14°N 177.86°E	7.7		7.8	ACSZ	$2.81 \times B11$ [real-time]
2006 Tonga	03 May 15:26:39 20.13°S 174.161°W	03 May 15:27:03.7 20.39°S 173.47°W	8.0		8.0	NTSZ	$6.6 \times b29$ [ad hoc]
2006 Kuril	15 Nov 11:14:16 46.607°N 153.230°E	15 Nov 11:15:08 46.71°N 154.33°E	8.3		8.1	KISZ	$4.0 \times A12 + 0.5 \times B12 + 2.0 \times A13 + 1.5 \times B13$ [real-time]
2007 Kuril	13 Jan 04:23:20 46.272°N 154.455°E	13 Jan 04:23:48.1 46.17°N 154.80°E	8.1		7.9	KISZ	$-3.64 \times B13$ [real-time]
2007 Solomon	01 Apr 20:39:56 8.481°S 156.978°E	01 Apr 20:40:38.9 7.76°S 156.34°E	8.1		8.2	NVSZ	$12.0 \times B10$ [preliminary]
2007 Peru	15 Aug 23:40:57 13.354°S 76.509°W	15 Aug 23:41:57.9 13.73°S 77.04°W	8.0		8.1	CSSZ	$0.9 \times A61 + 1.25 \times B61 + 5.6 \times A62 + 6.97 \times B62 + 3.5 \times Z62$ [preliminary]

Table 1: *Continued.*

		Earthquake / Seismic			Model		
Event	USGS		CMT	Tsunami Magnitude	Subduction Zone	Tsunami Source (Reference/Derivation)	
	Date Time (UTC) Epicenter	Date Time (UTC) Centroid	Magnitude Mw				
(a) Standard set for Pacific Ocean models, continued:							
2007 Chile	14 Nov 15:40:50 22.204°S 69.869°W	14 Nov 15:41:11.2 22.64°S 70.62°W	7.7	7.6	CSSZ	1.65 × Z73 [real-time]	
2009 Samoa	29 Sep 17:48:10 15.509°S 172.034°W	29 Sep 17:48:26.8 15.13°S 171.97°W	8.1	8.1	NTSZ	3.96 × A34 + 3.96 × B34 [real-time]	
2010 Chile	27 Feb 06:34:14 35.909°S 72.733°W	27 Feb 06:35:15.4 35.95°S 73.15°W	8.8	8.8	CSSZ	17.24 × A88 + 8.82 × A90 + 11.84 × B88 + 18.39 × B89 + 16.75 × B90 + 20.78 × Z88 + 7.06 × Z90 [real-time]	
2011 Tohoku	11 Mar 05:46:24 38.297°N 142.372°E	11 Mar 05:47:47.1 38.486°N 142.597°E	9.0	9.0	KISZ	4.66 × B24 + 12.23 × B25 + 26.31 × A26 + 21.27 × B26 + 22.75 × A27 + 4.98 × B27 (Tang <i>et al.</i> , 2012) [real-time]	
(b) Supplementary historical tsunami events employed for forecast model testing:							
1896 Sanriku	15 Jun 10:33:00 39.5°N 144.0°E		7.6	7.6	KISZ	1.413 × b25 [ad hoc]	
1992 Mendocino	25 Apr 18:06:04 40.368°N 124.316°W	25 Apr 18:06:11.8 38.56°N 123.31°W	7.2	7.2	ACSZ	0.355 × a65 <i>or</i> 0.355 × b65 [ad hoc]	
1995 Chile	30 Jul 05:11:24 23.340°S 70.294°W	30 Jul 05:11:56.9 24.17°S 70.74°W	8.0	8.0	CSSZ	2.812 × (a75 + b75) [ad hoc]	
1995 Kuril	03 Dec 18:01:09 44.663°N 149.300°E	03 Dec 18:01:36.1 44.82°N 150.17°E	7.9	7.9	KISZ	1.991 × (a17 + z17) [ad hoc]	
1996 Irian Jaya	17 Feb 05:59:31 0.891°S 136.952°E	17 Feb 06:00:02.8 0.67°S 136.62°E	8.2	8.2	NGSZ	2.7984 × (a9 + b9 + a10 + b10) [ad hoc]	
2009 Papua NG	03 Jan 19:43:51 0.414°S 132.885°E	03 Jan 19:44:09.0 0.38°S 132.83°E	7.6	7.6	NGSZ	0.7046 × (b13 + b14) [ad hoc]	
2009 Kuril	15 Jan 17:49:39 46.857°N 155.154°E	15 Jan 17:49:48.3 46.97°N 155.39°E	7.4	7.4	KISZ	0.7063 × b12 [ad hoc]	
2009 Vanuatu/	07 Oct 22:03:15 13.052°S 166.187°E	07 Oct 22:03:28.9 12.59°S 166.27°E	7.6	7.6	NVSZ	1.2 × B24 + 0.26 × A23 <i>followed after 15 minutes by</i>	
Santa Cruz	07 Oct 22:18:26 12.554°S 166.320°E	07 Oct 22:19:15.3 11.86°S 166.01°E	7.8	7.9	NVSZ	2.6 × B23 + 0.9 × A23 [preliminary] (Yong Wei, 2009 personal communication)	

Another local hazard that has been a frequent cause of damage to Arena Cove has been ocean wave action. Originating locally, or as swell from distant storms, such waves caused severe damage to the pier in 1983 that necessitated its replacement. Another impact of ocean waves, of relevance to tsunami detection and modeling, is in the noise they produce in the tide gauge record that can mask weaker tsunami signals. Harbor resonance in the case of Crescent City can amplify the tsunami and may be a factor too in the Arena Cove response.

1.3 Tsunami warning and risk assessment

The forecast model development described here will permit Arena Cove to be incorporated into the tsunami forecasting system, developed at NOAA's Center for Tsunami Research (NCTR) and now in operational use at the U.S. Tsunami Warning Centers (TWCs). The system has had considerable success in accurately forecasting the impact of both moderate and severe tsunami events in recent years, and in the following section, the methodology that permits such forecasts is discussed as prelude to a description of forecast model development for Arena Cove. With the model in hand, validated with historical events and with its stability verified by extensive testing against extreme scenarios, real-time forecasts will be available to inform local emergency response. Additionally, the synthetic scenarios investigated during model development and reported here provide an initial tsunami risk assessment, as described in Section 4.

2. Forecast Methodology

2.1 The tsunami model

In operational use, NOAA's tsunami forecast model is used to extend a precomputed deepwater solution into the shallows, and onshore as inundation, if appropriate. The model consists of a set of three nested grids, named A (outermost, with coarse resolution), B (intermediate), and C (innermost). The latter provides fine resolution that, in a real-time application of the MOST (Method of Splitting Tsunami) model (Titov and González, 1997; Titov and Synolakis, 1998), permits forecasts at spatial scales (as little as a few tens of meters) relevant to local emergency management. The validity of the MOST model applied in this manner and the operational effectiveness of the forecast system built around it have been demonstrated during unplanned tests in the Pacific basin, triggered by several mild to moderate tsunami events in the years since the 2004 Indian Ocean disaster (Wei *et al.*, 2008) and during the severe 2011 Tohoku (alternately referred to as Honshu) tsunami. Successful hindcasting of observed historic events, even mild ones, during forecast model development lends credence to an ability to accurately forecast the impact of future events. Such validation of tsunami modeling procedures is documented in other volumes of this series. Before proceeding to a description of the forecast model development for Arena Cove, California, it is useful to describe the steps in the overall forecast process.

2.2 NOAA's tsunami forecast system

Operational tsunami forecasts are generated at TWCs, staffed continuously around the clock in Alaska and Hawaii, using the SIFT tool developed at NCTR. The semi-automated process facilitates the steps by which TWC operators assimilate data from an appropriate subset of DART tsunami sensors, “invert” the data to determine the linear combination of precomputed propagation solutions that best match the observations, then initiate a set of forecast model runs if coastal communities are threatened, or, if warranted, cancel the warning. Steps in the process are as follows:

- When a submarine earthquake occurs, the global network of seismometers registers it. Based on the epicenter, the unit sources in the propagation database (Gica *et al.*, 2008) that are most likely to be involved in the event and the DART array elements (Spillane *et al.*, 2008) best placed to detect the waves' passage are identified. TWC operators can trigger DARTs into rapid sampling mode in the event that this did not occur automatically in response to the seismic signal.

- There is now an unavoidable delay while the tsunami waves are in transit to the DARTs. At least a quarter of a cycle of the first wave in the train must be sampled before moving to the “inversion” step.
- When sufficient data have accumulated at one or more DARTs, the observed time series are compared with the model series from the candidate unit sources. Since the latter are precomputed (using the MOST code), and the dynamics of tsunami waves in deep water are linear, a least squares approach can quickly identify the unit sources (and the appropriate scale factors for each) that best fit the observations. The inversion methodology is described by Percival *et al.* (2011).
- Drawing again on the propagation database, the scale factors are applied to produce a composite basin-wide solution with which to identify the coastal regions most threatened by the radiating waves.
- It is at this point that one or more forecast models are run. The composite propagation solution is employed as the boundary condition to the outermost (A-grid) domain of a nested set of three real-time MOST model grids that telescope with increasingly fine scale to the community of concern. A-grid results provide boundary conditions to the B grid, which, in turn, forces the innermost C grid. Nonlinear processes, including inundation, are modeled so that, relying on the validation procedures during model development, credible forecasts of the current event are available.
- Each forecast model provides quantitative and graphic forecast products with which to inform the emergency response or to serve as the basis for canceling or reducing the warnings. Unless the tsunami source is local, the forecast is generally available before the waves arrive. Even when lead time cannot be provided, the several hour duration of a significant event (in which the first wave may not be the most damaging) gives added value to the multi-hour forecasts provided.

Because multiple communities may be at risk, it may be necessary to run, simultaneously or in a prioritized manner, multiple forecast models. Each must be optimized to run efficiently in as little time as possible. The current standard is that an operational forecast model should be capable of simulating 4 hr of real time within about 10 min of CPU time on a fast workstation computer.

3. Model Development

3.1 Digital elevation models

Water depth determines local tsunami wave speed, and subaerial topography determines the extent to which tsunami waves inundate the land. Thus, a prerequisite for credible tsunami modeling is the availability of accurate gridded bathymetric and topographic datasets, termed digital elevation models, or DEMs. Given their expertise in this area and the number of coastal communities needing tsunami forecast capability, NCTR relies heavily on the NGDC to provide the DEMs needed. In the case of Arena Cove, California, the DEM was produced and documented by Friday *et al.* (2009). The DEM is a composite of multiple data sources merged and converted to a common datum of mean high water (MHW); the use of MHW as the “zero level” is standard in forecast models. The version of MOST currently employed does not explicitly include tidal fluctuations, and, since a tsunami may arrive at any stage of the tide, it is best to employ a “worst-case” approach by assuming high tide when forecasting inundation. For some forecast models, grounding of vessels and the strong and rapidly varying currents often associated with even mild tsunamis are of concern. For Arena Cove, which lacks a marina and shoreline infrastructure, low water impacts are less important.

The DEM provided by NGDC for the Arena Cove area is illustrated in **Figure 3**; its salient features listed in **Table 2** are reproduced from DEM documentation (Friday *et al.*, 2009). The NGDC report thoroughly describes the data sources and methods employed in constructing the DEM. With 1/3 arc sec (10 m) resolution, the DEM provides the basis for the B and C grids developed for both the reference and forecast models. NCTR maintains an atlas of lower-resolution gridded bathymetries that can be used for the A grids, as described in Section 3.4. All of the DEMs employed were verified for consistency with charts, satellite imagery, and other datasets during the course of MOST grid development.

Table 2: The main features of the Arena Cove digital elevation model (DEM).

Grid Area	Arena Cove, California
Coverage Area	123.43° to 124.43°W; 38.40° to 39.40°N
Coordinate System	Geographical decimal degrees
Horizontal Datum	World Geodetic System 1984 (WGS84)
Vertical Datum	Mean High Water (MHW)
Vertical Units	Meters
Cell Size	1/3 arc sec
Grid Format	ESRI Arc ASCII grid

The elevations and depths used in the development of this forecast model were based on the DEM provided by the NGDC; the author considers it to be a good representation of the local topography and bathymetry. As new DEMs become available, forecast models will be updated and report updates will be posted at nctr.pmel.noaa.gov/forecast_reports/.

3.2 Tides and sea level variation

Arena Cove's history of tidal observations dates back only to 1978. The tide station (9416841, 38°54.8'N, 123°42.4'W) is located near the end of the pier, whose concrete pilings raise the deck about 7.7 m above sea level and do not impede water movement within the cove. The instrumentation was upgraded in 2006 to include a tsunami-capable gauge sampling at 1 min intervals; some earlier data were sampled at 6 min intervals, and several historical events are only available as marigrams on microfiche. An ongoing project at NGDC will digitize the more critical images in this archive.

Station characteristics for 9416841 are provided in **Table 3**, based on the wealth of online tidal information available at NOAA's CO-OPS (Center for Operational Oceanographic Products and Services) website (tidesandcurrents.noaa.gov). Note the sizeable diurnal range of over 1.7 m, and that, while the long-term rate of change in sea level is low (compared to more tectonically active areas), there is substantial seasonal, interannual, and short-term variability. Owing to the relatively short history of the Arena Cove tide gauge, trends and cycles are reported for Crescent City to the north and Point Reyes to the south.

A sample section of the tide gauge record, again extracted from the CO-OPS website, is reproduced in **Figure 5**. Deviations (or residuals) from the astronomically predicted tide can be several cm and the variability strong. In particular, the highest water level reported for the Arena Cove gauge is 1.056 m above MHW (6 February 1998), so the use of MHW as the zero level of modeled sea level may underestimate the truly worst case. While the simultaneous arrival of the crest of a large tsunami at high tide during a storm surge has low probability, a feature of the simulated events reported below is that sustained oscillations at a resonant period may extend the duration of the threat. This effect is notorious at Crescent City, California, which is frequently the most heavily impacted U.S. West Coast location for remote events.

3.3 The CFL condition and other considerations for grid design

Water depth-dependent wave speed, in conjunction with the spacing of the spatial grid representation, places an upper limit on the time step permissible for stable numerical solutions employing an explicit scheme. This is the CFL (Courant-Friedrichs-Levy) limit, which requires careful consideration when the grids employed for a reference or forecast model are being designed. Finer-scale spatial grids, or greater water depths, require shorter time steps, thereby increasing the amount of computation required to simulate a specific real-time interval.

Table 3: Tidal characteristics of the Arena Cove tide gauge.**Arena Cove, California: Station 9416841 (38°54.8'N, 123°42.4'W)****Tidal Datum and Range Values (Epoch 1983–2001)**

MHHW (Mean Higher High Water)	10.609 m	Great Diurnal Range 1.787 m	Mean Range 1.232 m
MHW (Mean High Water)	10.405 m		
MSL (Mean Sea Level)	9.779 m		
MLW (Mean Low Water)	9.174 m		
MLLW (Mean Lower Low Water)	8.822 m		

Sea Level Trends and Cycles from Point Reyes, California, Station 9415020

Long-term Sea Level Trend	Increasing 2.10 ± 1.52 mm/yr
Seasonal Cycle Range	Min. -89 mm (April); Max. +59 mm (September)
Interannual Variation (from 1980)	Min. -20 mm (1988); Max. +21 mm (1997)

Sea Level Trends and Cycles from Crescent City, California, Station 9419750

Long-term Sea Level Trend	Decreasing 0.65 ± 0.36 mm/yr
Seasonal Cycle Range	Min. -87 mm (May); Max. +85 mm (January)
Interannual Variation (from 1980)	Min. -20 mm (1989); Max. +28 mm (1998)

Extremes (1991–2011)

Maximum	11.461 m on 6 February 1998
Minimum	8.017 m on 18 May 2003

Another feature of the application of gridded numerical solutions to the tsunami wave problem is the shortening that the wave train encounters in moving from deep water onto the shelf. In deep water, a grid spacing of 4 arc min (of latitude and longitude, corresponding to ~ 7 km) is normally used to represent propagating wave trains with a typical wavelength of the order of a few hundred kilometers. The stored results of such propagation model runs are typically decimated by a factor of 4, resulting in a database of ~ 30 km spacing (and 1 min temporal sampling) with which to generate the boundary conditions for the outermost (A grid) of the nested grids in a model solution. The extraction of the boundary conditions (of wave height and the two horizontal velocity components) is achieved by linear interpolation in space and time. To provide realistic interpolated values, the stored fields for these variables must be smoothly varying and have adequate sampling in space and time to resolve their structure. This necessitates the placement of the outer boundary of the forecast model domain well offshore. The presence of the Mendocino Escarpment is another incentive to do so, to ensure that its role in topographic steering of trans-Pacific wave trains is adequately represented.

Figure 6 illustrates the placement of the model domain in its west coast setting. The outermost A grid covers the entire region shown; embedded in it is the B grid, which covers most of Mendocino County. The innermost C grid, with the finest spatial resolution, spans the region north and south of Point Arena. A number of nearby communities where runups are mentioned in the historical record are

marked in red. The tsunami-capable tide gauges of the region, the closest of which are Point Reyes to the south and North Spit to the north, are indicated as black triangles. Almost directly offshore is DART 46411. This would play a major role in the detection of regionally generated waves. Its offshore location cleanly registers moderate to large tele-tsunamis and could, potentially, refine a local forecast that was initially based on DART array elements closer to the source. Red, green, and magenta lines indicate, using the color-convention employed in the USGS/NEIC (National Earthquake Information Center) online earthquake resources, the three types of fault that radiate from the triple junction off Cape Mendocino. To the south is the strike-slip San Andreas Fault, skirting the coastline north of San Francisco Bay before entering the ocean within the C-grid domain. The Mendocino Escarpment is dramatic evidence of the ridge fault extending offshore, but of most concern as a local source of tsunamis is the Cascadia Subduction Zone. The two southernmost pairs of the unit source set used to represent it fall within the A-grid domain. A “beachball” that visually represents the source mechanism marks the location of the 1992 Mendocino event, which was the last significant subduction event in Cascadia (at the time this report was written).

3.4 Specifics of the model grids

After several rounds of experimentation, the extents and resolutions of the nested grids for the reference and forecast models were chosen; these are illustrated in **Figures 7** and **8** and details are provided in **Tables 4** and **5**. The reference and forecast model grid pairs (A and B level) have the same extent, differing only in resolution. The C grid domain is, however, slightly larger for the reference than for the forecast model; the dimensions of the latter being reduced to achieve a shorter run time appropriate to operational use. The corresponding panels in the figures

Table 4: Specifics of the reference and forecast model grids employed for Arena Cove, California. For the paired values in the resolution and grid points columns, the zonal (east to west) value is listed first, followed by the meridional (north to south).

Reference Model for Arena Cove, California

Minimum offshore depth: 1.0 m; Water depth for dry land: 0.1 m; Friction coefficient (n^2): 0.0009; CPU time for a 4-hr simulation: 326 min

Grid	Zonal Extent		Meridional Extent		Resolution	Grid Points
A	128.00°W	121.50°W	36.00°N	42.50°N	30" × 30"	781 × 781
B	124.55°W	123.00°W	38.35°N	39.80°N	6" × 6"	931 × 871
C	123.85°W	123.60°W	38.82°N	39.03°N	1" × 1"	901 × 757

Forecast Model for Arena Cove, California

Minimum offshore depth: 1.0 m; Water depth for dry land: 0.1 m; Friction coefficient (n^2): 0.0009; CPU time for a 4-hr simulation: 9.5 min

Grid	Zonal Extent		Meridional Extent		Resolution	Grid Points
A	128.00°W	121.50°W	36.00°N	42.50°N	60" × 60"	391 × 391
B	124.55°W	123.00°W	38.35°N	39.80°N	24" × 24"	234 × 291
C	123.78°W	123.65°W	38.89°N	39.02°N	2" × 2"	235 × 313

CPU times for a 4-hr simulation are based on use of a single Intel® Xeon® E5670 2.93GHz processor.

Table 5: Grid file names and grid-related parameters for Arena Cove, California. The time steps for the A and B grids must be integer multiples of the basic time step chosen for the C grid.

Grid	File Name	Maximum Depth (m)	Minimum CFL (s)	Model Time Step (s)	Water Cells
A	ArenaCoveCA_RM_A	5002	3.350	3.0 (5×)	436,966
	ArenaCoveCA_FM_A	5005	6.689	6.0 (4×)	109,323
B	ArenaCoveCA_RM_B	3781	0.7559	0.6 (1×)	485,760
	ArenaCoveCA_FM_B	3776	2.893	1.5 (1×)	40,535
C	ArenaCoveCA_RM_C	143.6	0.6423	0.6	434,701
	ArenaCoveCA_FM_C	94.4	1.526	1.5	37,611

employ the same depth contours and color palette. Rectangles drawn in red for the A and B grid panels indicate the extent of the embedded grid; where appropriate the blue rectangles indicate the less extensive forecast model C grid. Superimposed in the C-grid panels is the network of rivers, creeks, and roads. The thick red line marks State Hwy 1, also called the Shoreline Highway.

Both C grids lie entirely within the NGDC-provided DEM; A and B grids include bathymetry and topography from other DEM datasets available at NCTR. Some smoothing and editing were necessary to eliminate erroneous points or grid features that tend to cause model instability. For example, “point” islands, where an isolated grid cell stands above water, are eliminated, as are narrow channels or inlets one grid-unit wide; these tend to resonate in the numerical solution. Large depth changes between adjacent grid cells can also cause numerical problems; customized tools (such as “bathcorr”) are available to correct many of these grid defects.

Details of the model grids are provided in **Tables 4** and **5**. The latter lists the maximum depth, the CFL time step requirement that must not be exceeded, and the actual time steps chosen for the reference and forecast model runs. Since the numerical solutions in the three grids proceed simultaneously in the current version of MOST employed by SIFT, there is a requirement that the A- and B-grid time steps be integer multiples of the (innermost) C-grid time step, in addition to satisfying the appropriate CFL requirement. For both reference and forecast models, the CFL requirement of the C grid was the most stringent. The values chosen are shown in **Table 5**, and are such that an integer multiple of each time step (20× for the forecast model; 50× for the reference model) is identically 30 sec, the chosen output time interval for both models. When run on an Intel® Xeon® E5670 2.93 GHz processor, the forecast model produces 4 hr of simulation in 9.5 min, within the desired 10 min value for this metric.

3.5 Model run input and output files

In addition to providing the bathymetry file names, the appropriate time step, and A and B grid multiples as provided in **Table 5** above, it is necessary to provide a number of additional parameters in an input file. These include the Manning friction coefficient (n), a depth threshold to determine when a grid point becomes inundated, and the threshold amplitude at the A-grid boundary that will start

the model. An upper limit on wave amplitude is specified in order to terminate the run if the waves grow beyond reasonable expectation. Standard MOST values are used: $n^2 = 0.0009$ for the friction coefficient (appropriate for natural channels and flood plains) and 0.1 m for the inundation threshold. The latter causes the inundation calculation to be avoided for insignificant water encroachments that are probably below the level of uncertainty in the topographic data. Inundation can, optionally, be ignored in the A and B grids, as is the norm in the (non-nested) MOST model runs that generate the propagation database. When A- and B-grid inundation is excluded, water depths less than a specified “minimum offshore depth” are treated as land; in effect, a “wall” is placed at the corresponding isobath. When invoked, a value of 1 m is applied as the threshold, although A and B inundation is normally permitted as a way to gain some knowledge of tsunami impact beyond the scope of the C-grid domain. Other parameter settings allow decimation of the output in space and/or time. As noted above, 30 sec output has been the target and output at every spatial node is preferred. These choices avoid aliasing in the output fields that may be suggestive of instability (particularly in graphical output) when none, in fact, exists.

Finally, the input file (supplied in Appendix A) provides options that control the output produced. Output of the three variables—wave amplitude, zonal (positive to the east) velocity, and meridional (positive to the north) velocity—can be written (in netCDF format) for any combination of A, B, and C grids. These files can be very large. A separate file, referred to as a SIFT file, contains the time series of wave amplitude at each time step at discrete cells of a selected grid. Normally, the time series at a “reference” or warning point, typically the location of a tide gauge, is selected to permit validation in the case of future or historical events. The SIFT file output also includes the distribution of the overall minimum and maximum wave amplitude and speed in each grid. By contrast with the complete space-time results of a run, the SIFT file (also netCDF) is very compact, and, if more than a single grid point is specified, a broader view of the response is provided.

By default, two additional output files are generated. A “listing” file summarizes run specifications, progress, and performance in terms of run time, as well as information to determine the reason, should a run not start or terminate early. A “restart” file is produced so that a run can be resumed from the time it ended, either normally or by operator intervention.

The input files described above are specific to the model itself. For an actual run, the program must be pointed toward the files that contain the boundary conditions of wave amplitude (H) and velocity components (U, V) to be imposed at the A-grid boundary. Time-varying conditions are generally extracted as a subset of a basin-wide propagation solution (either a single unit source or several, individually scaled and linearly combined) that mimics a particular event. These boundary-forcing files typically consist of 24 hr of values (beginning at the time of the earthquake), sampled at 1 min intervals and available on a 16 arc min grid. Occasionally, for more remote seismic sources or when delayed arrival of secondary waves due to reflections are a concern (as has been seen at Hawaii), the time span of the propagation run available for forcing is extended beyond one day.

4. Results and Discussion

Before proceeding to an extensive suite of model runs that explore the threat from various source regions to the Point Arena area in California, the stability of the model is tested in both low and extreme amplitude situations. The former we refer to as “micro-tsunami” testing, where the boundary forcing is at such a low level (but not precisely zero) that the response is expected to be negligible. These tests can be highly valuable in revealing localized instabilities that may result from undesirable features in the discretized bathymetric representation. Inlets or channels that are only one grid-cell wide may “ring” or resonate in a non-physical way in the numerical solution. An instability may not grow large enough to cause the model to fail but, in a run with typical tsunami amplitudes, may be masked by actual wave variability.

Forcing by extreme events, termed “mega-tsunami” events, is also tested. In addition to the need to test model stability under such circumstances, there is a parameter in the input file that truncates the run if a prescribed threshold is exceeded. For operational use, the threshold must be set high enough so that an extreme event run is not unnecessarily terminated. Both tests should be performed for test sources whose waves enter the model domain from different directions since, although stable for one set of incoming waves, an instability may be encountered for another. The micro- and mega-tsunami testing of the forecast and reference models is reported in the following subsections. Further evidence of stability is provided by the extensive set of scenarios, aimed at exploring the dependence of impact to source location, described later in the report and used in independent testing by other members of the NCTR team prior to the model’s release for operational use.

4.1 The micro-tsunami tests

Three micro-tsunami test cases (see **Table 6**) were run representing sources in the western Aleutians, the Philippines, and south of Japan. Based on sources from the propagation database (Gica *et al.*, 2008), their amplitudes were scaled down by a factor of 100 to mimic a Mw 6.1667 / Slip 0.01 m source rather than the Mw 7.5 / Slip 1 m standard. A number of grid cells in the B and C grids emerged as potential sources of instability. Generally, these were minor indentations of the coastline, barely resolved by the grids, or narrow channels. Also to be tested further is the area northwest of the Point Arena Light where the rugged seabed reveals several past water level stands. A limited number of grid cells in the outermost (A) grid required correction. These were generally associated with non-physical features in the topographic database, such as a track of ship-based soundings that were improperly merged with other data sources. After an iterative process of grid correction and retesting using these micro-tsunami sources, both the reference and forecast model grids were deemed satisfactory (as illustrated in the upper

panel of **Figure 9**) and the testing of extreme and historical events could begin. The lower panel of **Figure 9** illustrates a step in the process where a deficiency in the reference model grid generated a mild instability (in the EPSZ B19 micro-tsunami scenario—see **Table 6**), causing the reference model time series at the reference point, initially in close agreement with the forecast model, to develop unrealistic, high-frequency oscillations. Though still generally tracking the forecast model result and not growing without bound, the feature could behave erratically in simulating real events. Modification of the reference model bathymetry eliminated the problem, and tests involving other micro-tsunami sources (RNSZ B14 and ACSZ B6) did not reveal other issues.

Table 6: Synthetic tsunami events employed in Arena Cove, California, model testing. The reference and forecast model solutions of those shown in bold text were intercompared extensively.

Scenario	Source Zone	Tsunami Source	α [m]
Mega-tsunami (Mw 9.3) Scenario			
KISZ 1–10	Kamchatka-Kuril-Japan-Izu-Mariana-Yap	A1–10, B1–10	25
KISZ 22–31	Kamchatka-Kuril-Japan-Izu-Mariana-Yap	A22–31, B22–31	25
KISZ 32–41	Kamchatka-Kuril-Japan-Izu-Mariana-Yap	A32–41, B32–41	25
KISZ 56–65	Kamchatka-Kuril-Japan-Izu-Mariana-Yap	A56–65, B56–65	25
ACSZ 6–15	Aleutian-Alaska-Cascadia	A6–15, B6–15	25
ACSZ 16–25	Aleutian-Alaska-Cascadia	A16–25, B16–25	25
ACSZ 22–31	Aleutian-Alaska-Cascadia	A22–31, B22–31	25
ACSZ 50–59	Aleutian-Alaska-Cascadia	A50–59, B50–59	25
ACSZ 56–65	Aleutian-Alaska-Cascadia	A56–65, B56–65	25
CSSZ 1–10	Central and South America	A1–10, B1–10	25
CSSZ 37–46	Central and South America	A37–46, B37–46	25
CSSZ 89–98	Central and South America	A89–98, B89–98	25
CSSZ 102–111	Central and South America	A102–111, B102–111	25
NTSZ 30–39	New Zealand-Kermadec-Tonga	A30–39, B30–39	25
NVSZ 28–37	New Britain-Solomons-Vanuatu	A28–37, B28–37	25
MOSZ 1–10	Manus–Oceanic Convergent Boundary	A1–10, B1–10	25
NGSZ 3–12	North New Guinea	A3–12, B3–12	25
EPSZ 6–15	East Philippines	A6–15, B6–15	25
RNSZ 12–21	Ryukyu-Kyushu-Nankai	A12–21, B12–21	25
Mw 7.5 Scenario			
NTSZ 36	New Zealand-Kermadec-Tonga	B36	1
Micro-tsunami (Mw 6.5) Scenario			
EPSZ B19	East Philippines	B19	0.01
RNSZ B14	Ryukyu-Kyushu-Nankai	B14	0.01
ACSZ B6	Aleutian-Alaska-Cascadia	B6	0.01

4.2 The mega-tsunami tests

The record of tsunami impact on the northern California coast discussed in this report reveals that sources around the entire periphery of the Pacific can be felt. Indeed, the catastrophic Indian Ocean tsunami of 2004 was detectable at Arena Cove, as it was throughout the global ocean. A broad suite of 19 extreme events (termed mega-tsunamis), whose locations are standard for Pacific basin forecast model testing, are listed in **Table 6**, and their locations are shown in **Figure 10**. Unit source subduction zone acronyms (e.g., ACSZ, stretching from the Aleutians to Cascadia) are provided in Appendix B. To simulate each mega-tsunami source, 10 A–B pairs of unit sources are used with an evenly distributed slip of 25 m. As described by Gica *et al.* (2008), each unit source represents a 100×50 km area of the fault surface, with the long axis parallel to the plate boundary. Row B is shallowest, sloping from a nominal depth of 5 km (unless the USGS provides a depth estimate based on the earthquake catalogs). Row A is deeper, followed by rows Z, Y, X, etc. where appropriate. Thus, the mega-tsunami sources represent 1000 km long ruptures with a width of 100 km and corresponding magnitude of Mw 9.3.

Discussion of the entire set in greater detail is provided once the validity of the forecast model has been established. Here we focus on a subset of three synthetic cases, highlighted in **Figure 10** and **Table 6**, to contrast the forecast model with the more highly resolved reference model. The results are presented in **Figures 11–13**, with the time series at the reference point (the Arena Cove tide gauge) shown in the upper panel and the amplitude and current pattern at a selected time shown below. The black and red curves represent the reference and forecast model, respectively; the green line identifies the time at which the comparison in the lower panel was made. Inset in the lower panels are enlargements of the area around Arena Cove.

It is noticeable that, in all three of the cases shown, the reference model tends to oscillate longer and have somewhat larger amplitude than does the forecast model, although the two solutions are in close agreement for the first few tsunami waves. This is likely a physical reality: the more highly resolved bathymetry and coastline of the reference model provides greater scope for nonlinear features or reflected waves to develop. This observation suggests a caveat to operational use of the forecast model: while accurate portrayal of the early history of an event is to be expected, the duration of the event and the amplitude of later waves may be underestimated.

The snapshot comparisons in the lower panels of **Figures 11** and **12** are quite reasonable, illustrating that the solutions match not just at the reference point. It is worth noting too that, although the ACSZ 56–65 mega-tsunami event represents a massive Cascadia tsunami, the scale of impact to the Arena Cove area (~3 m) is not substantially greater than from trans-Pacific locations (KISZ 1–10 off Kamchatka and NTSZ 30–39 near Samoa.) The Crescent City response to the same synthetic Cascadia mega-tsunami event exceeds 10 m (Arcas and Uslu, 2010). It would appear that the energy propagated alongshore to the south, possibly with some sheltering by Cape Mendocino, is reduced, and that perhaps the greatest impact to Arena Cove may be associated with source regions elsewhere in the Pacific basin.

In **Figure 13**, the comparison time was intentionally chosen later in the event as a counterexample. At the warning point and nearby, the forecast and reference models may be in reasonable agreement, but the broader wave patterns may have substantial phase differences. The comparisons in these lower panels are restricted to the portion of C-grid area common to both models. Waves generated by reflections in the larger reference model C grid will impinge on the common domain as the solution proceeds, so the greatest disparities are to be expected at the northern and southern forecast model boundaries. However, **Figure 13** and other “snapshot” comparisons show that the effect is quite minor.

Before proceeding to validate the model with historical events, one other synthetic event is standard in the testing protocol: a moderate source of Mw 7.5 at a remote location. A single unit source near Samoa (NTSZ B36) is employed, and its representation by the reference and forecast model are compared in **Figure 14**. Such an event results in a response of about 2 cm in Arena Cove sea level, and there is excellent agreement between both model representations in the earlier portion of the event.

Overall, the close agreement between the first wave arrival time and waveform and the general range of variation of the two model representations in synthetic scenarios (even though the amplitude and phase is not always well-matched for later waves) suggest that the forecast model is performing well, and that we can confidently proceed to model real events.

4.3 Model validation with historical events

We now proceed to examine, for the historical cases highlighted in **Table 1a** and **Figure 4**, how well the reference and forecast model solutions compare with observation. Since the observations are limited to the tide gauge records or runup reports in Arena Cove, the purpose of the lower panels is only to illustrate the agreement between the models.

The results displayed and described below represent the large 1946 Unimak and 1964 Alaska events and three more recent ones: 2006 Kuril (which has been extensively studied), 2009 Samoa, and 2010 Chile. The latter three events occurred subsequent to the installation of an improved tide gauge at Arena Cove. In Section 4.6, the Tohoku tsunami of 11 March 2011 is discussed. The event occurred while this report was undergoing internal review at NCTR, but the forecast model was available for use in real-time circumstances. Another difference between the earlier and more recent events is that the source characterization for the former is based on the literature, with the source mechanism estimated from the seismic record. The 2006 Kuril event was the first substantial event for which direct observation of the tsunami wave train was available from multiple deep-water DART sites. As such, its source characteristics, and those for the 2009 Samoa, 2010 Chile, and 2011 Tohoku events are better suited to tsunami modeling and forecast; those based on seismic data only may suffer from the defect that earthquakes differ in their ability to generate tsunami waves. An extreme case of this is the 1896 Sanriku event, which is modeled and briefly discussed

in Section 4.4. It was referred to as a “tsunami-earthquake” (Dudley and Lee, 1998), causing devastating losses in Japan despite its modest magnitude and scant warning in the form of ground motion.

Even in the case of source characterizations based on DART detection and inversion, one should bear in mind that perfect agreement between the model wave and observation is unlikely. For one thing, the DART sites used in the inversion process may be well described by a linear combination of unit source functions but their placement may limit the ability to predict basin-wide energy propagation. Ideally, one might hope to refine the model solution in light of DART observations closer to the impact site. The deep-water waves in the far field (e.g., 46411, for Arena Cove) may, however, fall below the DART detection threshold. Neither are the tide gauge observations, available for comparison with model prediction, perfect. They may include noise, possibly amplified by harbor resonances and wind wave activity.

The 1946 Unimak and 1964 Alaska events were widely felt along the U.S. West Coast, although the greatest impact was to the Hawaiian Islands. Reported runups at Arena Cove were 2.40 and 1.83 m, respectively, comparable in the case of 1964 Alaska (but somewhat lower for 1946 Unimak) to the modeled responses shown in **Figures 15** (1946 Unimak) and **16** (1964 Alaska). The reference and forecast model solutions match well, both in the time series and in the amplitude and velocity field at the selected comparison time.

For the more recent events, where time series at Arena Cove permit direct intercomparison with the reference and forecast model predictions, the results are presented in **Figures 17–19**. For the 2006 Kuril event (**Figure 17**), the reported 61 cm runup at Arena Cove exceeds, by a factor of about 2, the amplitude of the tide gauge oscillations. Particularly for the early waves, the model gives a reasonable representation of both the amplitude and timing of the observations. The time axis is in model hours and the discrepancy in the first wave arrival time is about 5 min, just 1% of its transoceanic travel time.

For the 2009 Samoa event (**Figure 18**), the reported runup at Arena Cove is 44 cm, which may correspond to later in the record when harbor resonances may have been excited. For the early waves, the amplitude of the observations is closer to 20 cm, and, though it does reasonably well in predicting the early timing and the sequence of waves, the model underestimates the amplitude by about a third. For the 2010 Chile event (**Figure 19**), the amplitude of the observations is replicated more closely. Again though, the reported runup of 35 cm is substantially greater than the greatest positive excursion of the de-tided observations as displayed.

Considering the above results, the main discrepancy appears to be the mismatch between reported runup and the processed sea level time series. Some possible explanations come to mind. Runup is defined as maximum elevation above the predicted tide, which may not include seasonal or meteorologically driven departures, which, as illustrated in **Figure 5**, can be several centimeters. Another possibility is that the overall maximum of the tide gauge record may be aliased by high-frequency variability, which was smoothed somewhat by a 3-point running average in the preparation of these graphics.

4.4 Further historical simulations

The above analysis has documented good agreement between the forecast model and the slower-running reference version. This permits us to simulate the balance of historical cases where impacts to Arena Cove and northern California have been reported with the forecast model alone. These runs are used to further validate the stability of the forecast model, but also provide some information on the exposure of the region to tsunamis generated at various points on the periphery of the Pacific.

In **Figures 20–24**, the full set of observed records at Arena Cove (or proxy sites in some cases) are compared with forecast model prediction. Also provided for each event is the state of the tide at Arena Cove. While probably of little concern for weak events, this may be a factor in the impact of larger ones. Reported runup is included in each case, but as noted earlier, this may be only loosely related to the plotted series. In each case, the forecast model series is shown in black and the observations are drawn in red. Although studies of the global ocean response to the 2004 Indian Ocean tsunami suggest a runup of 19 cm in Arena Cove, the signal is largely obscured by noise. An attempt was made to employ global ocean model results (on a coarser grid than is available for the Pacific propagation database) to drive the Arena Cove forecast model; the results were unsatisfactory and will not be presented. When a better-resolved global solution is available, this event may be added to the suite employed for forecast model testing, since it should shed light on the extent to which bathymetric resolution may impact arrival time accuracy.

The sequence begins with a cautionary tale: the “tsunami-earthquake”-induced 1896 Sanriku event (upper left panel, **Figure 20**). This was modeled by a suitably positioned unit source (KISZ B25) with the slip appropriate to the reported Mw 7.6 magnitude. As shown, such an event would be expected to generate only a few centimeters signal at Arena Cove. Large runups occurred (1 m in the case of the nearby town of Mendocino), illustrating the fact that direct observation of deep-water waves is needed for realistic forecasting. The depth and frequency of seafloor motion for this event was such that the earthquake magnitude poorly indicated its devastating tsunami-generating potential to Japan’s Sanriku coast.

Next, we consider the set of events from 1946 to 1964 that were felt in or near Arena Cove. During this time, a tide gauge had not yet been installed and the DART array was still in the future. (1946 Unimak and 1964 Alaska were shown earlier.) In each case the source was represented by a weighted group of unit sources from the propagation database or constructed to match source characteristics appearing in the literature (see **Table 1**; Tang *et al.*, 2006).

A number of other events between 1994 (East Kuril) and 2003 (Rat Island), listed in **Table 1** and illustrated in **Figures 21** and **22**, generated weak responses in Arena Cove. In the case of the 1994 East Kuril event, although the match is quite good, the presence of substantial noise in the tide gauge record in advance of the waves’ arrival suggests a limitation on the detection of weak tsunami signals. Particularly in winter months, the tide gauge record at Arena Cove can be extremely noisy. This is true for the 1996 Irian Jaya event; the tide gauge records for the Chile and Kuril events of 1995 are not readily available. For the 1996 Andreanof event, the model seems to capture the timing and periodicity of the Arena Cove

response, as it does perhaps for the 2003 Rat Island event. For the 2001 Peru and 2003 Hokkaido events, the match is less convincing. The 2003 Rat Island event is notable in the history of tsunami forecasting and the DART array. Based on data from early elements of the DART array of the Aleutian Islands and without the conveniences of the SIFT system for inversion, an estimate for the likely impact of this event on the Hawaiian Islands (Titov *et al.*, 2005) demonstrated the utility of direct sea level observation in tsunami forecasting.

The next set of Pacific basin historical events, depicted in **Figure 23**, are the 2006 Tonga through 2007 Peru events. The previously examined Kuril event of 15 November 2006, excluded from this set, was observed at several DART sites; it serves as a benchmark event for NCTR. The 2006 Tonga event is reported by NGDC as producing a 27 cm runup at Crescent City, California, but unfortunately, only 6 min sampled tide gauge data are available at Arena Cove. Though the arrival time and first wave shape correspond reasonably well, the amplitude of the observations is considerably less than the model predicts. For the 2006 Kuril event, the tsunami-capable instrument, with its 1-min sampling, was in place and the early waves of the event were well represented by the forecast model. The same is true of the 2007 Kuril event, which also played an important role in the development of the SIFT forecast tool. Unlike most preceding events, whose source mechanism is a reverse-thrust fault sending a leading peak toward the offshore DART sites, this was a “normal” thrust event from which a leading trough propagated. As seen in **Figure 23**, this observed time series at Arena Cove is well matched by the model.

For the 2007 Solomon event, the observations were weak and intermittent, although the amplitude of the model signal and its inclusion of larger late waves seems consonant with the data. Also shown in **Figure 23**, the 2007 Peru event was only weakly felt at Arena Cove, and one might be tempted to view the observations as noise. By shifting the model result to the right by about 10 min, it is suggested that the early event history is mimicked. Waves traveling from South America to the U.S. West Coast occasionally arrive later than the propagation model predicts, perhaps due to the model bathymetry being smoother than the real ocean. Tsunami waves travel slower in shallower water, and therefore real waves may be delayed in passing through rugged ocean regions, such as the Galapagos. Similar delays have been encountered in other forecasts, and it remains to be seen whether, as more accurate bathymetric data become available, arrival time forecasts will improve. It should be emphasized that, as a percentage of the overall travel time, these delays are quite minor.

Another event off South America, 2007 Chile, occurred late in the same year. The Arena Cove response, shown in **Figure 24**, was quite weak and difficult to match with model prediction. Two events from early 2009, also appearing in **Figure 24**, are available for study. The predicted signal from the first, near Bird’s Head in Papua New Guinea, arrived at a noisy period at the Arena Cove tide gauge, and little, if anything, can be gleaned from the comparison. Two weeks later, an event of similar magnitude occurred off the Kuril Islands where tsunami waves impacting the west coast frequently originate. As seen in the lower left panel of **Figure 24**, the Arena Cove forecast model is reasonably successful in representing that response. The final event in this set, 2009 Vanuatu, is discussed below.

We now arrive at the events that were most recent at the time this report was initially written. The 2009 Samoa event was the most damaging to U.S. territory in recent years, and, although the DART array performed well in providing data to provide an accurate forecast, the proximity of the source to U.S. and Western Samoa did not permit any lead time there. This was a sizeable event, and, even as far away as Arena Cove, a runup of 44 cm was reported. As seen in **Figure 25**, the Arena Cove forecast model performs very well in replicating the early waves, though the later waves may be underestimated. This is an instance in which the reference model (see **Figure 18**) may, in light of the substantial lead-time inherent in such remote source situations, be a worthwhile option. With a workstation-level computer, the run time of the forecast model is presently about 9.5 min of wall-clock time for 4 hr of simulation. With advances in computing power, or the migration of operational computing to supercomputers, it may be possible to depart from the current standard of about 10 min per 4 hr of simulation with a forecast model, perhaps even to run the basin-wide solution in real time with enhanced resolution.

Just days after the 2009 Samoa event, another occurred off Vanuatu. Though much less damaging, this event had a new feature to exercise the tsunami community. The 2009 Vanuatu case was a composite event with two earthquakes in a 15 min period. Though not yet part of the standard set of historic events for forecast model evaluation, the separate source characterizations have been established at NCTR (Yong Wei, personal communication). Blending the two forcing histories with an appropriate time delay provides the input needed for a forecast (or reference) model run, and the result for the mild response at Arena Cove is quite good. The final historical event analyzed for the initial development of this report is associated with the major earthquake that struck Chile on 27 February 2010. Causing major damage and loss of life locally, the tsunami waves propagated widely throughout the Pacific. The waves, seen at DART 32412, provided a good estimate of the remote hazard, particularly to Hawaii, indicating that wide-scale evacuation was not necessary. On the U.S. West Coast, noticeable tsunami effects were observed matching predictions. At Arena Cove, had this model been available and included in the SIFT system then, it would have been another point of success for the forecast system in the emergency response to the 2010 Chile event. As seen in **Figure 25**, there is very close agreement between the forecast model hindcast and tide gauge observation. On 11 March 2011, as this report was undergoing internal review, the Tohoku region of Honshu, Japan, was struck by a huge earthquake, generating a tsunami that caused local devastation and serious impacts throughout the Pacific basin. The forecast model for Arena Cove was employed in real time, and the results are described briefly in Section 4.6.

4.5 The Mendocino earthquake of 25 April 1992

Of special interest to northern California is the Mendocino earthquake of 25 April 1992. This has the distinction of being the most recent substantial thrust event on the Cascadia Subduction Zone. Strike-slip events are commonplace offshore in this region, as shown in **Figure 26**. The upper panels show earthquake epicenters and some fault mechanisms from the USGS/NEIC catalogs in the period 1900–2010. Most are strike-slip, with only the 1991 and 1992 events having

the signature of thrust faulting, with the greater potential to generate significant vertical displacements of the seafloor. The epicenter of the 1992 event was on land to the southeast of the plate triple junction off Cape Mendocino. Uplift on the order of 1 m of a 25 km stretch of the nearshore, between Cape Mendocino and Punta Gorda to the south, was evident in a die-off of intertidal organisms, reported by Carver *et al.* (1994). Presumably extending offshore too, this deformation is not well represented by either of the southernmost unit sources now available in the propagation database (ACSZ A65 and B65). The model predictions based on either of these unit sources with an appropriate scale factor for the magnitude 7.2 event underestimate the tide gauge signal at Arena Cove, as seen in **Figure 26**. Another feature of interest for this event, described by González *et al.* (1995), is that its proximity to shore may have generated a train of coastal-trapped edge waves. Traveling slower than normal tsunami waves taking a deep-water route, the edge waves may have extended the duration of the event at nearby locations to the north and south. This possibility, and the suggestion that the ACSZ source line should be extended at least one unit farther south, make this an event worth further study. The reference and forecast models for Arena Cove and other existing or planned West Coast models (Eureka, Crescent City, etc.) have a major role in ongoing risk assessment studies for Cascadia.

4.6 The Tohoku tsunami of 11 March 2011

As this report was in development, a severe earthquake and consequent tsunami occurred in the Tohoku region off the east coast of Honshu, Japan. The SIFT forecast system, ingesting timely data from nearby DART sites, performed well and provided the basis for appropriate response at those sites for which forecast models were available. Among these was Arena Cove, so it seems appropriate to add 2011 Tohoku (alternately referred to as 2011 Honshu) to the suite of historical events for which observations, and both forecast model and reference model results, are available. The results appear in **Figure 27** where, in the upper panel, the reference and forecast model time series at the Arena Cove tide gauge (black and red lines, respectively) are compared with the 1 min tide gauge record (in blue).

While the largest tsunami waves fortuitously arrived near low water for the U.S. West Coast, and the NCTR models employ MHW to represent “worst case” conditions, the agreement is excellent. As at other sites, there was a slight discrepancy in the arrival time (9 min in the case of Arena Cove); this has been compensated for in **Figure 27**. This error is < 1.6% of the overall travel time and is believed to be associated with the relatively coarse grid of the propagation database, which provides the boundary conditions of the finer-scale nested forecast and reference model grids.

After the first few waves, the timing and amplitude of crests and troughs lose synchronicity, both between the reference and forecast model and between these and the observations. Nonetheless, the character of the response is well replicated and the maximum runup agrees well with the reported 1.55 m provided by NGDC. The latter is the difference between actual and predicted sea level and suggests that, in the case of Arena Cove itself, the forecast wave height is not overly sensitive to the state of the tide, although the extent of inundation may be overstated.

The second row of **Figure 27** contrasts the reference and forecast model solutions at a time, indicated by the green line in the upper panel, where the solutions have begun to diverge. It illustrates that both wave amplitude and tsunami-induced currents are in good agreement through most of the region shown. As before, there is some nearshore discrepancy at the northern and southern limits of the C grid and near the complex topography off Point Arena Light. The lower panels of the figure contrast the reference and forecast model predictions for maximum wave amplitude. No reports of amplitude or inundation are available for comparison with these predictions, but the agreement would appear to be best near shore for this event. The maxima, in particular, predicted for Arena Cove and the inundation near the mouth of the Garcia River and much of Manchester Beach match well. If there is error, the forecast model appears to err on the conservative side, overstating the likely impact. Other historical cases, comparing reference and forecast model predictions to observation, may weaken this as a general conclusion though it does come from the event generating the strongest signal. In the upper panels of **Figures 18** and **19** the reference model may be a better match, particularly for later waves, while for the 2006 Kuril case (**Figure 17**), neither model replicates well what may be noise in the tide gauge record.

To summarize the analysis of historical events, it would appear that the Arena Cove forecast model is capable of producing accurate forecasts for this open coast site on the U.S. West Coast. Though the tsunami waves may be difficult to detect amid the noise at the tide gauge during winter storms, the objective of producing credible forecasts of tsunami impact appears to have been met.

4.7 Simulation of the remaining synthetic mega-tsunami events

We conclude this section with a summary of other model runs, included to verify its stability, that provide useful information on the exposure of Arena Cove to potentially hazardous future events within the Pacific. As noted earlier, the sparse instrumental record of actual events needs to be augmented with credible scenarios to permit risk assessment. While not pretending to be a full-blown risk assessment for the Arena Cove–Manchester Beach area, the full set of mega-tsunami events modeled during stability testing can provide some early estimates.

Results for the set of 19 mega-tsunami events based on the forecast model are presented in **Figure 28**. At the center of each source zone (1000×100 km in extent, with the long axis aligned with the local plate boundary and a uniform slip distribution corresponding to an event magnitude of 9.3) a color-coded square represents the impact at Arena Cove. The measure of impact employed is the maximum amplitude of the predicted time series at the reference point (for the Arena Cove forecast model, the tide gauge location near the head of the pier.) There is not any simple relationship between source orientation, location, or great circle distance to Arena Cove; focusing associated with seafloor features can more than compensate for the decay associated with geometric spreading. In **Figure 29**, forecast model prediction of the inundation that might result from some of these scenarios are drawn together with (in the lower right panel) an ensemble representing the selection employed in the CalEMA study, whose inundation line is drawn in red.

5. Conclusions

In conclusion, good agreement between observations and model predictions for a subset of historical events, including the recent 2011 Tohoku tsunami, has been established, and the stability of the model for numerous synthetic events has been demonstrated. The reliability of the forecast model, designed to run rapidly in real-time emergency conditions, has been proven by the favorable comparison with reference model predictions, particularly during the early hours of an event. The model will be included in the SIFT system employed operationally at the Tsunami Warning Centers, and will permit the Point Arena–Manchester area of California to be added to the coastal communities for which forecast capability is available. Additionally, this model provides a useful tool in risk assessment for the Arena Cove area.

Further tests have been made by other members of the group at NCTR, and will continue to be made by staff at the Tsunami Warning Centers and others, perhaps in training situations. Among the many related tools developed at NCTR is ComMIT (the Community Model Interface for Tsunamis; Titov *et al.*, 2011), which provides a highly intuitive graphical environment in which to exercise and explore forecast models for any combination of propagation database unit sources. Were any of these avenues to reveal a problem with the model, its origin (most likely in some quirk of the bathymetric files) would be located and corrected, and the revised version would then be re-installed for operational use. The development of the forecast system is a dynamic process, with new models added (and old ones revisited) from the current list of U.S. interests and globally. As algorithms and methodologies to represent meteo- or landslide-generated tsunamis become available in the coming years, the utility of current forecast models beyond purely seismic events could well expand.

6. Acknowledgments

Many members of the NCTR group provided valuable assistance in the production of this report. In particular, Nicolas Arcos edited the first draft for content and style; a later internal review was provided by Edison Gica. Jean Newman performed the SIFT testing reported in Appendix C. CalEMA and other California entities distribute GIS online datasets used in the graphics. The modeling could not proceed without the detailed DEM produced at NGDC by the painstaking combination of numerous bathymetric and topographic surveys. Imagery used in the earlier figures has been reproduced with permission from the California Coastal Records Project (www.californiacoastline.org) and the Mendocino County Historical Society. This publication is partially funded by the Joint Institute for the Study of the Atmosphere and Ocean (JISAO) under NOAA Cooperative Agreements NA17RJ1232 and NA10OAR4320148. This is JISAO Contribution No. 2087, PMEL Contribution No. 3390, and NOAA ISI ID300.

7. References

- Arcas, D.R., and B. Uslu (2010): A Tsunami Forecast Model for Crescent City, California. US Department of Commerce, NOAA OAR Special Report, PMEL Tsunami Forecast Series: Vol. 2, 112 pp.
- Barberopoulou, A., J. C. Borrero, B. Uslu, M. R. Legg, and C. E. Synolakis (2011): A second generation of tsunami inundation maps for the state of California. *Pure and Appl. Geophys.*, 168(11), 2133–2146.
- Carver, G.A., A.S. Jayko, D.W. Valentine, and W.H. Li (1994): Coastal uplift associated with the 1992 Cape Mendocino earthquake, northern California. *Geology*, 22(3), 195–198.
- Census Bureau (2010): United States Census Bureau American FactFinder Community Facts. URL: factfinder2.census.gov/faces/nav/jsf/pages/community_facts.xhtml.
- Dudley, W.C., and M. Lee (1998): *Tsunami!*, University of Hawai'i Press, Honolulu, Hawaii, 362 pp.
- Dunbar, P. (2007): Increasing public awareness of natural hazards via the internet. *Nat. Hazards*, 42(3) doi:10.1007/s11069-006-9072-3, 529–536.
- Fine, I.V., A.B. Rabinovich, B.D. Bornhold, R.E. Thomson, and E.A. Kulikov (2005): The Grand Banks landslide-generated tsunami of November 18, 1929: Preliminary analysis and numerical modeling. *Mar. Geol.*, 215(1), 45–57.
- Friday, D.Z., L.A. Taylor, B.W. Eakins, R.R. Warnken, K.S. Carignan, R.J. Caldwell, E. Lim, and P.R. Medley (2009): Digital Elevation Model of Arena Cove, California: Procedures, Data Sources and Analysis. ngdc.noaa.gov/mgg/inundation/tsunami/data/arena_cove_ca/arena_cove_ca.pdf
- Gica, E., M. Spillane, V.V. Titov, C.D. Chamberlin, and J.C. Newman (2008): Development of the forecast propagation database for NOAA's Short-term Inundation Forecast for Tsunamis (SIFT). NOAA Tech. Memo. OAR PMEL-139, NTIS: PB2008-109391, 89 pp.
- González, F.I., K. Satake, E.F. Boss, and H.O. Mofjeld (1995): Edge wave and non-trapped modes of the 25 April 1992 Cape Mendocino tsunami. *Pure and Appl. Geophys.*, 144(3–4), 409–426, doi:10.1007/BF00874375.
- Haugan, J. (2005): Dog holes and wire chutes. *Maritime Life and Traditions*, No. 29, Winter.

- Kanamori, H., and J.J. Cipar (1974): Focal process of the great Chilean earthquake, May 22, 1960. *Phys. Earth Planet. Inter.*, *9*, 128–136.
- Lander, J.F., and P.A. Lockridge (1989): United States tsunamis (including United States possessions): 1690–1988. US Department of Commerce, NOAA, NESDIS, and NGDC, Publication 41-2, 265 pp.
- López, A.M., and E.A. Okal (2006): A seismological reassessment of the source of the 1946 Aleutian “tsunami” earthquake. *Geophys. J. Int.*, *165*(3), 835–849, doi:10.1111/j.1365-246x.2006.02899.x.
- O’Brien, M.P. (1946): Preliminary Report on Seismic Sea Waves from Aleutian Earthquake of April 1, 1946, Tech. Rep. HE 116207, Wave Project, Fluid Mechanics Lab., University of California, Berkeley.
- Percival, D.B., D.W. Denbo, M.C. Eble, E. Gica, H.O. Mofjeld, M.C. Spillane, L. Tang, and V.V. Titov (2011): Extraction of tsunami source coefficients via inversion of DART® buoy data. *Nat. Hazards*, *58*(1), doi:10.1007/s11069-010-9688-1, 567–590.
- Spillane, M.C., E. Gica, V.V. Titov, and H.O. Mofjeld (2008): Tsunameter network design for the U.S. DART® arrays in the Pacific and Atlantic oceans. NOAA Tech. Memo. OAR PMEL-143, 165 pp.
- Tang, L., C. Chamberlin, E. Tolkova, M. Spillane, V.V. Titov, E.N. Bernard, and H.O. Mofjeld (2006): Assessment of potential tsunami impact for Pearl Harbor, Hawaii. NOAA Tech. Memo. OAR PMEL-131, NTIS: PB2007-100617, 36 pp.
- Tang, L., V.V. Titov, and C.D. Chamberlin (2009): Development, testing, and applications of site-specific tsunami inundation models for real-time forecasting. *J. Geophys. Res.*, *114*, C12025, doi:10.1029/2009JC005476.
- Tang, L., V.V. Titov, E. Bernard, Y. Wei, C. Chamberlin, J.C. Newman, H. Mofjeld, D. Arcas, M. Eble, C. Moore, B. Uslu, C. Pells, M.C. Spillane, L.M. Wright, and E. Gica (2012): Direct energy estimation of the 2011 Japan tsunami using deep-ocean pressure measurements. *J. Geophys. Res.*, *117*, C08008, doi:10.1029/2011JC007635.
- Titov, V., and F.I. González (1997): Implementation and testing of the Method of Splitting Tsunami (MOST) model. NOAA Tech. Memo. ERL PMEL-112, NTIS: PB98-122773, NOAA/Pacific Marine Environmental Laboratory, Seattle, WA, 11 pp.
- Titov, V.V., and C.E. Synolakis (1998): Numerical modeling of tidal wave runup. *J. Waterw. Port Coast. Ocean Eng.*, *124*(4), 157–171.

- Titov, V.V., F.I. González, E.N. Bernard, M.C. Eble, H.O. Mofjeld, J.C. Newman, and A.J. Venturato (2005): Real-time tsunami forecasting: Challenges and solutions. *Nat. Hazards*, 35(1) Special Issue, U.S. National Tsunami Hazard Mitigation Program, 41–58.
- Titov, V.V., C. Moore, D.J.M. Greenslade, C. Pattiaratchi, R. Badal, C.E. Synolakis, and U. Kânoğlu (2011): A new tool for inundation modeling: Community Modeling Interface for Tsunamis (ComMIT). *Pure Appl. Geophys.*, 168(11), 2121–2131, doi:10.1007/s00024-011-0292-4.
- U.S. Secretary of War (1914): Harbor of Refuge at Point Arena, or Elsewhere on the Pacific Coast, Between San Francisco and Humboldt Bay, California. Report to 63rd Congress, House of Representatives, Washington D.C., Document No. 1369, 39 pp.
- Wei, Y., E. Bernard, L. Tang, R. Weiss, V. Titov, C. Moore, M. Spillane, M. Hopkins, and U. Kânoğlu (2008): Real-time experimental forecast of the Peruvian tsunami of August 2007 for U.S. coastlines. *Geophys. Res. Lett.*, 35, L04609, doi:10.1029/2007GL032250.

FIGURES



Figure 1: The Point Arena area of southern Mendocino County, California. Arena Cove is indicated by the red arrow.

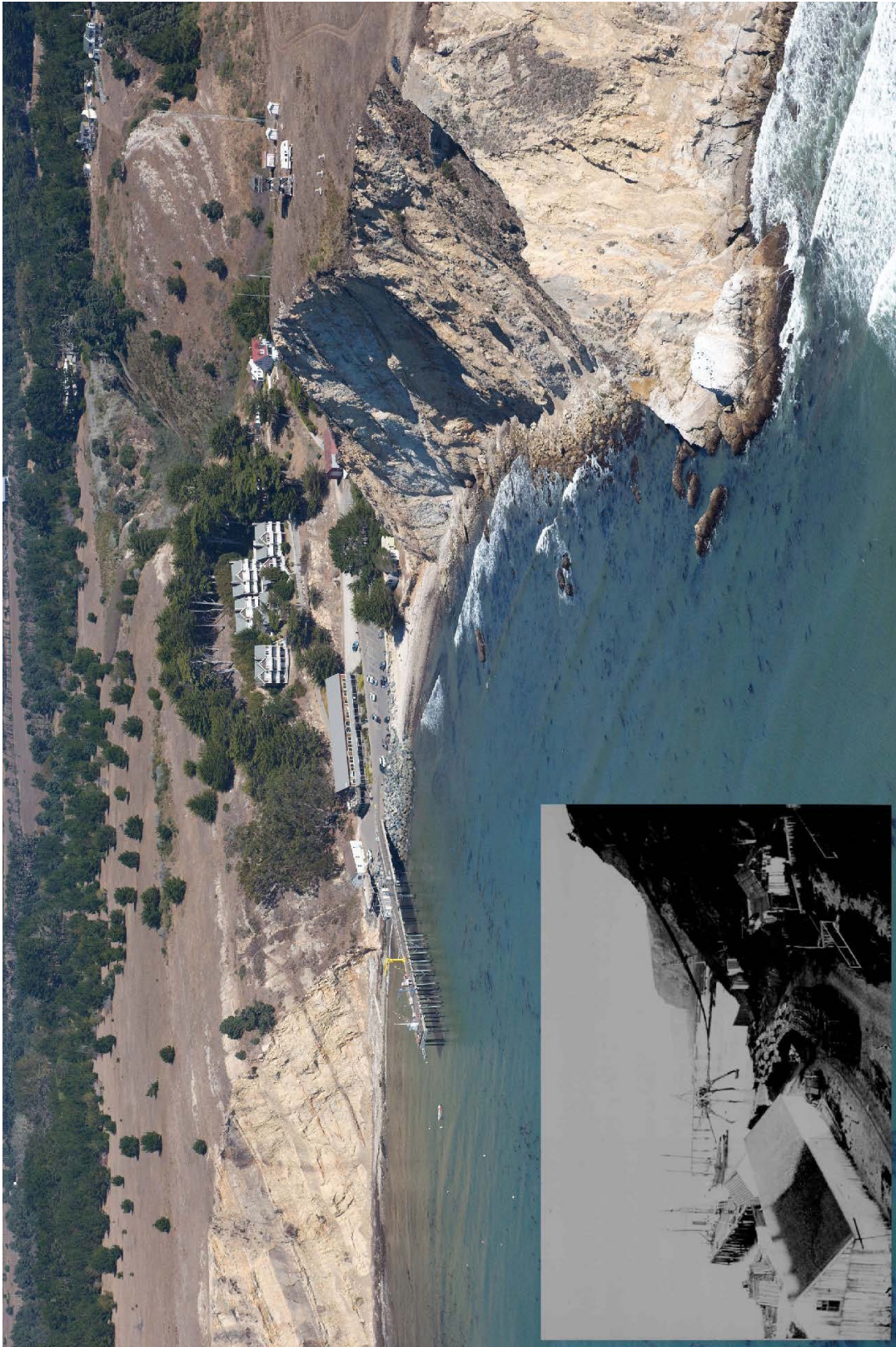


Figure 2: Views of present-day Arena Cove, California (Photographer: Kenneth Adelman) and its appearance in the early 1900s (inset).

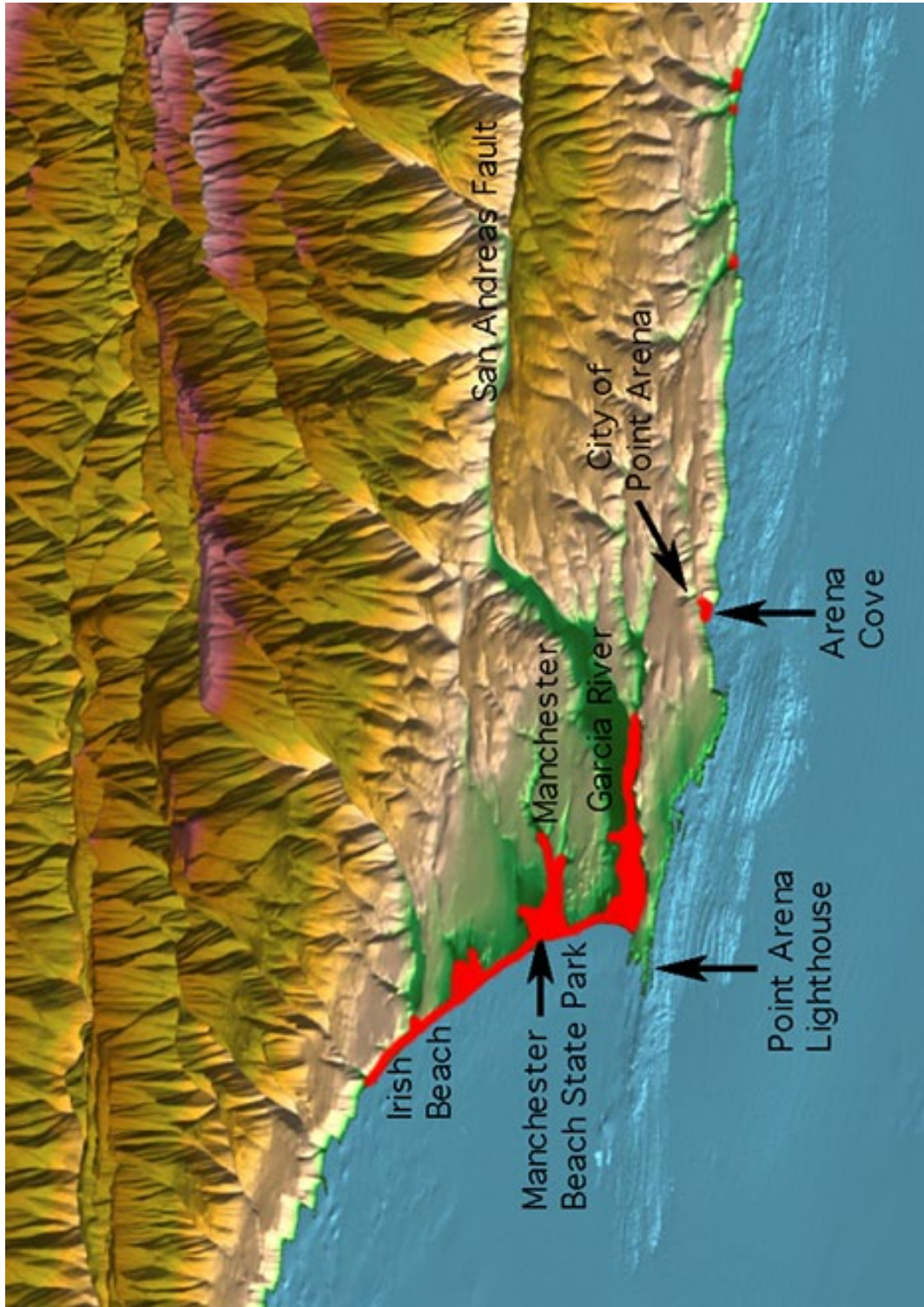


Figure 3: Extract from the oblique 3-D view of the Arena Cove digital elevation model provided by NGDC; sites of potential inundation identified by CalEMA are highlighted in red.

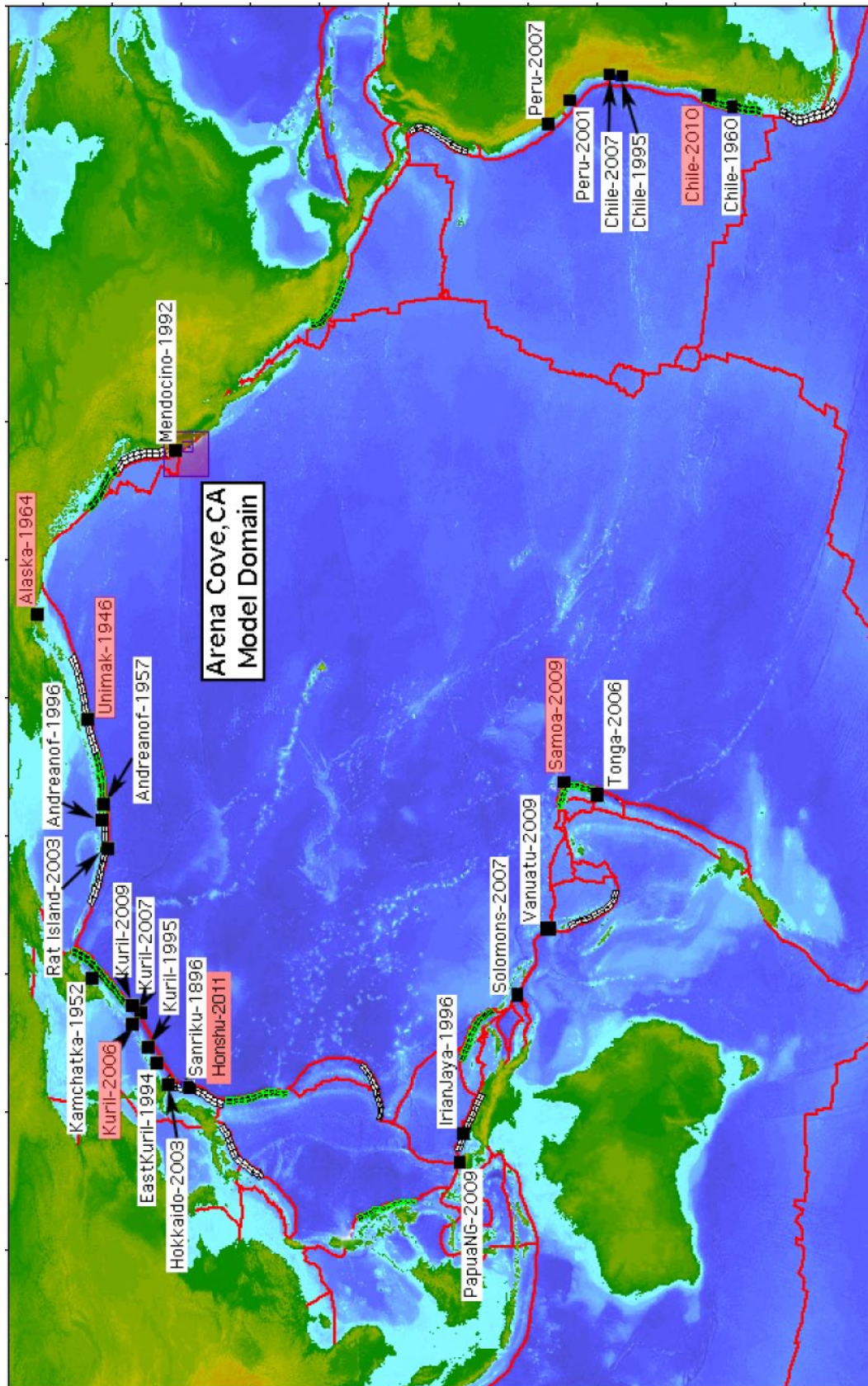


Figure 4: Distribution of the historical tsunami sources employed for the development of the Arena Cove forecast model. Those highlighted in red are more extensively investigated using the reference model.

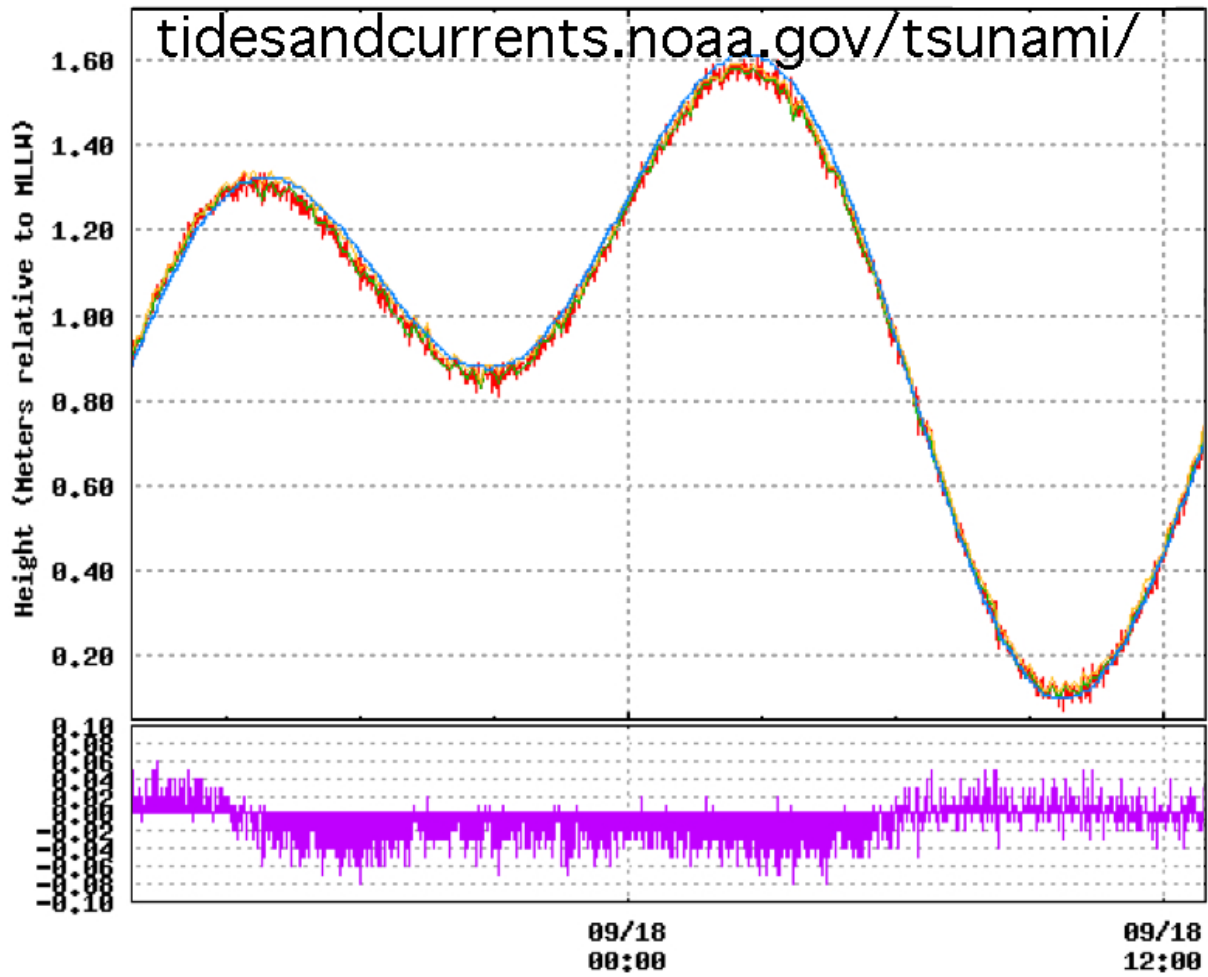


Figure 5: A sample time interval from the tsunami-capable tide gauge at Arena Cove, California, unrelated to tsunami activity.

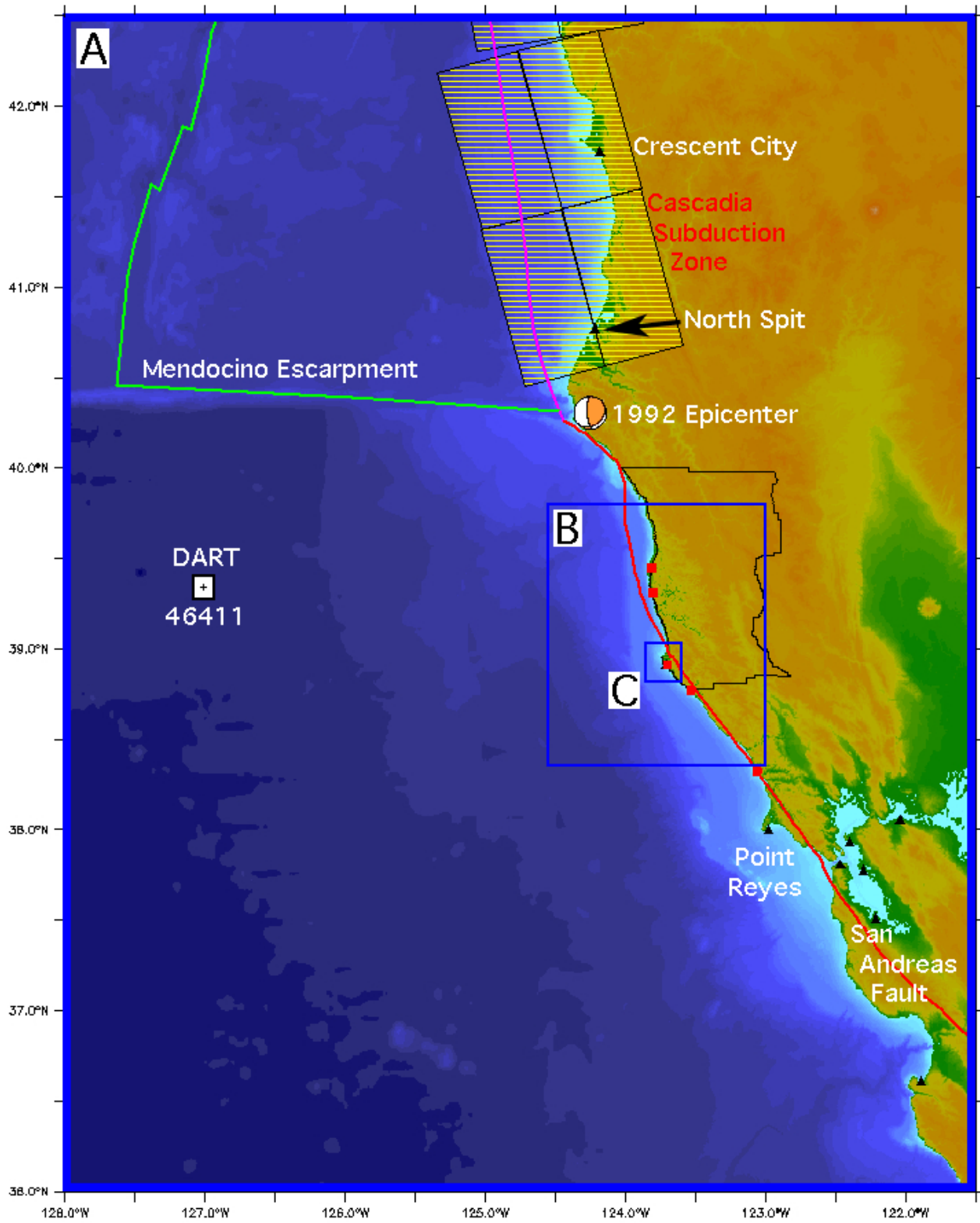


Figure 6: The setting of the Arena Cove model. Rectangles indicate the extents of the nested grids; communities within the model domain are marked in red. Tide gauge locations are drawn as black triangles; 46411 is the closest DART. Plate boundaries are shown, as are the southernmost unit sources representing Cascadia.

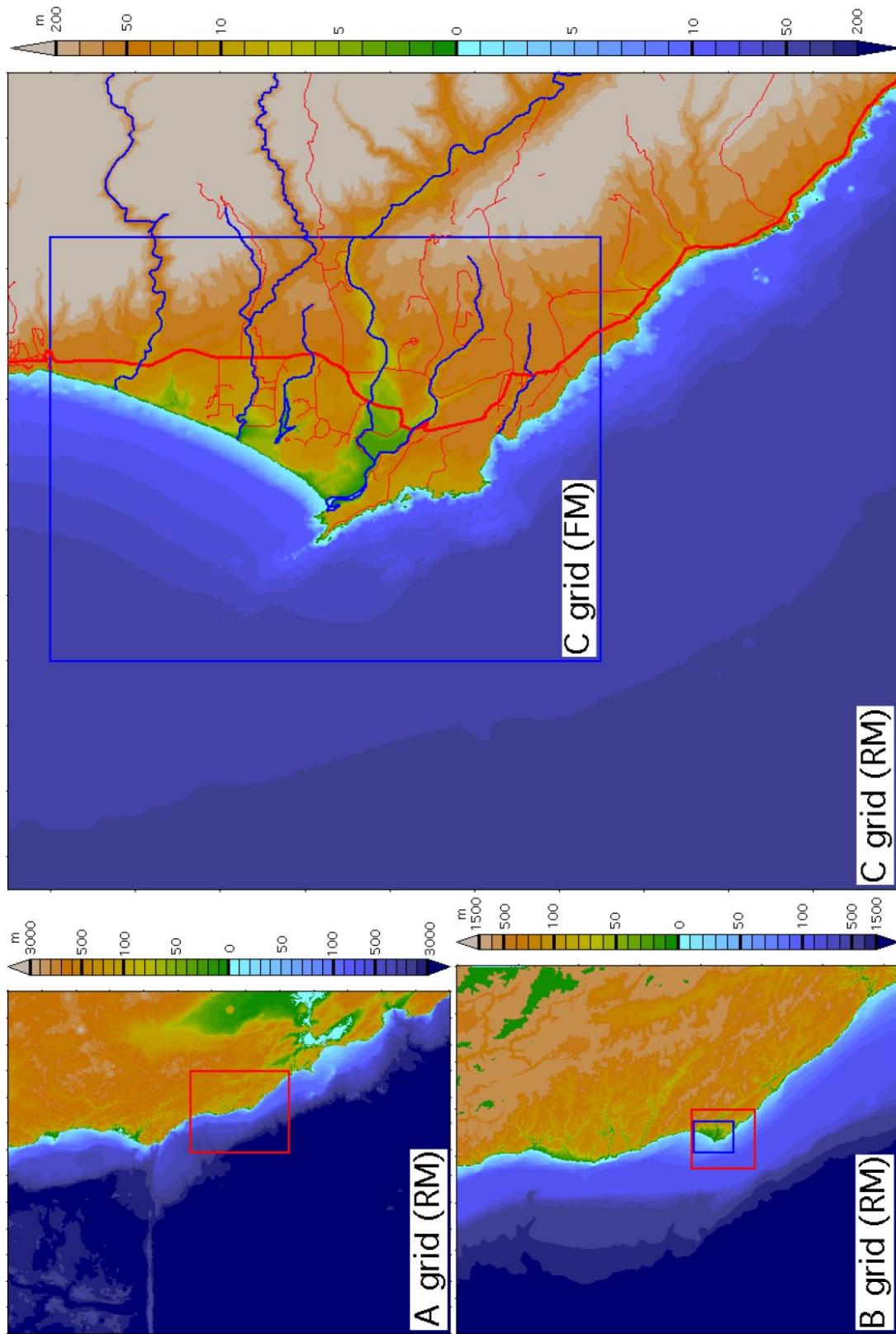


Figure 7. Nested grid representation for the Arena Cove, California, reference model (RM). Rectangles, drawn in red, indicate the placement of the next nesting level. Blue rectangles delineate the forecast model (FM) grid boundaries. Rivers and roads are marked in the C grid panel.

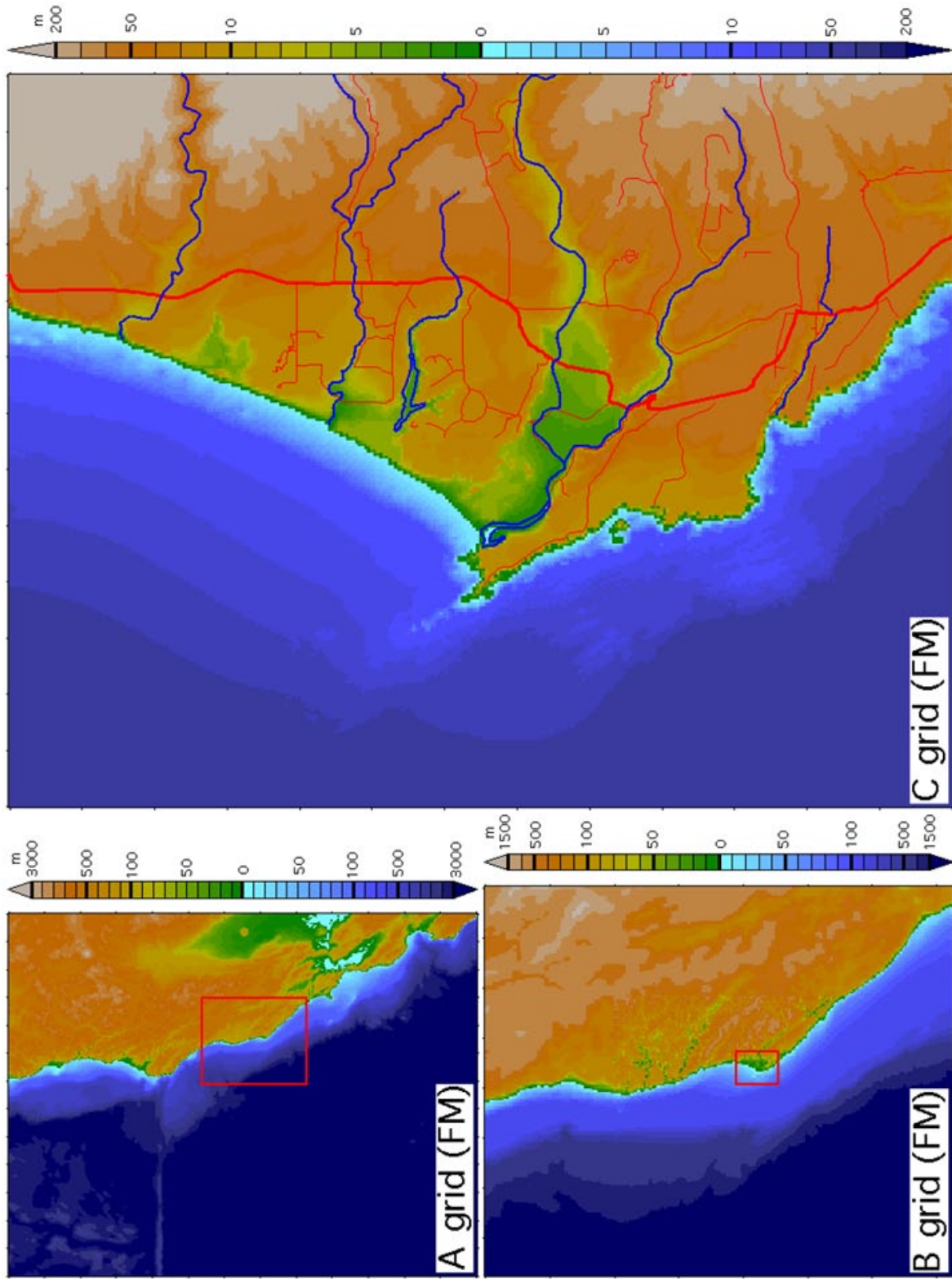


Figure 8: Nested grid representation for the Arena Cove, California, forecast model (FM). Rectangles are drawn to indicate the placement of the next nesting level. Rivers and roads are marked in the C grid panel

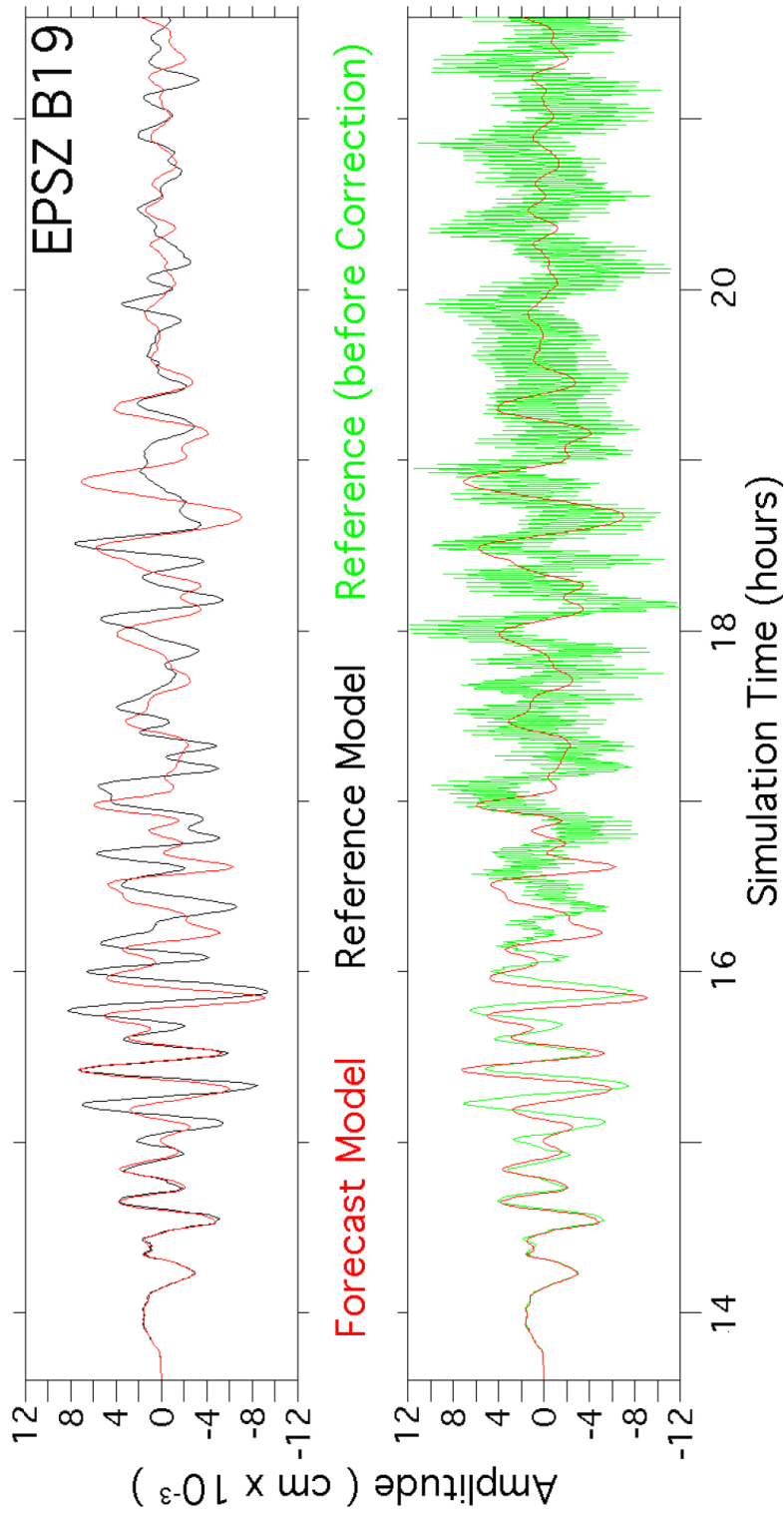


Figure 9: Comparison of the reference and forecast model time series at the warning point for micro-tsunami scenario EPSZ B19. Upper panel: Illustration of the close agreement between the reference (black) and forecast (red) model responses. Lower panel: The signature of model instability in the reference model (green) prior to finalization of its bathymetry.

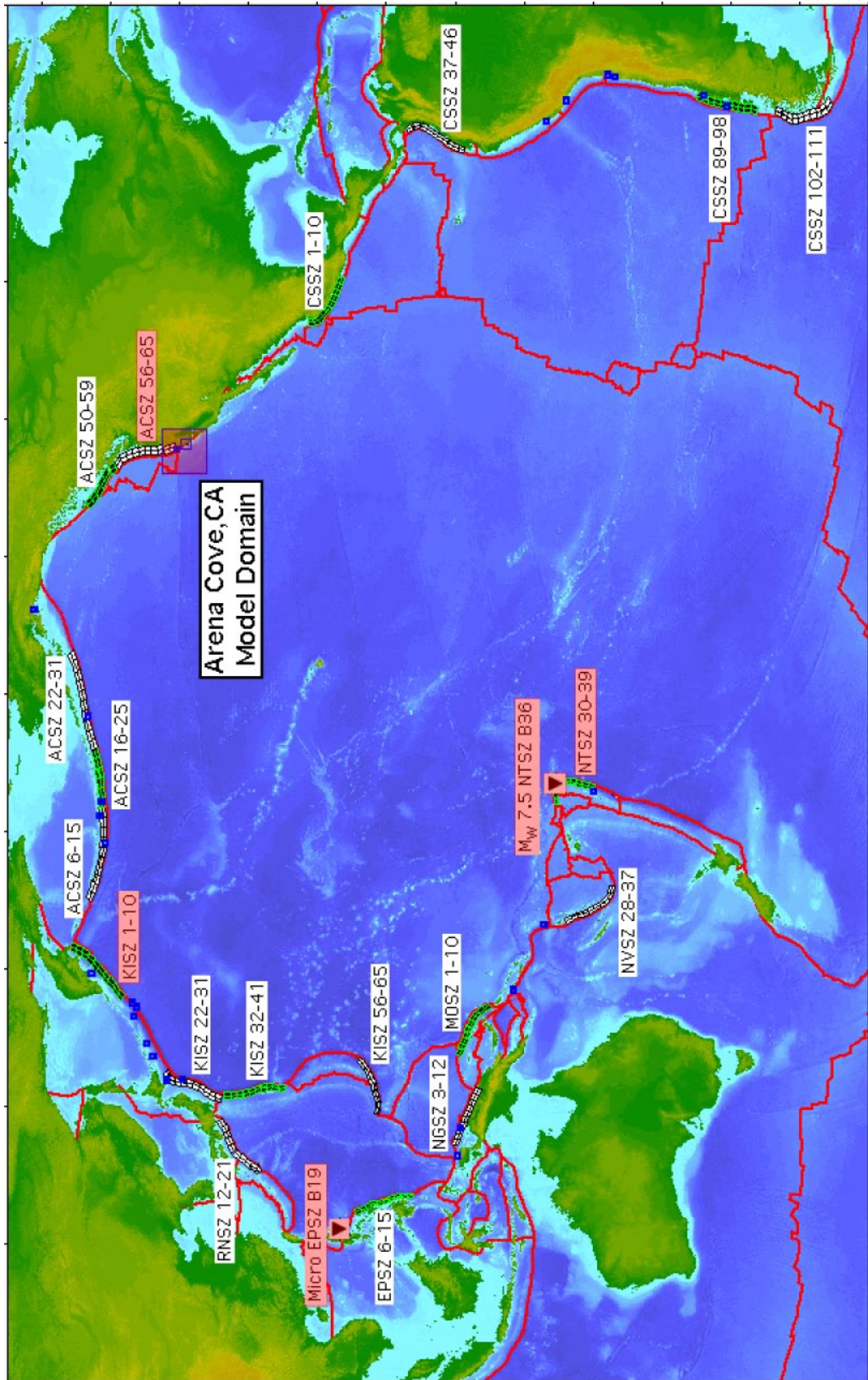


Figure 10: Locations of synthetic tsunami scenarios employed in the development of the Arena Cove model. Those highlighted in red are more extensively investigated in this report.

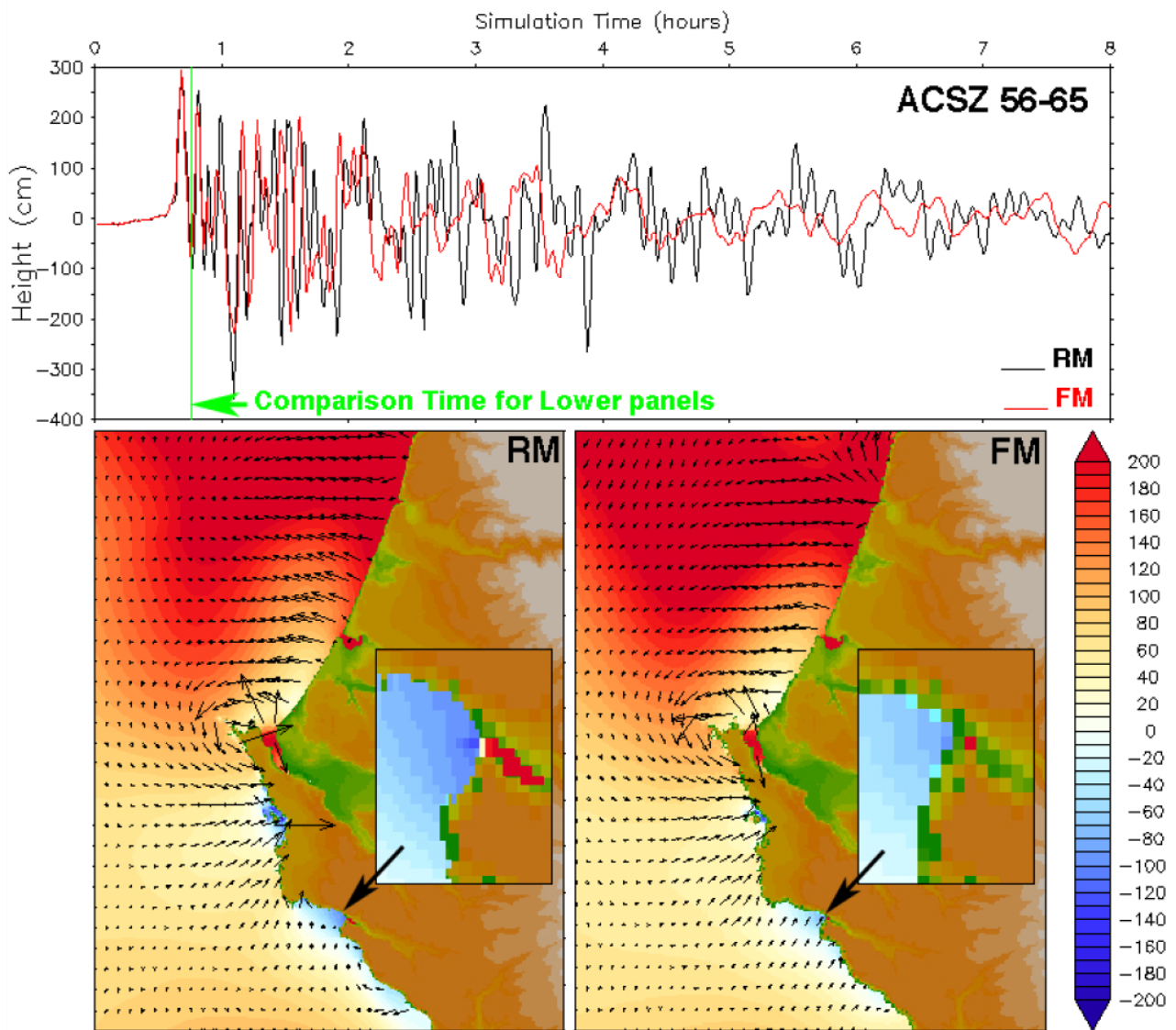


Figure 11: Comparison of reference and forecast model results for the synthetic ACSZ 56–65 mega-tsunami event representing the Cascadia Subduction Zone. Time series at the tide gauge location in Arena Cove are shown in the upper panel. The lower panels contrast the reference (RM) and forecast (FM) model amplitude and velocity fields at the time indicated in the upper panel. Insets are enlargements of Arena Cove, left pixelated to reflect the discrete grid resolution.

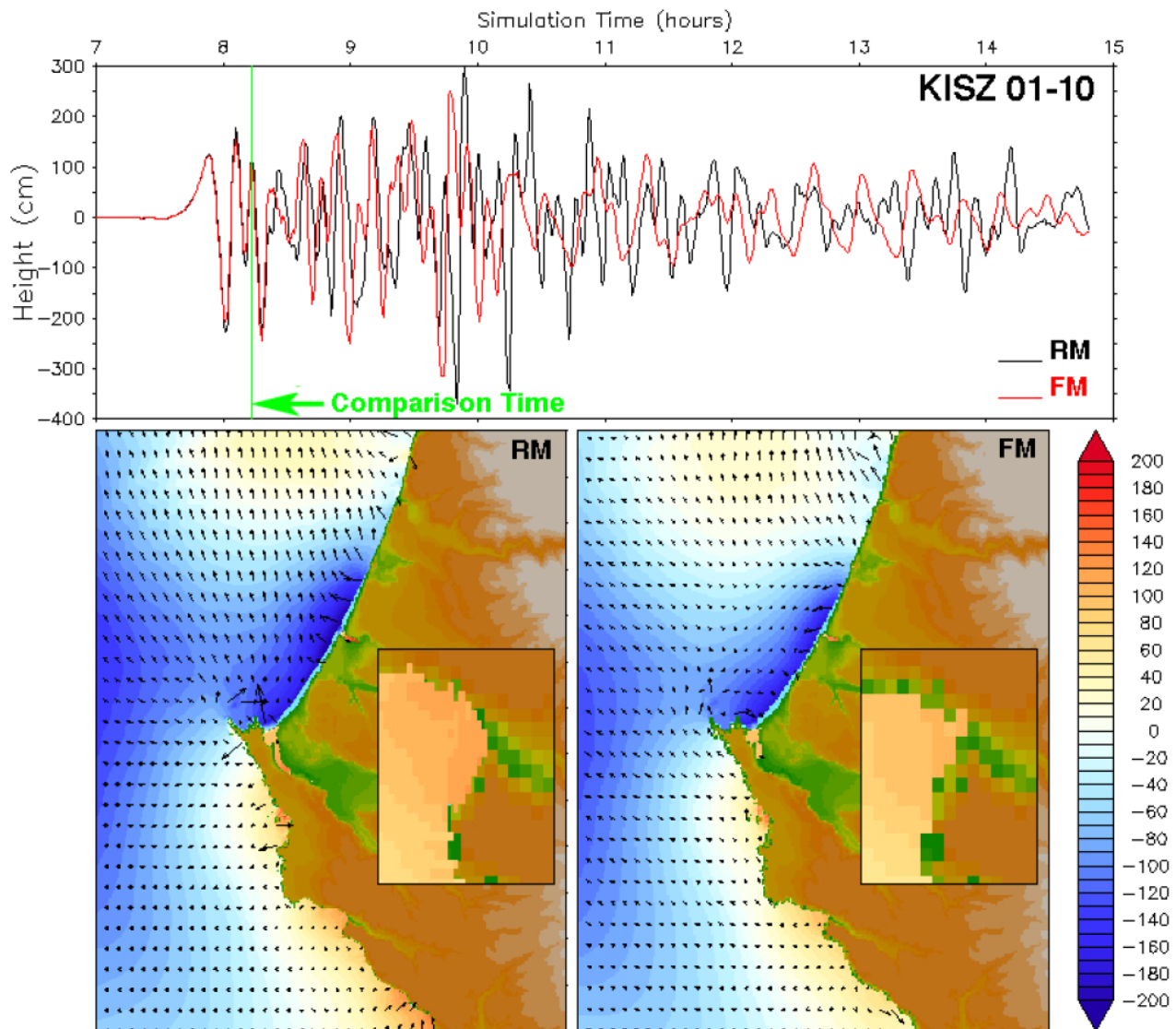


Figure 12: Comparison of reference and forecast model results for the synthetic KISZ 01–10 mega-tsunami event representing Kamchatka. Time series at the tide gauge location in Arena Cove are shown in the upper panel. The lower panels contrast the reference (RM) and forecast (FM) model amplitude and velocity fields at the time indicated in the upper panel. Insets are enlargements of Arena Cove, left pixelated to reflect the discrete grid resolution.

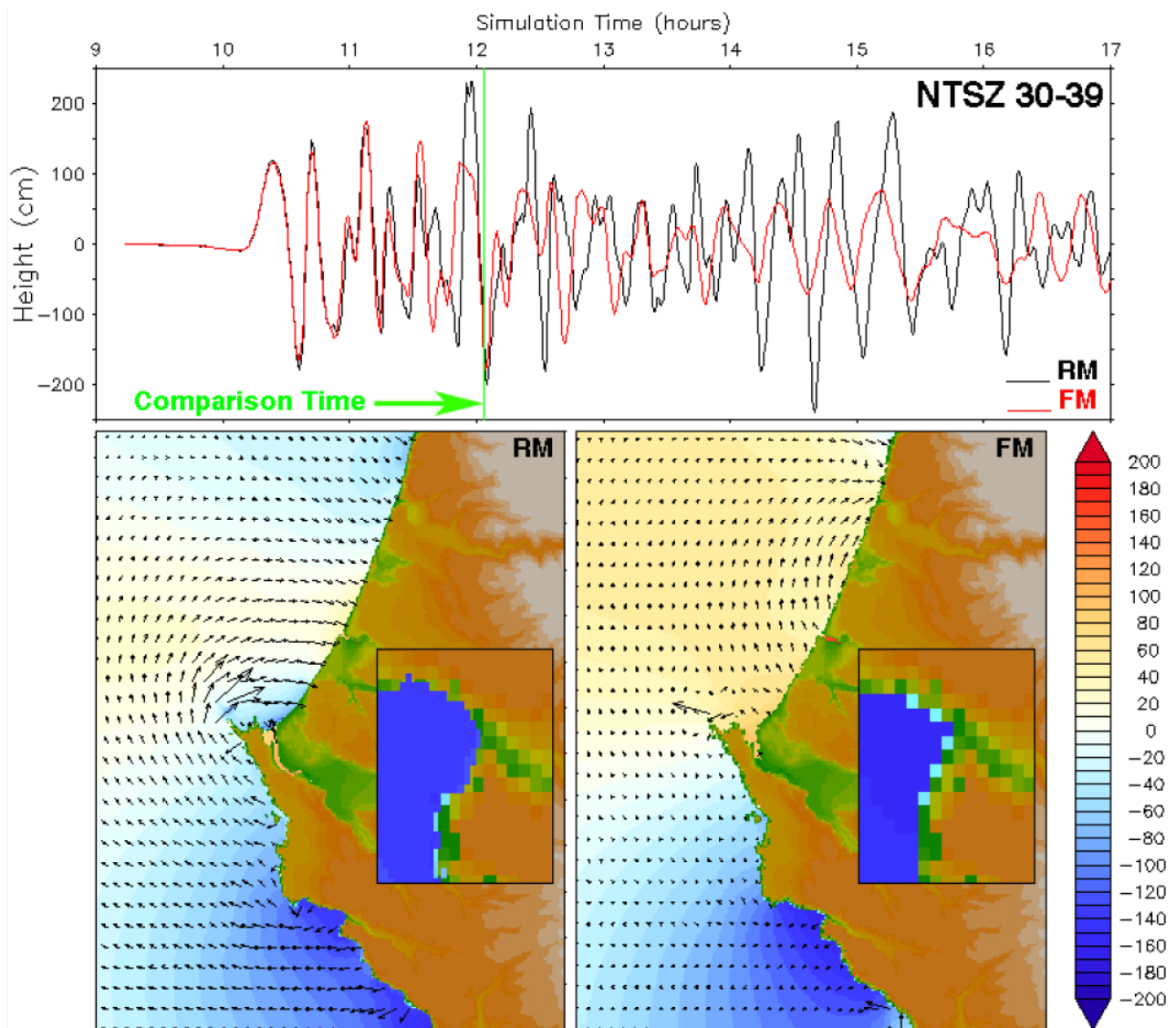


Figure 13: Comparison of reference and forecast model results for the synthetic NTSZ 30–39 mega-tsunami event representing Samoa. Time series at the tide gauge location in Arena Cove are shown in the upper panel. The lower panels contrast the reference (RM) and forecast (FM) model amplitude and velocity fields at the time indicated in the upper panel. Insets are enlargements of Arena Cove, left pixilated to reflect the discrete grid resolution.

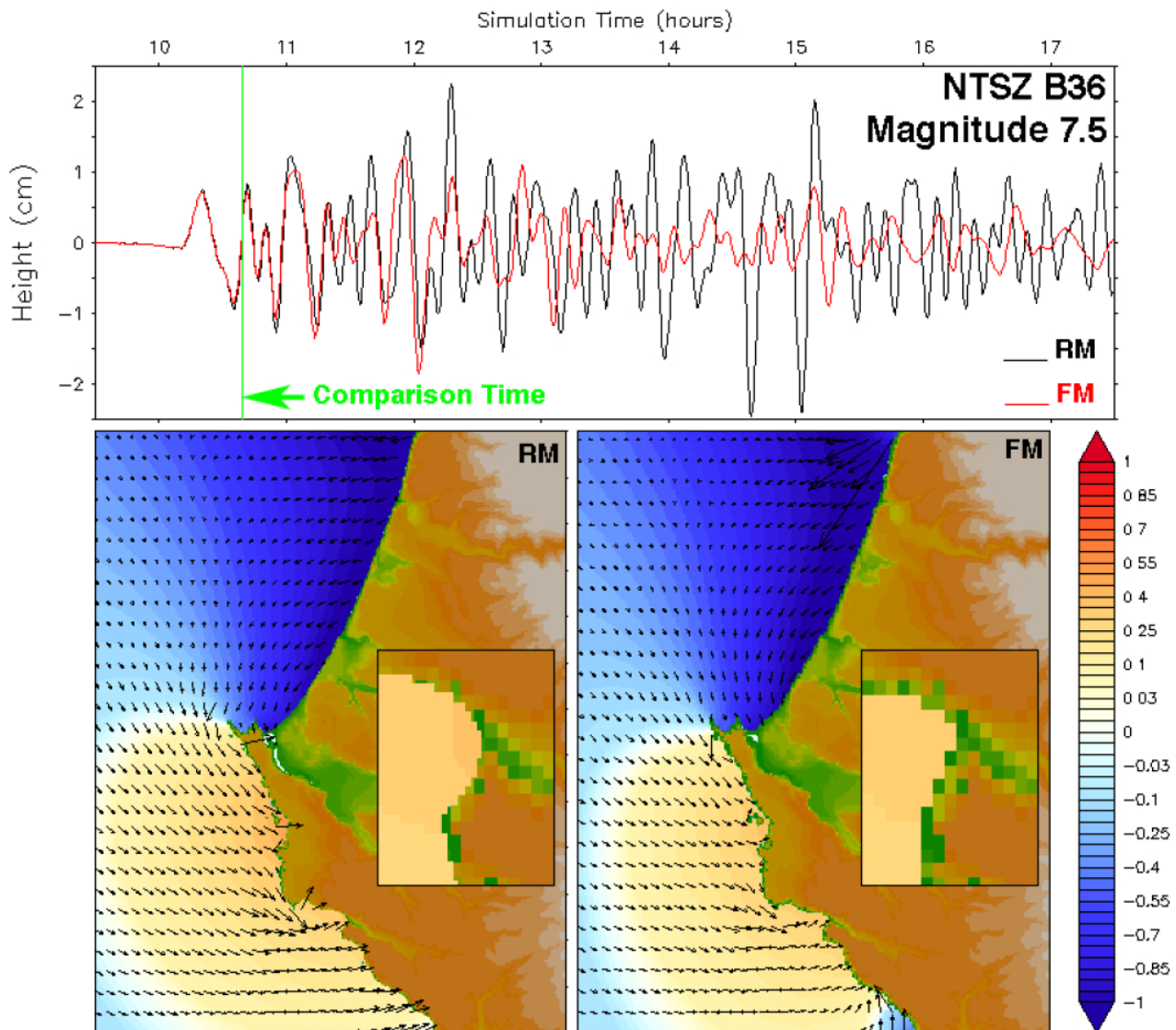


Figure 14: Comparison of reference and forecast model results for the synthetic moderate event at NTSZ B36 near Samoa. Time series at the tide gauge location in Arena Cove are shown in the upper panel. The lower panels contrast the reference (RM) and forecast (FM) model amplitude and velocity fields at the time indicated in the upper panel. Insets are enlargements of Arena Cove, left pixelated to reflect the discrete grid resolution.

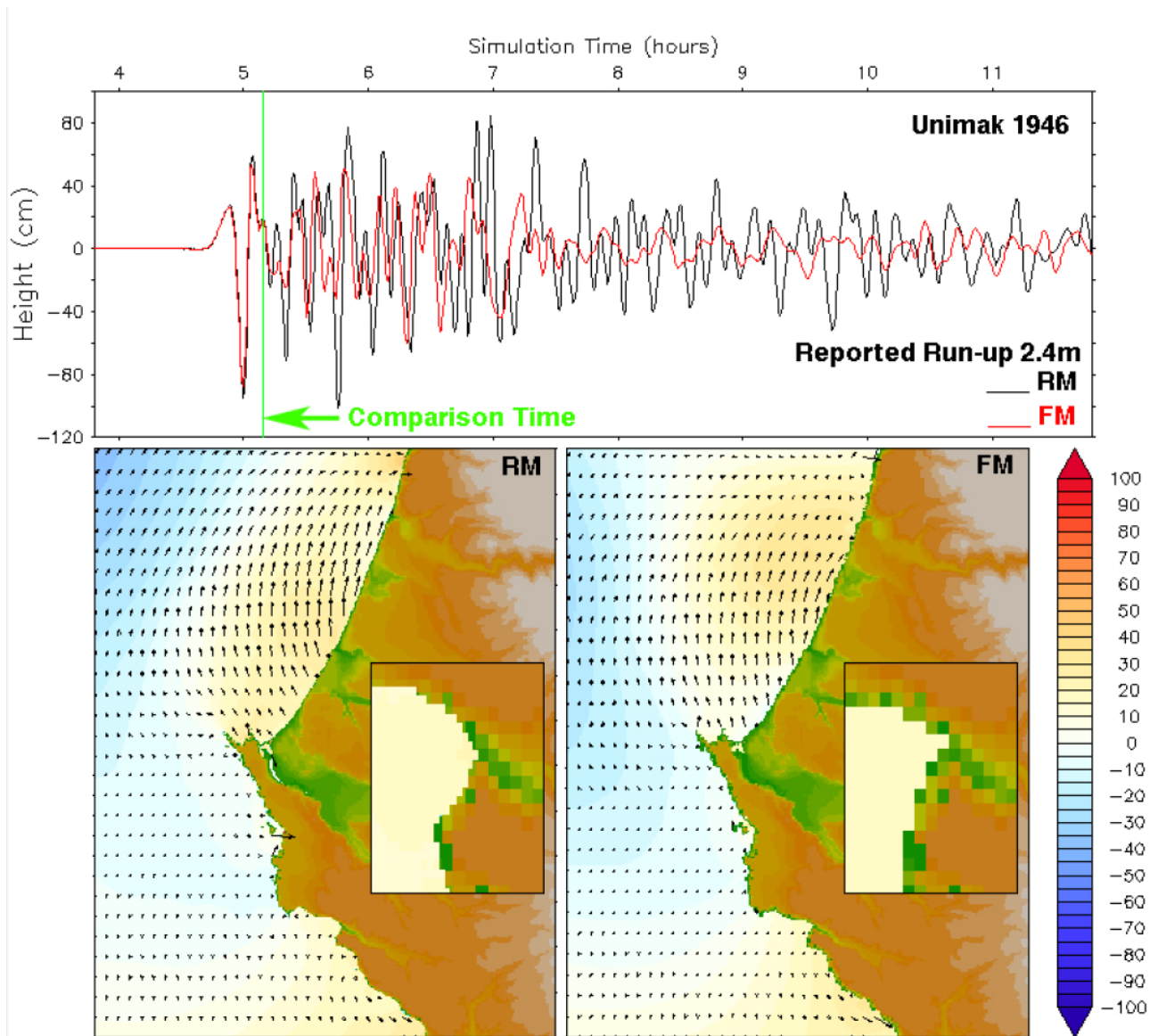


Figure 15: Comparison of reference (RM) and forecast (FM) model results for the historical 1946 Unimak tsunami (prior to tide gauge installation).

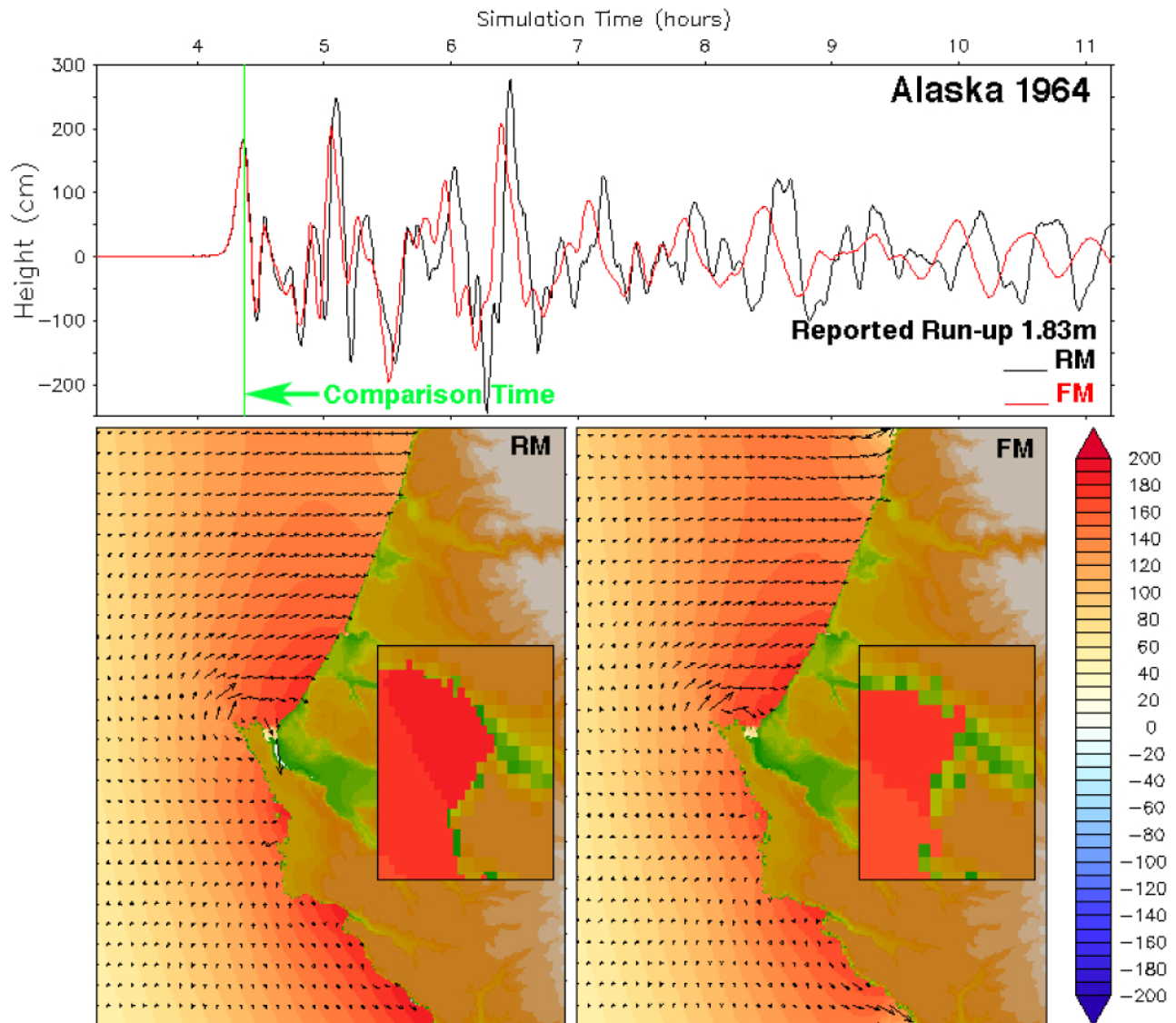


Figure 16: Comparison of reference (RM) and forecast (FM) model response for the historical 1964 Alaska tsunami (prior to tide gauge installation).

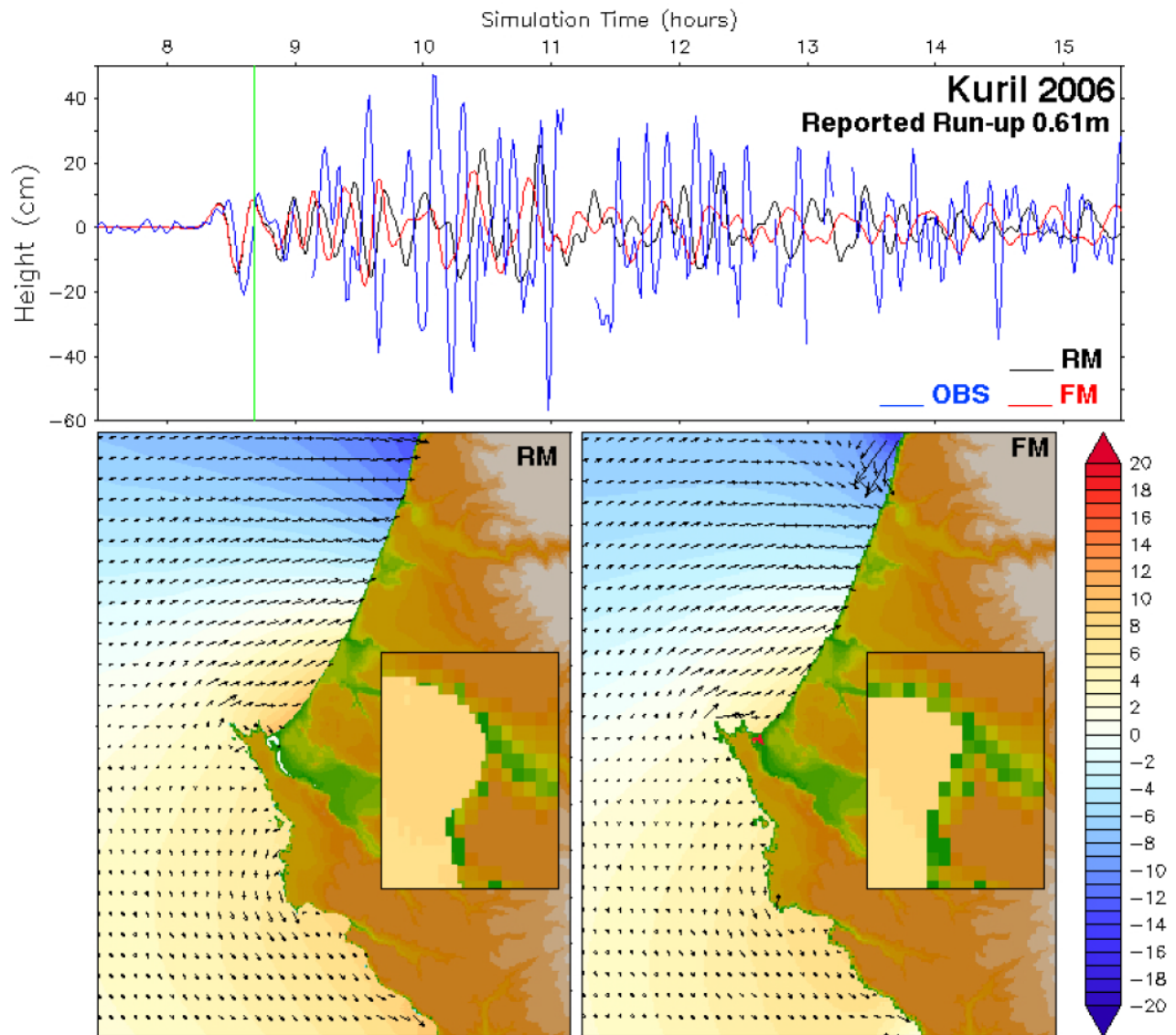


Figure 17: Comparison of reference (RM) and forecast (FM) model results for the 2006 Kuril event with sea level fluctuations, observed by the tsunami-capable Arena Cove tide gauge.

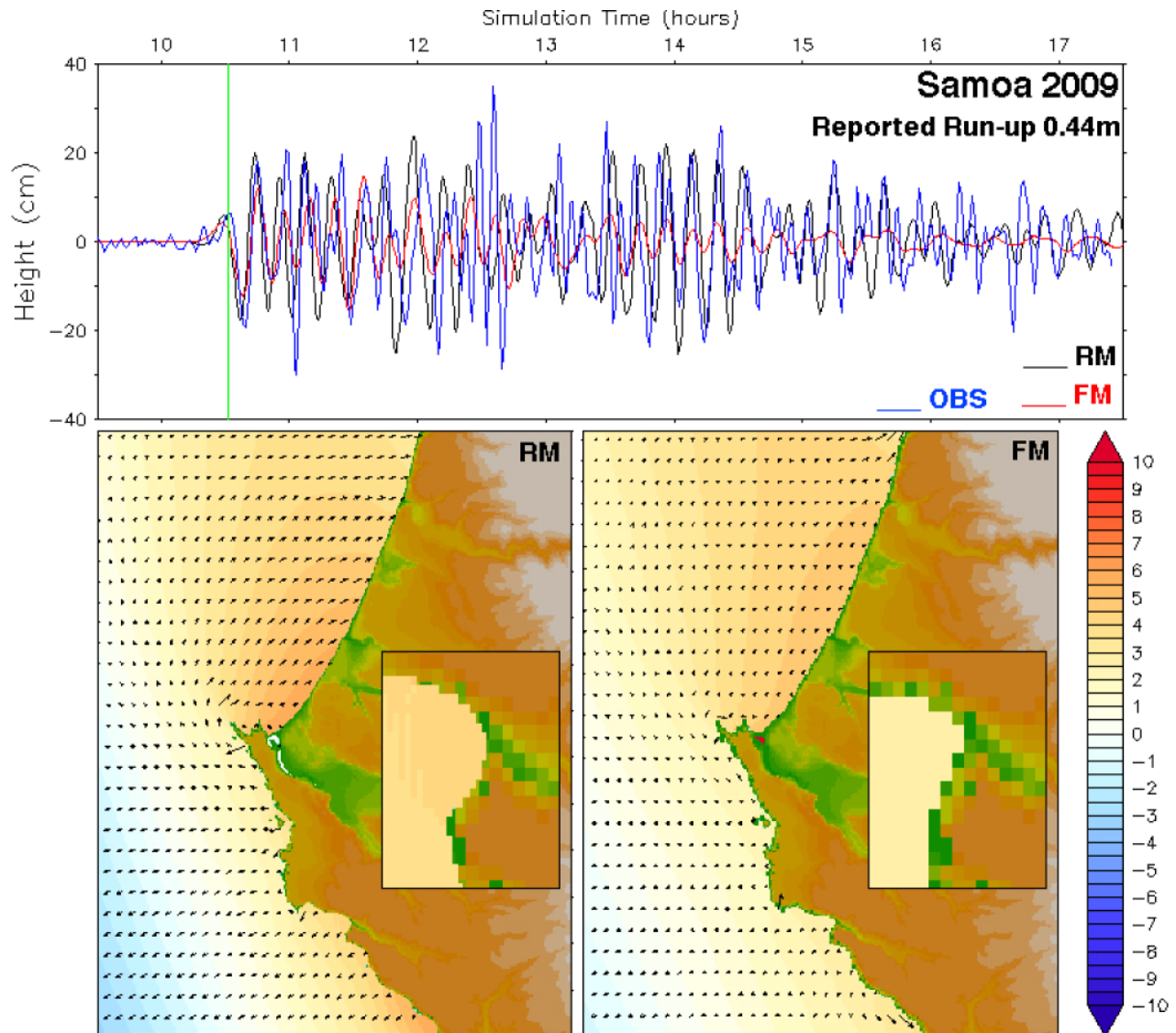


Figure 18: Comparison of reference (RM) and forecast (FM) model hindcasts of the 2009 Samoa event with sea level fluctuations in Arena Cove.

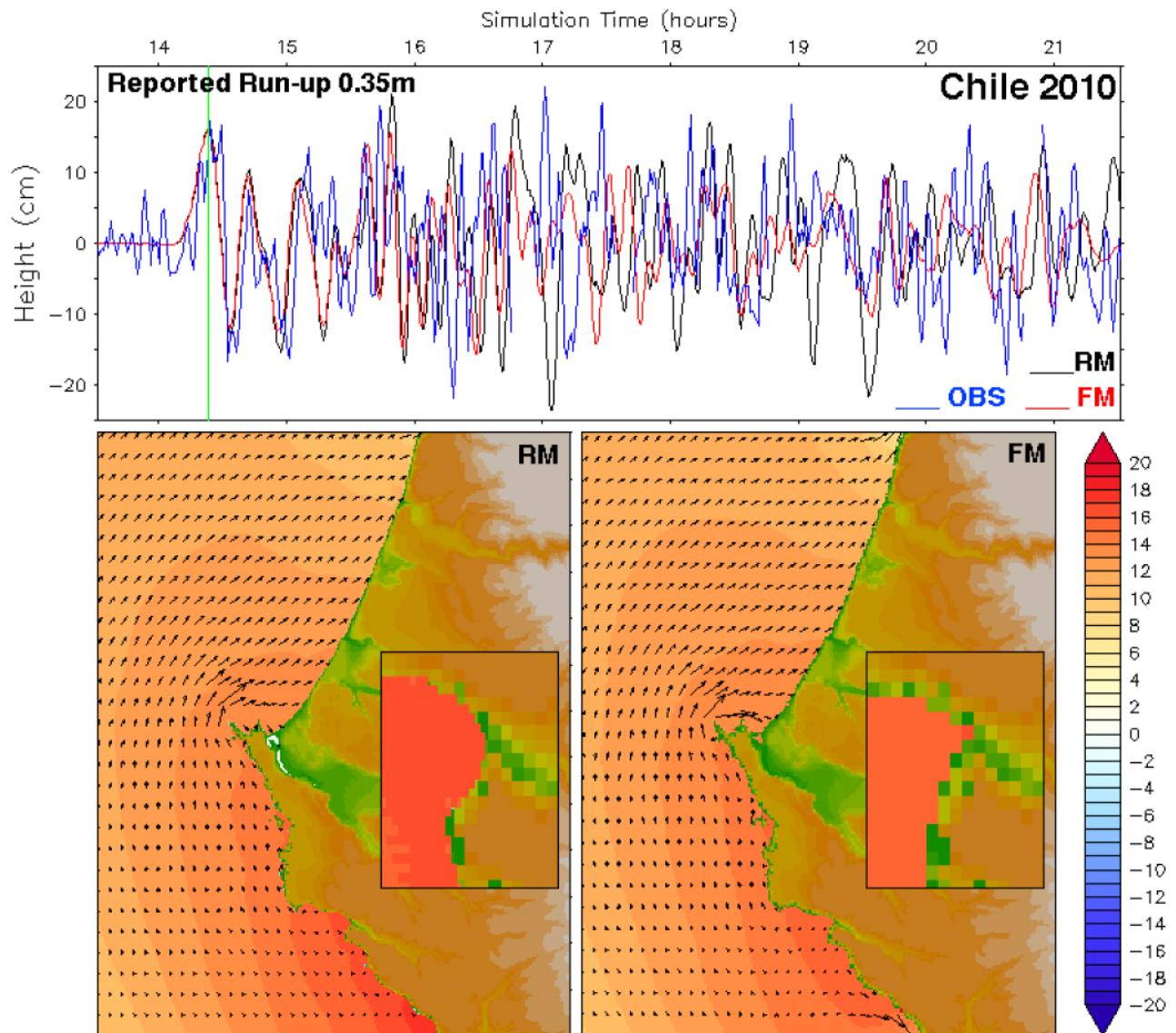


Figure 19: Comparison of reference (RM) and forecast (FM) model hindcasts of the 2010 Chile event with sea level fluctuations in Arena Cove.

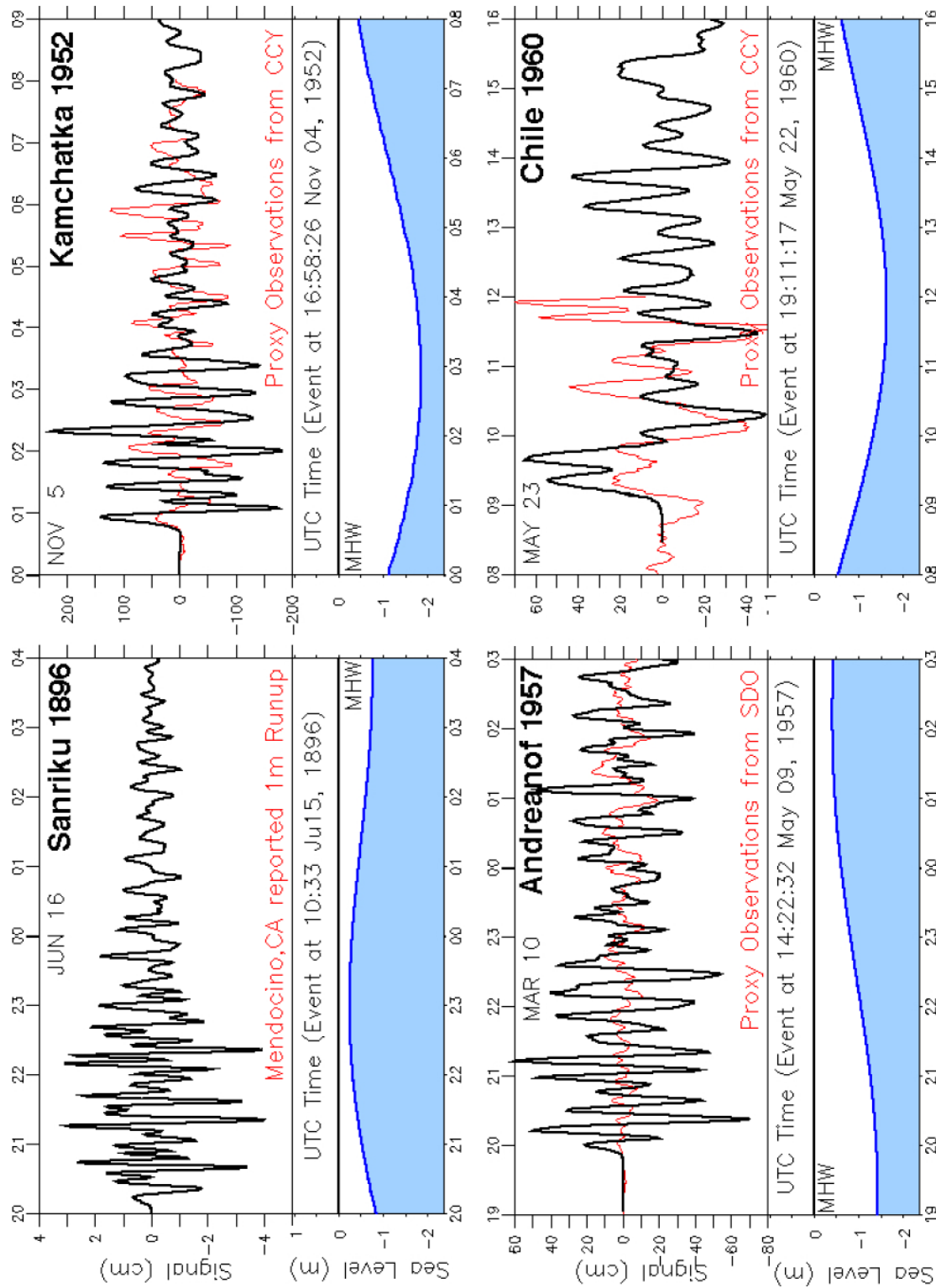


Figure 20: Simulated model response to the historical 1896 Sanriku, 1952 Kamchatka, 1957 Andreeanof, and 1960 Chile events. Proxy observations (in red) are provided, where available, from other California locations. The 1896 Sanriku result is not expected to match the observed runup at nearby Mendocino. The state of the tide is shown, and times are given as UTC.

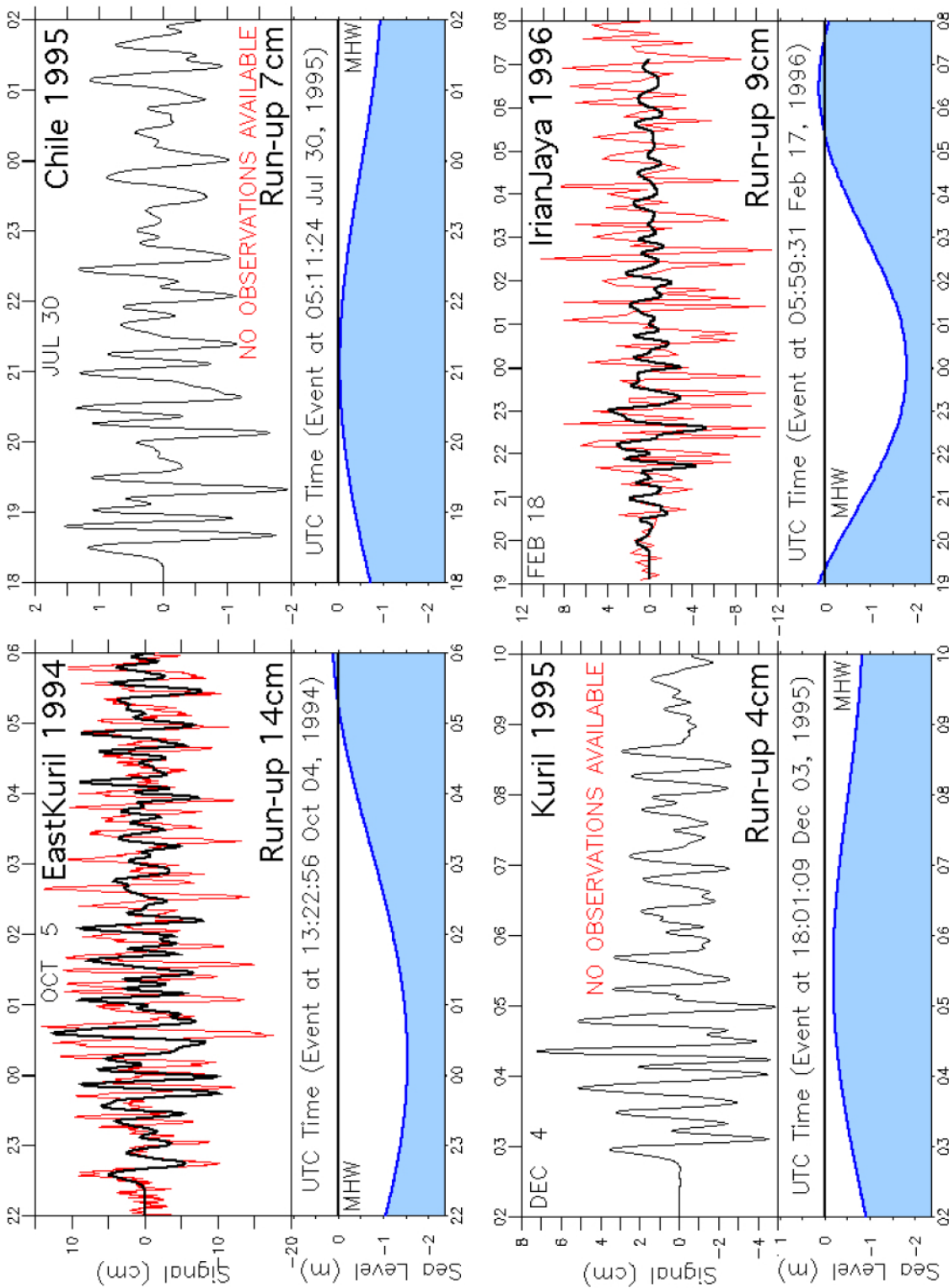


Figure 21: Forecast model response to the 1994 East Kuril, 1995 Chile, and 1996 Irian Jaya events. Tide gauge data (in red), where available, are from Arena Cove.

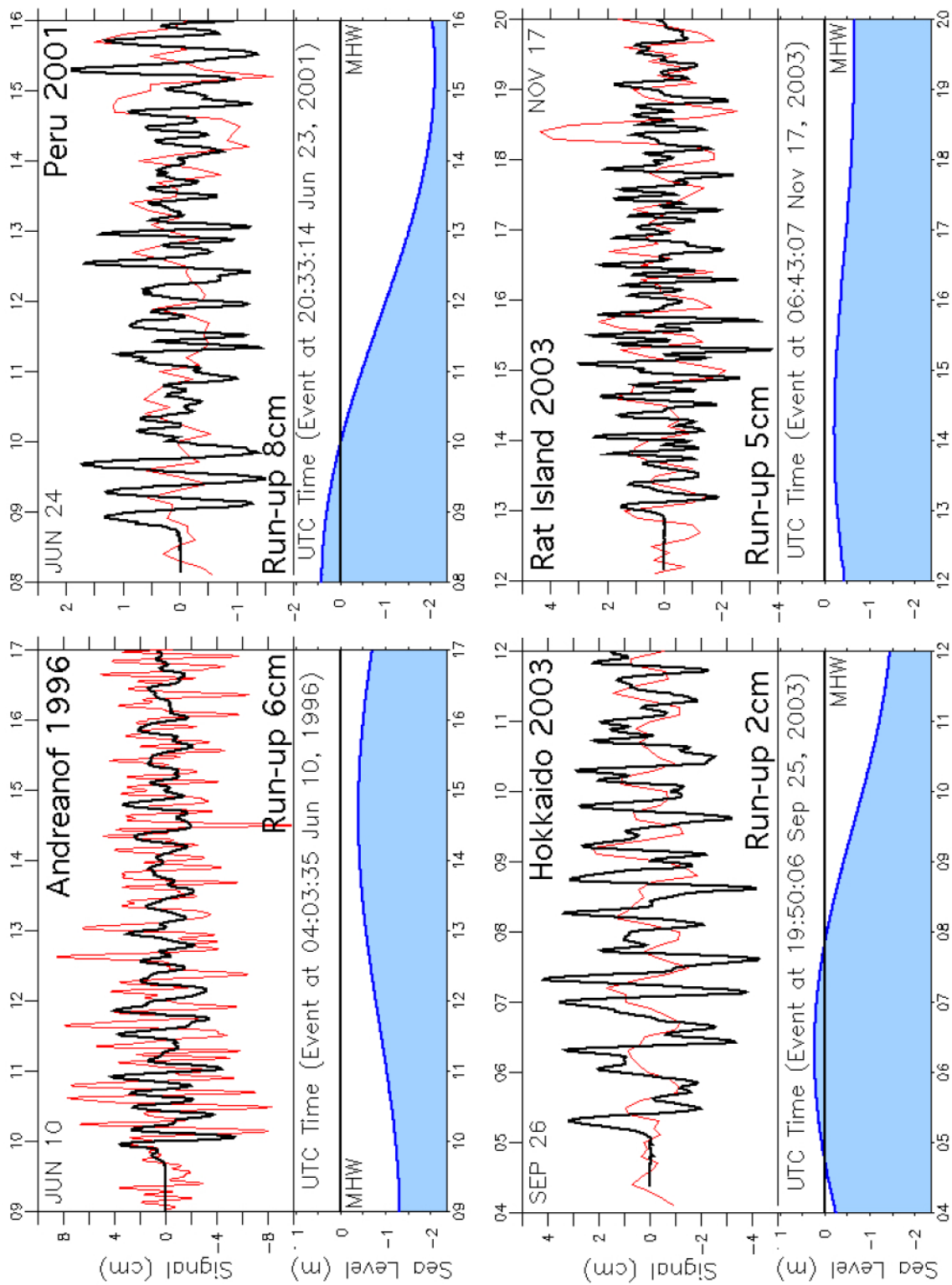


Figure 22: Forecast model response to the 1996 Andeanof, 2001 Peru, 2003 Hokkaido, and 2003 Rat Island events. Tide gauge data (in red) are from Arena Cove.

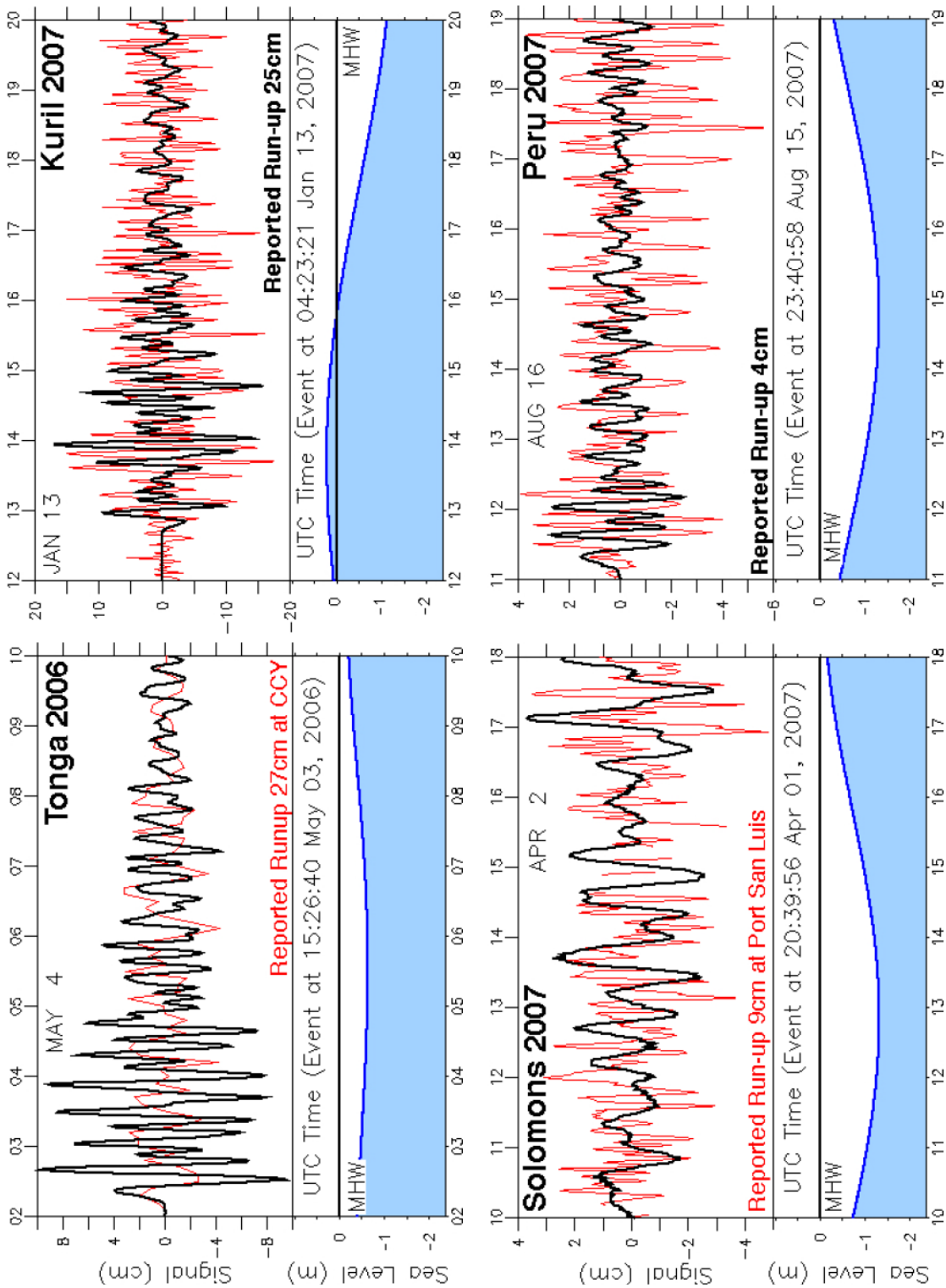


Figure 23: Forecast model response to the 2006 Tonga, 2007 Kuril, 2007 Solomons, and 2007 Peru events. Tide gauge data (in red) are from Arena Cove.

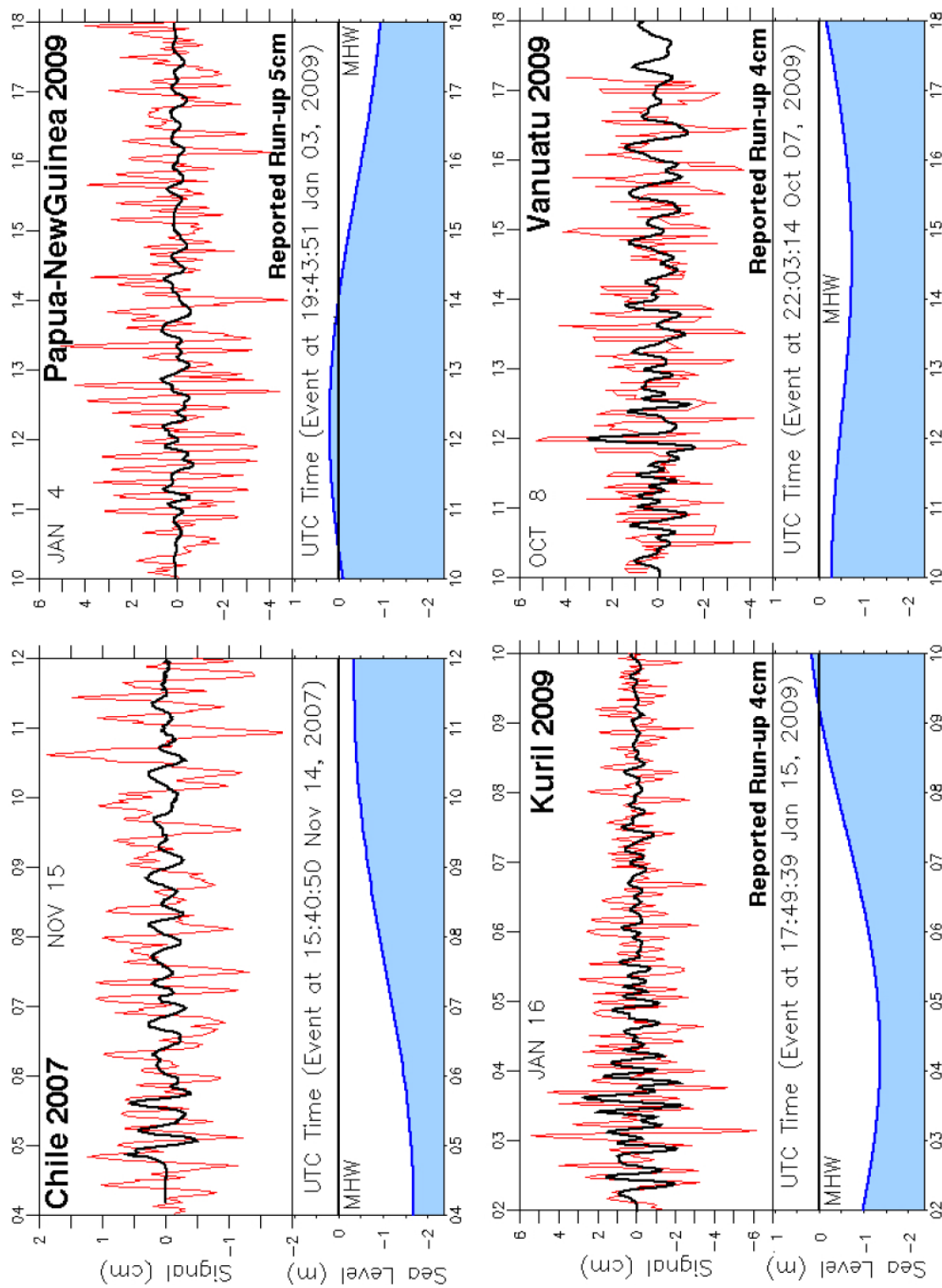


Figure 24: Forecast model response to the 2007 Chile, 2009 Papua New Guinea, 2009 Kuril, and 2009 Vanuatu events. Tide gauge data (in red) are from Arena Cove.

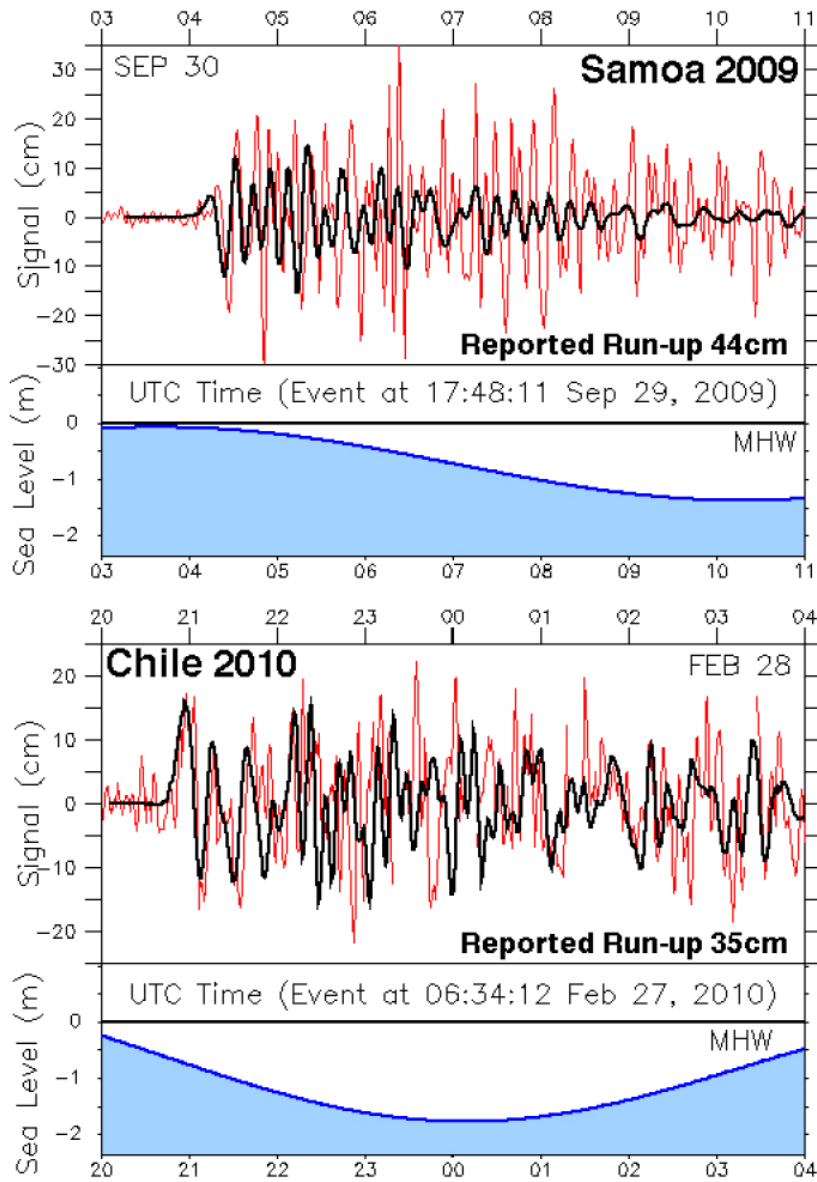


Figure 25: Forecast model response to the 2009 Samoa and 2010 Chile events. Tide gauge data (in red) are from Arena Cove.

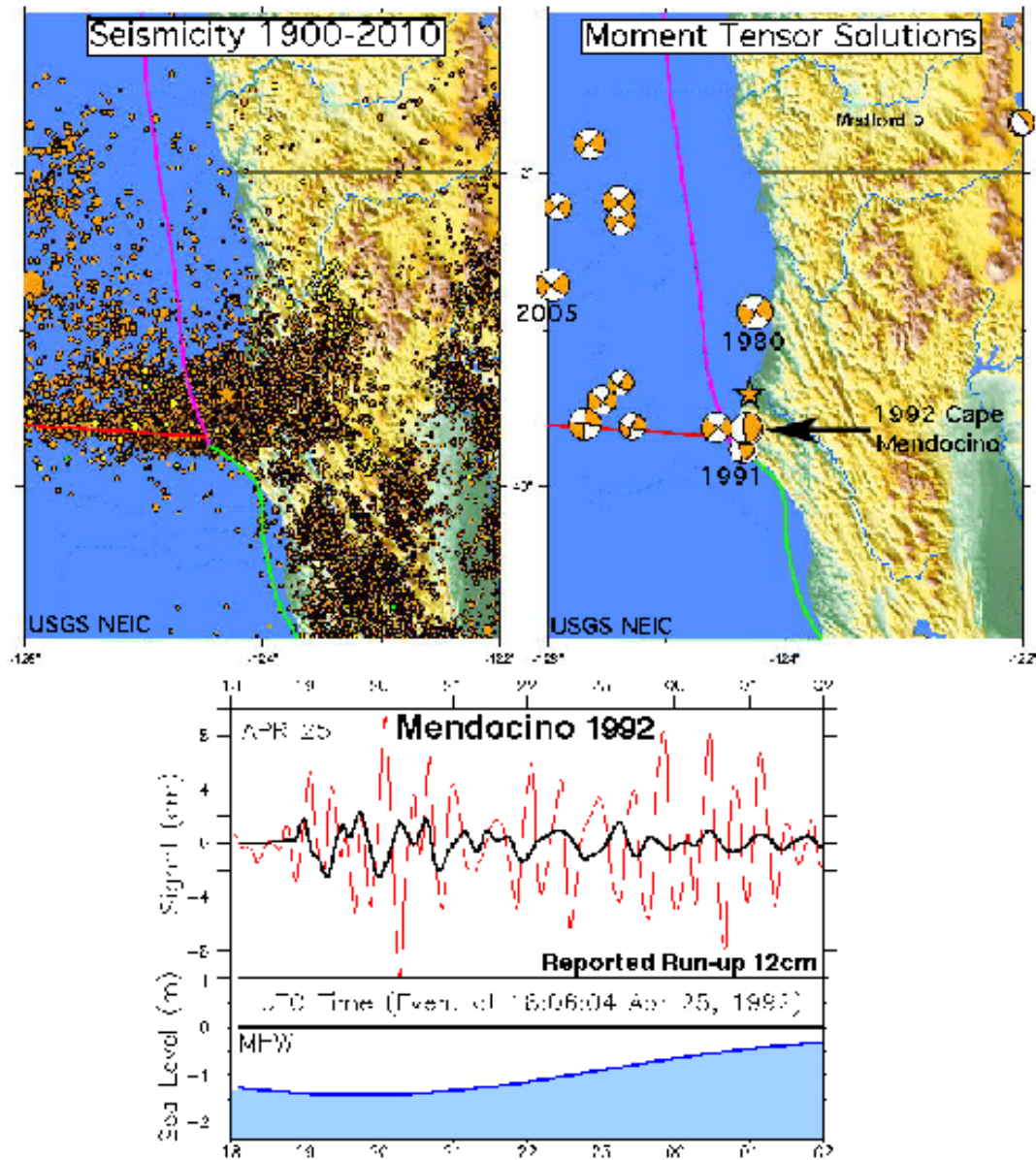


Figure 26: Seismicity in the vicinity of Cape Mendocino and the source mechanisms of recent earthquakes, adapted from USGS/NEIC products. The lower panel shows the poor agreement between the model and Arena Cove tide gauge observations that is likely due to inadequate source representation in the model.

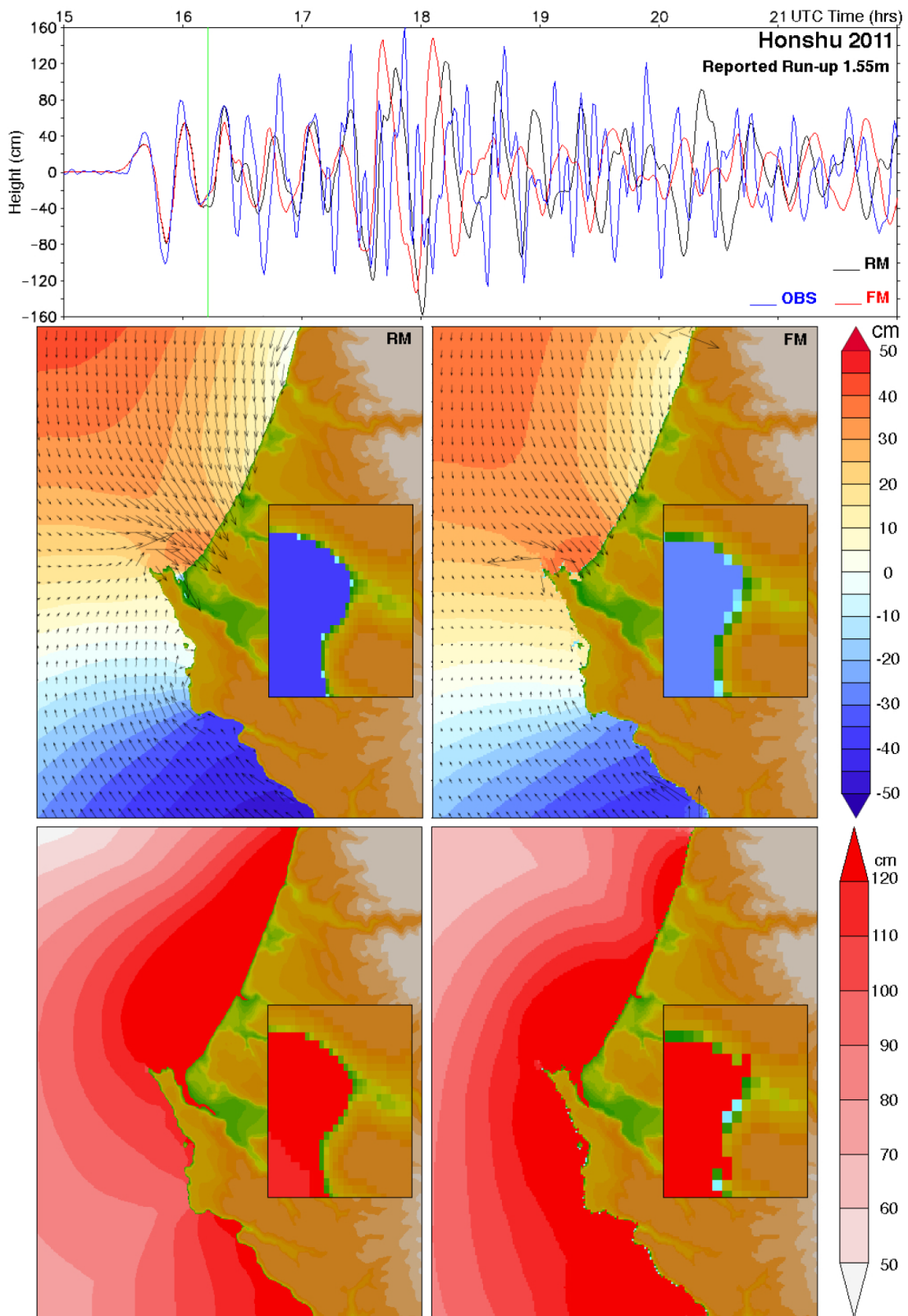


Figure 27: Comparison of real-time forecast (FM) and hindcast reference (RM) model representations of the 2011 Tohoku (Honshu) event with sea level observations in Arena Cove.

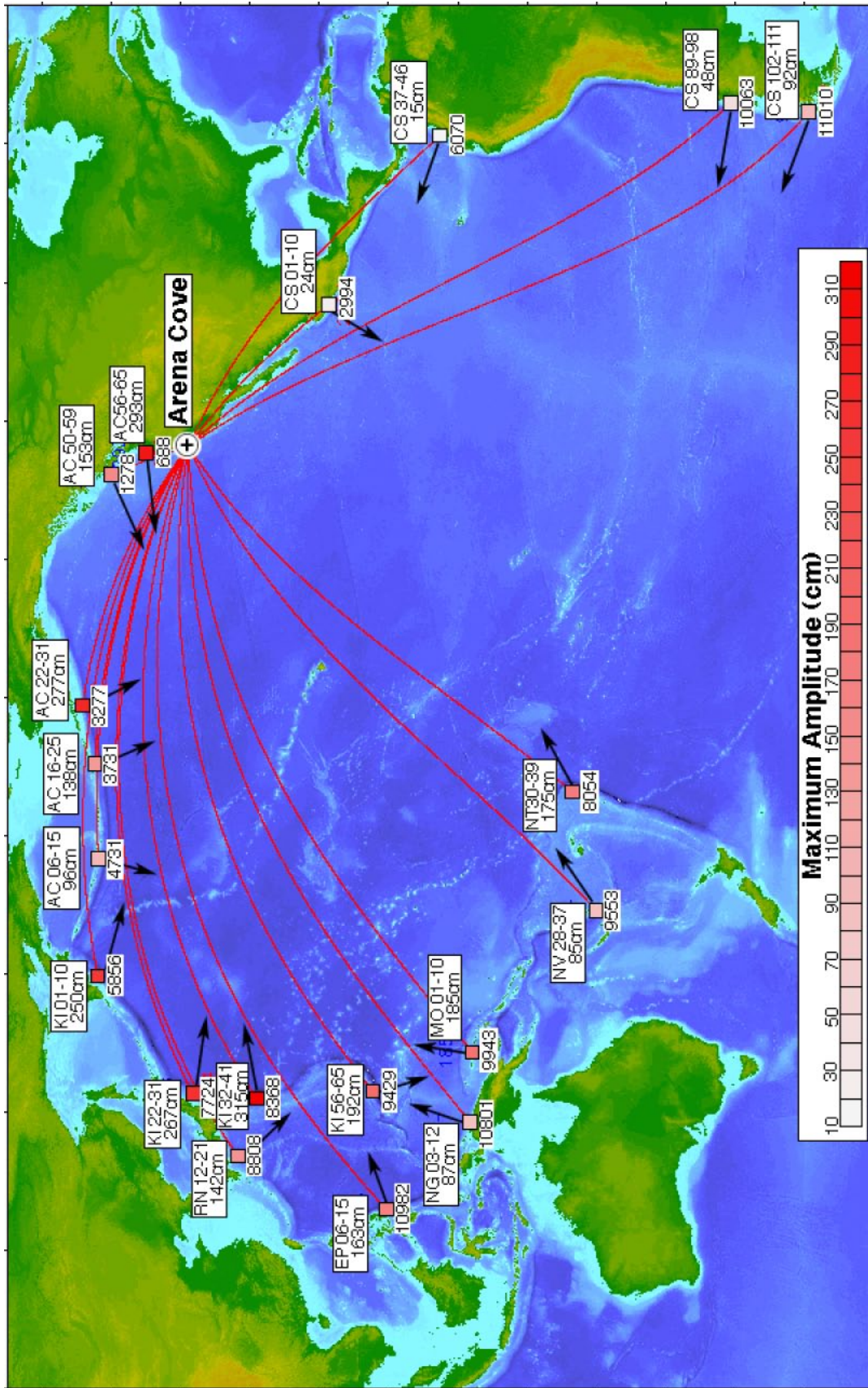


Figure 28: Predicted maximum sea level (from the forecast model) at the Arena Cove tide gauge for the mega-tsunami scenarios described in Table 6. Great circle routes are shown in red (with distances in km); black arrows indicate the normal to the strike direction.

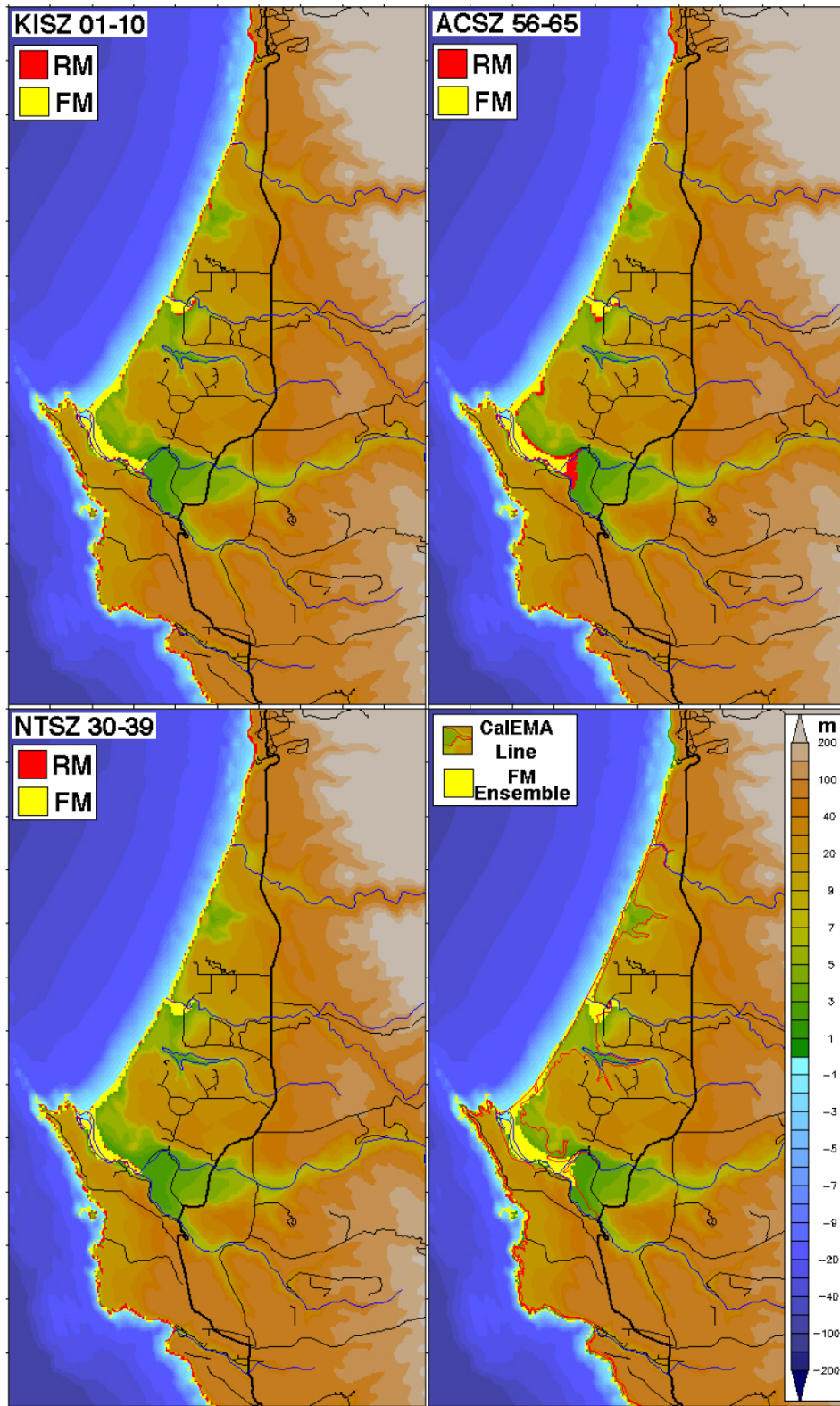


Figure 29: Comparison of reference (RM) and forecast (FM) model predictions for inundation of the Arena Cove / Manchester Beach region for selected mega-tsunami scenarios and (lower right) for the ensemble employed in the CalEMA study.

Appendix A. Model input files for Arena Cove, California

As discussed in Section 3.5, input files providing model parameters, the file names of the nested grids, and the output specifications are necessary in order to run the model in either its reference or forecast mode. These files are provided below; each record contains the value(s) and an annotation of purpose.

A1. Reference model *.in file for Arena Cove, California

The following table contains the parameter and file choices used in the input file for the SIFT implementation (most3_facts_nc.in) of the reference model (RM) for Arena Cove, California. When run on an Intel® Xeon® E5670 2.93 GHz processor during development the model simulated 4 hr in 5.43 CPU hr.

0.001	Minimum amplitude of input offshore wave (m)
1	Minimum depth of offshore (m)
0.1	Dry land depth of inundation (m)
0.0009	Friction coefficient (n**2)
1	Let A Grid and B Grid run up
900.0	Max eta before blow-up (m)
0.6	Time step (sec)
48000	Total number of time steps in run
5	Time steps between A-grid computations
1	Time steps between B-grid computations
50	Time steps between output steps
0	Time steps before saving first output step
1	Save output every n-th grid point, n=
ArenaCoveCA_RM_A.most	A-grid bathymetry file
ArenaCoveCA_RM_B.most	B-grid bathymetry file
ArenaCoveCA_RM_C.most	C-grid bathymetry file
./	Directory of source files
./	Directory for output files
1 1 1 1	netCDF output for A, B, C, SIFT
1	Number of time series locations
3 500 417	Grid & cell indices for reference point

A2. Forecast model *.in file for Arena Cove, California

The following table contains the parameter and file choices used in the input file for the SIFT implementation (most3_facts_nc.in) of the optimized forecast model (FM) for Arena Cove, California. When run on an Intel® Xeon® E5670 2.93 GHz processor the model simulated 4 hr in 9.5 min, satisfying the 10 min target for this metric.

0.001	Minimum amplitude of input offshore wave (m)
1	Minimum depth of offshore (m)
0.1	Dry land depth of inundation (m)
0.0009	Friction coefficient (n**2)
1	Let A Grid and B Grid run up
900.0	Max eta before blow-up (m)
1.5	Time step (sec)
19200	Total number of time steps in run
4	Time steps between A-grid computations
1	Time steps between B-grid computations
20	Time steps between output steps
0	Time steps before saving first output step
1	Save output every n-th grid point, n=
ArenaCoveCA_FM_A.most	A-grid bathymetry file
ArenaCoveCA_FM_B.most	B-grid bathymetry file
ArenaCoveCA_FM_C.most	C-grid bathymetry file
./	Directory of source files
./	Directory for output files
1 1 1 1	netCDF output for A, B, C, SIFT
1	Number of time series locations
3 125 254	Grid & cell indices for 236.28888889 38.91458333

Appendix B. Propagation Database

Pacific Ocean Unit Sources

The NOAA propagation database presented in this section is the representation of the database as of March 2013, and may not be the most current version of the database available upon publication.

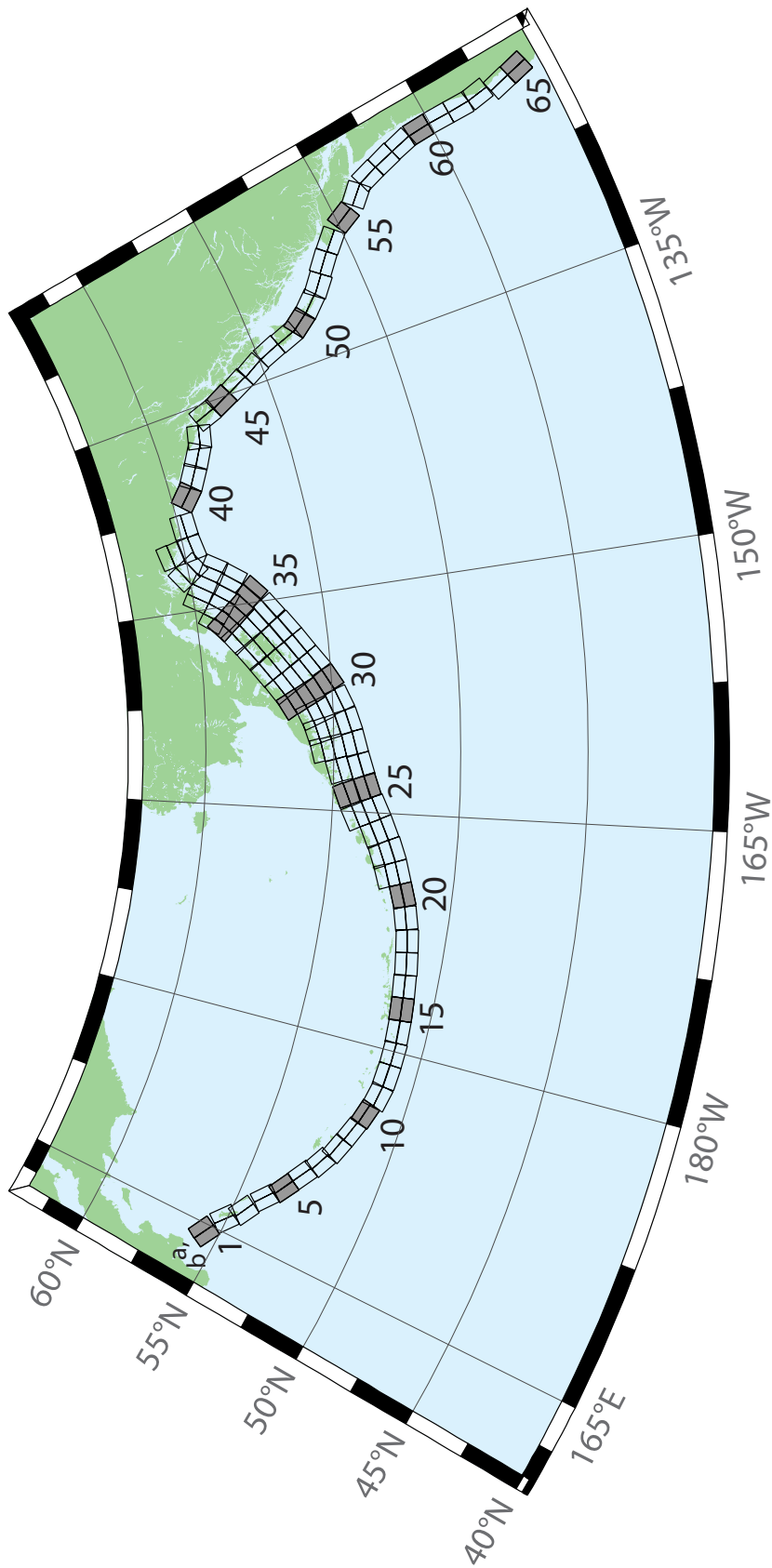


Figure B1: Aleutian–Alaska–Cascadia Subduction Zone unit sources.

Table B1: Earthquake parameters for Aleutian–Alaska–Cascadia Subduction Zone unit sources.

Segment	Description	Longitude (°E)	Latitude (°N)	Strike (°)	Dip (°)	Depth (km)
acsz-1a	Aleutian–Alaska–Cascadia	164.7994	55.9606	299	17	19.61
acsz-1b	Aleutian–Alaska–Cascadia	164.4310	55.5849	299	17	5
acsz-2a	Aleutian–Alaska–Cascadia	166.3418	55.4016	310.2	17	19.61
acsz-2b	Aleutian–Alaska–Cascadia	165.8578	55.0734	310.2	17	5
acsz-3a	Aleutian–Alaska–Cascadia	167.2939	54.8919	300.2	23.36	24.82
acsz-3b	Aleutian–Alaska–Cascadia	166.9362	54.5356	300.2	23.36	5
acsz-4a	Aleutian–Alaska–Cascadia	168.7131	54.2852	310.2	38.51	25.33
acsz-4b	Aleutian–Alaska–Cascadia	168.3269	54.0168	310.2	24	5
acsz-5a	Aleutian–Alaska–Cascadia	169.7447	53.7808	302.8	37.02	23.54
acsz-5b	Aleutian–Alaska–Cascadia	169.4185	53.4793	302.8	21.77	5
acsz-6a	Aleutian–Alaska–Cascadia	171.0144	53.3054	303.2	35.31	22.92
acsz-6b	Aleutian–Alaska–Cascadia	170.6813	52.9986	303.2	21	5
acsz-7a	Aleutian–Alaska–Cascadia	172.1500	52.8528	298.2	35.56	20.16
acsz-7b	Aleutian–Alaska–Cascadia	171.8665	52.5307	298.2	17.65	5
acsz-8a	Aleutian–Alaska–Cascadia	173.2726	52.4579	290.8	37.92	20.35
acsz-8b	Aleutian–Alaska–Cascadia	173.0681	52.1266	290.8	17.88	5
acsz-9a	Aleutian–Alaska–Cascadia	174.5866	52.1434	289	39.09	21.05
acsz-9b	Aleutian–Alaska–Cascadia	174.4027	51.8138	289	18.73	5
acsz-10a	Aleutian–Alaska–Cascadia	175.8784	51.8526	286.1	40.51	20.87
acsz-10b	Aleutian–Alaska–Cascadia	175.7265	51.5245	286.1	18.51	5
acsz-11a	Aleutian–Alaska–Cascadia	177.1140	51.6488	280	15	17.94
acsz-11b	Aleutian–Alaska–Cascadia	176.9937	51.2215	280	15	5
acsz-12a	Aleutian–Alaska–Cascadia	178.4500	51.5690	273	15	17.94
acsz-12b	Aleutian–Alaska–Cascadia	178.4130	51.1200	273	15	5
acsz-13a	Aleutian–Alaska–Cascadia	179.8550	51.5340	271	15	17.94
acsz-13b	Aleutian–Alaska–Cascadia	179.8420	51.0850	271	15	5
acsz-14a	Aleutian–Alaska–Cascadia	181.2340	51.5780	267	15	17.94
acsz-14b	Aleutian–Alaska–Cascadia	181.2720	51.1290	267	15	5
acsz-15a	Aleutian–Alaska–Cascadia	182.6380	51.6470	265	15	17.94
acsz-15b	Aleutian–Alaska–Cascadia	182.7000	51.2000	265	15	5
acsz-16a	Aleutian–Alaska–Cascadia	184.0550	51.7250	264	15	17.94
acsz-16b	Aleutian–Alaska–Cascadia	184.1280	51.2780	264	15	5
acsz-17a	Aleutian–Alaska–Cascadia	185.4560	51.8170	262	15	17.94
acsz-17b	Aleutian–Alaska–Cascadia	185.5560	51.3720	262	15	5
acsz-18a	Aleutian–Alaska–Cascadia	186.8680	51.9410	261	15	17.94
acsz-18b	Aleutian–Alaska–Cascadia	186.9810	51.4970	261	15	5
acsz-19a	Aleutian–Alaska–Cascadia	188.2430	52.1280	257	15	17.94
acsz-19b	Aleutian–Alaska–Cascadia	188.4060	51.6900	257	15	5

continued on next page

Table B1: (continued)

Segment	Description	Longitude (°E)	Latitude (°N)	Strike (°)	Dip (°)	Depth (km)
acsz-20a	Aleutian–Alaska–Cascadia	189.5810	52.3550	251	15	17.94
acsz-20b	Aleutian–Alaska–Cascadia	189.8180	51.9300	251	15	5
acsz-21a	Aleutian–Alaska–Cascadia	190.9570	52.6470	251	15	17.94
acsz-21b	Aleutian–Alaska–Cascadia	191.1960	52.2220	251	15	5
acsz-21z	Aleutian–Alaska–Cascadia	190.7399	53.0443	250.8	15	30.88
acsz-22a	Aleutian–Alaska–Cascadia	192.2940	52.9430	247	15	17.94
acsz-22b	Aleutian–Alaska–Cascadia	192.5820	52.5300	247	15	5
acsz-22z	Aleutian–Alaska–Cascadia	192.0074	53.3347	247.8	15	30.88
acsz-23a	Aleutian–Alaska–Cascadia	193.6270	53.3070	245	15	17.94
acsz-23b	Aleutian–Alaska–Cascadia	193.9410	52.9000	245	15	5
acsz-23z	Aleutian–Alaska–Cascadia	193.2991	53.6768	244.6	15	30.88
acsz-24a	Aleutian–Alaska–Cascadia	194.9740	53.6870	245	15	17.94
acsz-24b	Aleutian–Alaska–Cascadia	195.2910	53.2800	245	15	5
acsz-24y	Aleutian–Alaska–Cascadia	194.3645	54.4604	244.4	15	43.82
acsz-24z	Aleutian–Alaska–Cascadia	194.6793	54.0674	244.6	15	30.88
acsz-25a	Aleutian–Alaska–Cascadia	196.4340	54.0760	250	15	17.94
acsz-25b	Aleutian–Alaska–Cascadia	196.6930	53.6543	250	15	5
acsz-25y	Aleutian–Alaska–Cascadia	195.9009	54.8572	247.9	15	43.82
acsz-25z	Aleutian–Alaska–Cascadia	196.1761	54.4536	248.1	15	30.88
acsz-26a	Aleutian–Alaska–Cascadia	197.8970	54.3600	253	15	17.94
acsz-26b	Aleutian–Alaska–Cascadia	198.1200	53.9300	253	15	5
acsz-26y	Aleutian–Alaska–Cascadia	197.5498	55.1934	253.1	15	43.82
acsz-26z	Aleutian–Alaska–Cascadia	197.7620	54.7770	253.3	15	30.88
acsz-27a	Aleutian–Alaska–Cascadia	199.4340	54.5960	256	15	17.94
acsz-27b	Aleutian–Alaska–Cascadia	199.6200	54.1600	256	15	5
acsz-27x	Aleutian–Alaska–Cascadia	198.9736	55.8631	256.5	15	56.24
acsz-27y	Aleutian–Alaska–Cascadia	199.1454	55.4401	256.6	15	43.82
acsz-27z	Aleutian–Alaska–Cascadia	199.3135	55.0170	256.8	15	30.88
acsz-28a	Aleutian–Alaska–Cascadia	200.8820	54.8300	253	15	17.94
acsz-28b	Aleutian–Alaska–Cascadia	201.1080	54.4000	253	15	5
acsz-28x	Aleutian–Alaska–Cascadia	200.1929	56.0559	252.5	15	56.24
acsz-28y	Aleutian–Alaska–Cascadia	200.4167	55.6406	252.7	15	43.82
acsz-28z	Aleutian–Alaska–Cascadia	200.6360	55.2249	252.9	15	30.88
acsz-29a	Aleutian–Alaska–Cascadia	202.2610	55.1330	247	15	17.94
acsz-29b	Aleutian–Alaska–Cascadia	202.5650	54.7200	247	15	5
acsz-29x	Aleutian–Alaska–Cascadia	201.2606	56.2861	245.7	15	56.24
acsz-29y	Aleutian–Alaska–Cascadia	201.5733	55.8888	246	15	43.82
acsz-29z	Aleutian–Alaska–Cascadia	201.8797	55.4908	246.2	15	30.88

continued on next page

Table B1: (continued)

Segment	Description	Longitude (°E)	Latitude (°N)	Strike (°)	Dip (°)	Depth (km)
acsz-30a	Aleutian–Alaska–Cascadia	203.6040	55.5090	240	15	17.94
acsz-30b	Aleutian–Alaska–Cascadia	203.9970	55.1200	240	15	5
acsz-30w	Aleutian–Alaska–Cascadia	201.9901	56.9855	239.5	15	69.12
acsz-30x	Aleutian–Alaska–Cascadia	202.3851	56.6094	239.8	15	56.24
acsz-30y	Aleutian–Alaska–Cascadia	202.7724	56.2320	240.2	15	43.82
acsz-30z	Aleutian–Alaska–Cascadia	203.1521	55.8534	240.5	15	30.88
acsz-31a	Aleutian–Alaska–Cascadia	204.8950	55.9700	236	15	17.94
acsz-31b	Aleutian–Alaska–Cascadia	205.3400	55.5980	236	15	5
acsz-31w	Aleutian–Alaska–Cascadia	203.0825	57.3740	234.5	15	69.12
acsz-31x	Aleutian–Alaska–Cascadia	203.5408	57.0182	234.9	15	56.24
acsz-31y	Aleutian–Alaska–Cascadia	203.9904	56.6607	235.3	15	43.82
acsz-31z	Aleutian–Alaska–Cascadia	204.4315	56.3016	235.7	15	30.88
acsz-32a	Aleutian–Alaska–Cascadia	206.2080	56.4730	236	15	17.94
acsz-32b	Aleutian–Alaska–Cascadia	206.6580	56.1000	236	15	5
acsz-32w	Aleutian–Alaska–Cascadia	204.4129	57.8908	234.3	15	69.12
acsz-32x	Aleutian–Alaska–Cascadia	204.8802	57.5358	234.7	15	56.24
acsz-32y	Aleutian–Alaska–Cascadia	205.3385	57.1792	235.1	15	43.82
acsz-32z	Aleutian–Alaska–Cascadia	205.7880	56.8210	235.5	15	30.88
acsz-33a	Aleutian–Alaska–Cascadia	207.5370	56.9750	236	15	17.94
acsz-33b	Aleutian–Alaska–Cascadia	207.9930	56.6030	236	15	5
acsz-33w	Aleutian–Alaska–Cascadia	205.7126	58.3917	234.2	15	69.12
acsz-33x	Aleutian–Alaska–Cascadia	206.1873	58.0371	234.6	15	56.24
acsz-33y	Aleutian–Alaska–Cascadia	206.6527	57.6808	235	15	43.82
acsz-33z	Aleutian–Alaska–Cascadia	207.1091	57.3227	235.4	15	30.88
acsz-34a	Aleutian–Alaska–Cascadia	208.9371	57.5124	236	15	17.94
acsz-34b	Aleutian–Alaska–Cascadia	209.4000	57.1400	236	15	5
acsz-34w	Aleutian–Alaska–Cascadia	206.9772	58.8804	233.5	15	69.12
acsz-34x	Aleutian–Alaska–Cascadia	207.4677	58.5291	233.9	15	56.24
acsz-34y	Aleutian–Alaska–Cascadia	207.9485	58.1760	234.3	15	43.82
acsz-34z	Aleutian–Alaska–Cascadia	208.4198	57.8213	234.7	15	30.88
acsz-35a	Aleutian–Alaska–Cascadia	210.2597	58.0441	230	15	17.94
acsz-35b	Aleutian–Alaska–Cascadia	210.8000	57.7000	230	15	5
acsz-35w	Aleutian–Alaska–Cascadia	208.0204	59.3199	228.8	15	69.12
acsz-35x	Aleutian–Alaska–Cascadia	208.5715	58.9906	229.3	15	56.24
acsz-35y	Aleutian–Alaska–Cascadia	209.1122	58.6590	229.7	15	43.82
acsz-35z	Aleutian–Alaska–Cascadia	209.6425	58.3252	230.2	15	30.88
acsz-36a	Aleutian–Alaska–Cascadia	211.3249	58.6565	218	15	17.94
acsz-36b	Aleutian–Alaska–Cascadia	212.0000	58.3800	218	15	5

continued on next page

Table B1: (continued)

Segment	Description	Longitude (°E)	Latitude (°N)	Strike (°)	Dip (°)	Depth (km)
acsz-36w	Aleutian–Alaska–Cascadia	208.5003	59.5894	215.6	15	69.12
acsz-36x	Aleutian–Alaska–Cascadia	209.1909	59.3342	216.2	15	56.24
acsz-36y	Aleutian–Alaska–Cascadia	209.8711	59.0753	216.8	15	43.82
acsz-36z	Aleutian–Alaska–Cascadia	210.5412	58.8129	217.3	15	30.88
acsz-37a	Aleutian–Alaska–Cascadia	212.2505	59.2720	213.7	15	17.94
acsz-37b	Aleutian–Alaska–Cascadia	212.9519	59.0312	213.7	15	5
acsz-37x	Aleutian–Alaska–Cascadia	210.1726	60.0644	213	15	56.24
acsz-37y	Aleutian–Alaska–Cascadia	210.8955	59.8251	213.7	15	43.82
acsz-37z	Aleutian–Alaska–Cascadia	211.6079	59.5820	214.3	15	30.88
acsz-38a	Aleutian–Alaska–Cascadia	214.6555	60.1351	260.1	0	15
acsz-38b	Aleutian–Alaska–Cascadia	214.8088	59.6927	260.1	0	15
acsz-38y	Aleutian–Alaska–Cascadia	214.3737	60.9838	259	0	15
acsz-38z	Aleutian–Alaska–Cascadia	214.5362	60.5429	259	0	15
acsz-39a	Aleutian–Alaska–Cascadia	216.5607	60.2480	267	0	15
acsz-39b	Aleutian–Alaska–Cascadia	216.6068	59.7994	267	0	15
acsz-40a	Aleutian–Alaska–Cascadia	219.3069	59.7574	310.9	0	15
acsz-40b	Aleutian–Alaska–Cascadia	218.7288	59.4180	310.9	0	15
acsz-41a	Aleutian–Alaska–Cascadia	220.4832	59.3390	300.7	0	15
acsz-41b	Aleutian–Alaska–Cascadia	220.0382	58.9529	300.7	0	15
acsz-42a	Aleutian–Alaska–Cascadia	221.8835	58.9310	298.9	0	15
acsz-42b	Aleutian–Alaska–Cascadia	221.4671	58.5379	298.9	0	15
acsz-43a	Aleutian–Alaska–Cascadia	222.9711	58.6934	282.3	0	15
acsz-43b	Aleutian–Alaska–Cascadia	222.7887	58.2546	282.3	0	15
acsz-44a	Aleutian–Alaska–Cascadia	224.9379	57.9054	340.9	12	11.09
acsz-44b	Aleutian–Alaska–Cascadia	224.1596	57.7617	340.9	7	5
acsz-45a	Aleutian–Alaska–Cascadia	225.4994	57.1634	334.1	12	11.09
acsz-45b	Aleutian–Alaska–Cascadia	224.7740	56.9718	334.1	7	5
acsz-46a	Aleutian–Alaska–Cascadia	226.1459	56.3552	334.1	12	11.09
acsz-46b	Aleutian–Alaska–Cascadia	225.4358	56.1636	334.1	7	5
acsz-47a	Aleutian–Alaska–Cascadia	226.7731	55.5830	332.3	12	11.09
acsz-47b	Aleutian–Alaska–Cascadia	226.0887	55.3785	332.3	7	5
acsz-48a	Aleutian–Alaska–Cascadia	227.4799	54.6763	339.4	12	11.09
acsz-48b	Aleutian–Alaska–Cascadia	226.7713	54.5217	339.4	7	5
acsz-49a	Aleutian–Alaska–Cascadia	227.9482	53.8155	341.2	12	11.09
acsz-49b	Aleutian–Alaska–Cascadia	227.2462	53.6737	341.2	7	5
acsz-50a	Aleutian–Alaska–Cascadia	228.3970	53.2509	324.5	12	11.09
acsz-50b	Aleutian–Alaska–Cascadia	227.8027	52.9958	324.5	7	5
acsz-51a	Aleutian–Alaska–Cascadia	229.1844	52.6297	318.4	12	11.09

continued on next page

Table B1: (continued)

Segment	Description	Longitude (°E)	Latitude (°N)	Strike (°)	Dip (°)	Depth (km)
acsz-51b	Aleutian–Alaska–Cascadia	228.6470	52.3378	318.4	7	5
acsz-52a	Aleutian–Alaska–Cascadia	230.0306	52.0768	310.9	12	11.09
acsz-52b	Aleutian–Alaska–Cascadia	229.5665	51.7445	310.9	7	5
acsz-53a	Aleutian–Alaska–Cascadia	231.1735	51.5258	310.9	12	11.09
acsz-53b	Aleutian–Alaska–Cascadia	230.7150	51.1935	310.9	7	5
acsz-54a	Aleutian–Alaska–Cascadia	232.2453	50.8809	314.1	12	11.09
acsz-54b	Aleutian–Alaska–Cascadia	231.7639	50.5655	314.1	7	5
acsz-55a	Aleutian–Alaska–Cascadia	233.3066	49.9032	333.7	12	11.09
acsz-55b	Aleutian–Alaska–Cascadia	232.6975	49.7086	333.7	7	5
acsz-56a	Aleutian–Alaska–Cascadia	234.0588	49.1702	315	11	12.82
acsz-56b	Aleutian–Alaska–Cascadia	233.5849	48.8584	315	9	5
acsz-57a	Aleutian–Alaska–Cascadia	234.9041	48.2596	341	11	12.82
acsz-57b	Aleutian–Alaska–Cascadia	234.2797	48.1161	341	9	5
acsz-58a	Aleutian–Alaska–Cascadia	235.3021	47.3812	344	11	12.82
acsz-58b	Aleutian–Alaska–Cascadia	234.6776	47.2597	344	9	5
acsz-59a	Aleutian–Alaska–Cascadia	235.6432	46.5082	345	11	12.82
acsz-59b	Aleutian–Alaska–Cascadia	235.0257	46.3941	345	9	5
acsz-60a	Aleutian–Alaska–Cascadia	235.8640	45.5429	356	11	12.82
acsz-60b	Aleutian–Alaska–Cascadia	235.2363	45.5121	356	9	5
acsz-61a	Aleutian–Alaska–Cascadia	235.9106	44.6227	359	11	12.82
acsz-61b	Aleutian–Alaska–Cascadia	235.2913	44.6150	359	9	5
acsz-62a	Aleutian–Alaska–Cascadia	235.9229	43.7245	359	11	12.82
acsz-62b	Aleutian–Alaska–Cascadia	235.3130	43.7168	359	9	5
acsz-63a	Aleutian–Alaska–Cascadia	236.0220	42.9020	350	11	12.82
acsz-63b	Aleutian–Alaska–Cascadia	235.4300	42.8254	350	9	5
acsz-64a	Aleutian–Alaska–Cascadia	235.9638	41.9818	345	11	12.82
acsz-64b	Aleutian–Alaska–Cascadia	235.3919	41.8677	345	9	5
acsz-65a	Aleutian–Alaska–Cascadia	236.2643	41.1141	345	11	12.82
acsz-65b	Aleutian–Alaska–Cascadia	235.7000	41.0000	345	9	5
acsz-238a	Aleutian–Alaska–Cascadia	213.2878	59.8406	236.8	15	17.94
acsz-238y	Aleutian–Alaska–Cascadia	212.3424	60.5664	236.8	15	43.82
acsz-238z	Aleutian–Alaska–Cascadia	212.8119	60.2035	236.8	15	30.88

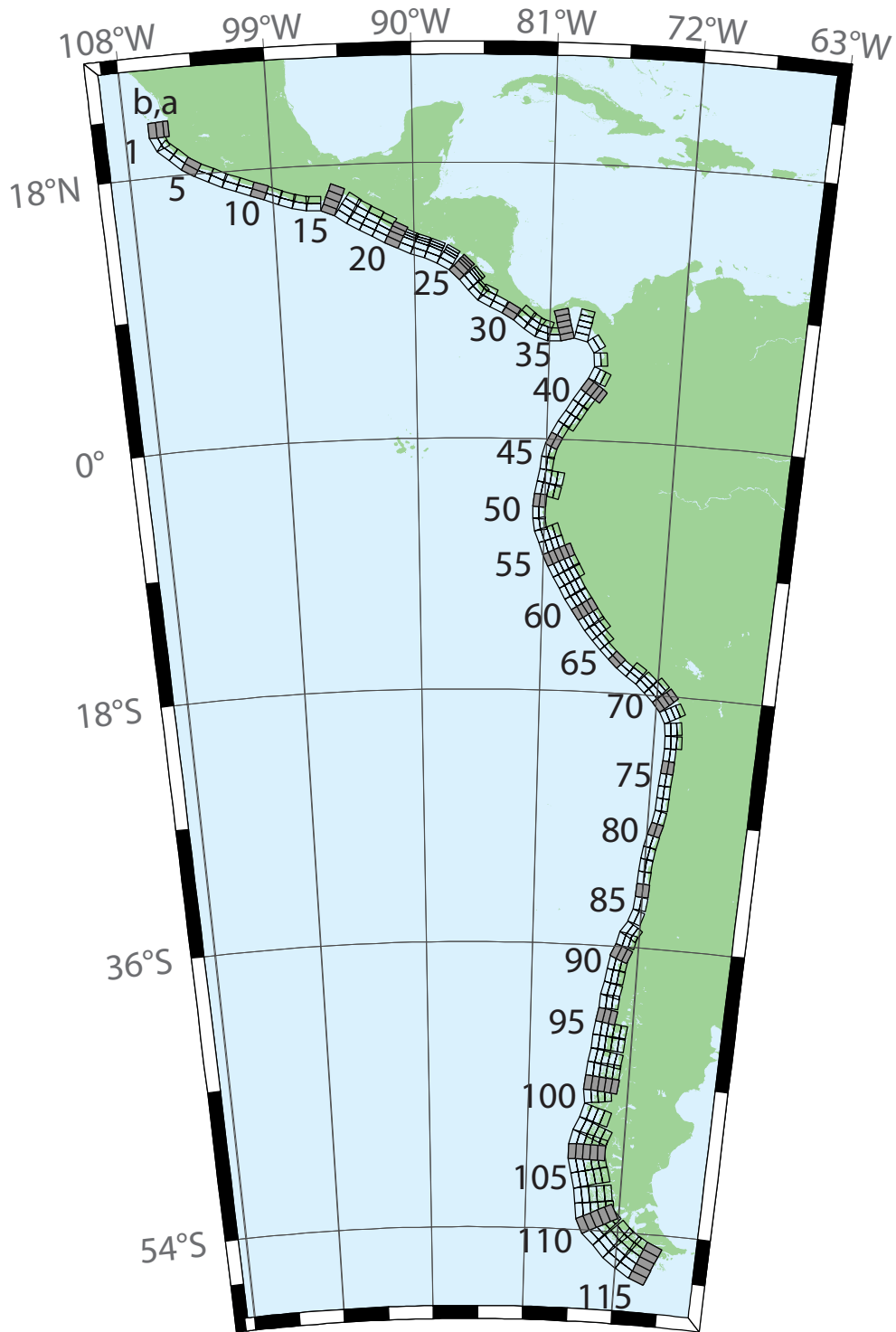


Figure B2: Central and South America Subduction Zone unit sources.

Table B2: Earthquake parameters for Central and South America Subduction Zone unit sources.

Segment	Description	Longitude (°E)	Latitude (°N)	Strike (°)	Dip (°)	Depth (km)
cssz-1a	Central and South America	254.4573	20.8170	359	19	15.4
cssz-1b	Central and South America	254.0035	20.8094	359	12	5
cssz-1z	Central and South America	254.7664	20.8222	359	50	31.67
cssz-2a	Central and South America	254.5765	20.2806	336.8	19	15.4
cssz-2b	Central and South America	254.1607	20.1130	336.8	12	5
cssz-3a	Central and South America	254.8789	19.8923	310.6	18.31	15.27
cssz-3b	Central and South America	254.5841	19.5685	310.6	11.85	5
cssz-4a	Central and South America	255.6167	19.2649	313.4	17.62	15.12
cssz-4b	Central and South America	255.3056	18.9537	313.4	11.68	5
cssz-5a	Central and South America	256.2240	18.8148	302.7	16.92	15
cssz-5b	Central and South America	255.9790	18.4532	302.7	11.54	5
cssz-6a	Central and South America	256.9425	18.4383	295.1	16.23	14.87
cssz-6b	Central and South America	256.7495	18.0479	295.1	11.38	5
cssz-7a	Central and South America	257.8137	18.0339	296.9	15.54	14.74
cssz-7b	Central and South America	257.6079	17.6480	296.9	11.23	5
cssz-8a	Central and South America	258.5779	17.7151	290.4	14.85	14.61
cssz-8b	Central and South America	258.4191	17.3082	290.4	11.08	5
cssz-9a	Central and South America	259.4578	17.4024	290.5	14.15	14.47
cssz-9b	Central and South America	259.2983	16.9944	290.5	10.92	5
cssz-10a	Central and South America	260.3385	17.0861	290.8	13.46	14.34
cssz-10b	Central and South America	260.1768	16.6776	290.8	10.77	5
cssz-11a	Central and South America	261.2255	16.7554	291.8	12.77	14.21
cssz-11b	Central and South America	261.0556	16.3487	291.8	10.62	5
cssz-12a	Central and South America	262.0561	16.4603	288.9	12.08	14.08
cssz-12b	Central and South America	261.9082	16.0447	288.9	10.46	5
cssz-13a	Central and South America	262.8638	16.2381	283.2	11.38	13.95
cssz-13b	Central and South America	262.7593	15.8094	283.2	10.31	5
cssz-14a	Central and South America	263.6066	16.1435	272.1	10.69	13.81
cssz-14b	Central and South America	263.5901	15.7024	272.1	10.15	5
cssz-15a	Central and South America	264.8259	15.8829	293	10	13.68
cssz-15b	Central and South America	264.6462	15.4758	293	10	5
cssz-15y	Central and South America	265.1865	16.6971	293	10	31.05
cssz-15z	Central and South America	265.0060	16.2900	293	10	22.36
cssz-16a	Central and South America	265.7928	15.3507	304.9	15	15.82
cssz-16b	Central and South America	265.5353	14.9951	304.9	12.5	5
cssz-16y	Central and South America	266.3092	16.0619	304.9	15	41.7
cssz-16z	Central and South America	266.0508	15.7063	304.9	15	28.76
cssz-17a	Central and South America	266.4947	14.9019	299.5	20	17.94
cssz-17b	Central and South America	266.2797	14.5346	299.5	15	5
cssz-17y	Central and South America	266.9259	15.6365	299.5	20	52.14

continued on next page

Table B2: (continued)

Segment	Description	Longitude (°E)	Latitude (°N)	Strike (°)	Dip (°)	Depth (km)
cssz-17z	Central and South America	266.7101	15.2692	299.5	20	35.04
cssz-18a	Central and South America	267.2827	14.4768	298	21.5	17.94
cssz-18b	Central and South America	267.0802	14.1078	298	15	5
cssz-18y	Central and South America	267.6888	15.2148	298	21.5	54.59
cssz-18z	Central and South America	267.4856	14.8458	298	21.5	36.27
cssz-19a	Central and South America	268.0919	14.0560	297.6	23	17.94
cssz-19b	Central and South America	267.8943	13.6897	297.6	15	5
cssz-19y	Central and South America	268.4880	14.7886	297.6	23	57.01
cssz-19z	Central and South America	268.2898	14.4223	297.6	23	37.48
cssz-20a	Central and South America	268.8929	13.6558	296.2	24	17.94
cssz-20b	Central and South America	268.7064	13.2877	296.2	15	5
cssz-20y	Central and South America	269.1796	14.2206	296.2	45.5	73.94
cssz-20z	Central and South America	269.0362	13.9382	296.2	45.5	38.28
cssz-21a	Central and South America	269.6797	13.3031	292.6	25	17.94
cssz-21b	Central and South America	269.5187	12.9274	292.6	15	5
cssz-21x	Central and South America	269.8797	13.7690	292.6	68	131.8
cssz-21y	Central and South America	269.8130	13.6137	292.6	68	85.43
cssz-21z	Central and South America	269.7463	13.4584	292.6	68	39.07
cssz-22a	Central and South America	270.4823	13.0079	288.6	25	17.94
cssz-22b	Central and South America	270.3492	12.6221	288.6	15	5
cssz-22x	Central and South America	270.6476	13.4864	288.6	68	131.8
cssz-22y	Central and South America	270.5925	13.3269	288.6	68	85.43
cssz-22z	Central and South America	270.5374	13.1674	288.6	68	39.07
cssz-23a	Central and South America	271.3961	12.6734	292.4	25	17.94
cssz-23b	Central and South America	271.2369	12.2972	292.4	15	5
cssz-23x	Central and South America	271.5938	13.1399	292.4	68	131.8
cssz-23y	Central and South America	271.5279	12.9844	292.4	68	85.43
cssz-23z	Central and South America	271.4620	12.8289	292.4	68	39.07
cssz-24a	Central and South America	272.3203	12.2251	300.2	25	17.94
cssz-24b	Central and South America	272.1107	11.8734	300.2	15	5
cssz-24x	Central and South America	272.5917	12.6799	300.2	67	131.1
cssz-24y	Central and South America	272.5012	12.5283	300.2	67	85.1
cssz-24z	Central and South America	272.4107	12.3767	300.2	67	39.07
cssz-25a	Central and South America	273.2075	11.5684	313.8	25	17.94
cssz-25b	Central and South America	272.9200	11.2746	313.8	15	5
cssz-25x	Central and South America	273.5950	11.9641	313.8	66	130.4
cssz-25y	Central and South America	273.4658	11.8322	313.8	66	84.75
cssz-25z	Central and South America	273.3366	11.7003	313.8	66	39.07
cssz-26a	Central and South America	273.8943	10.8402	320.4	25	17.94

continued on next page

Table B2: (continued)

Segment	Description	Longitude (°E)	Latitude (°N)	Strike (°)	Dip (°)	Depth (km)
cssz-26b	Central and South America	273.5750	10.5808	320.4	15	5
cssz-26x	Central and South America	274.3246	11.1894	320.4	66	130.4
cssz-26y	Central and South America	274.1811	11.0730	320.4	66	84.75
cssz-26z	Central and South America	274.0377	10.9566	320.4	66	39.07
cssz-27a	Central and South America	274.4569	10.2177	316.1	25	17.94
cssz-27b	Central and South America	274.1590	9.9354	316.1	15	5
cssz-27z	Central and South America	274.5907	10.3444	316.1	66	39.07
cssz-28a	Central and South America	274.9586	9.8695	297.1	22	14.54
cssz-28b	Central and South America	274.7661	9.4988	297.1	11	5
cssz-28z	Central and South America	275.1118	10.1643	297.1	42.5	33.27
cssz-29a	Central and South America	275.7686	9.4789	296.6	19	11.09
cssz-29b	Central and South America	275.5759	9.0992	296.6	7	5
cssz-30a	Central and South America	276.6346	8.9973	302.2	19	9.36
cssz-30b	Central and South America	276.4053	8.6381	302.2	5	5
cssz-31a	Central and South America	277.4554	8.4152	309.1	19	7.62
cssz-31b	Central and South America	277.1851	8.0854	309.1	3	5
cssz-31z	Central and South America	277.7260	8.7450	309.1	19	23.9
cssz-32a	Central and South America	278.1112	7.9425	303	18.67	8.49
cssz-32b	Central and South America	277.8775	7.5855	303	4	5
cssz-32z	Central and South America	278.3407	8.2927	303	21.67	24.49
cssz-33a	Central and South America	278.7082	7.6620	287.6	18.33	10.23
cssz-33b	Central and South America	278.5785	7.2555	287.6	6	5
cssz-33z	Central and South America	278.8328	8.0522	287.6	24.33	25.95
cssz-34a	Central and South America	279.3184	7.5592	269.5	18	17.94
cssz-34b	Central and South America	279.3223	7.1320	269.5	15	5
cssz-35a	Central and South America	280.0039	7.6543	255.9	17.67	14.54
cssz-35b	Central and South America	280.1090	7.2392	255.9	11	5
cssz-35x	Central and South America	279.7156	8.7898	255.9	29.67	79.22
cssz-35y	Central and South America	279.8118	8.4113	255.9	29.67	54.47
cssz-35z	Central and South America	279.9079	8.0328	255.9	29.67	29.72
cssz-36a	Central and South America	281.2882	7.6778	282.5	17.33	11.09
cssz-36b	Central and South America	281.1948	7.2592	282.5	7	5
cssz-36x	Central and South America	281.5368	8.7896	282.5	32.33	79.47
cssz-36y	Central and South America	281.4539	8.4190	282.5	32.33	52.73
cssz-36z	Central and South America	281.3710	8.0484	282.5	32.33	25.99
cssz-37a	Central and South America	282.5252	6.8289	326.9	17	10.23
cssz-37b	Central and South America	282.1629	6.5944	326.9	6	5
cssz-38a	Central and South America	282.9469	5.5973	355.4	17	10.23
cssz-38b	Central and South America	282.5167	5.5626	355.4	6	5

continued on next page

Table B2: (continued)

Segment	Description	Longitude (°E)	Latitude (°N)	Strike (°)	Dip (°)	Depth (km)
cssz-39a	Central and South America	282.7236	4.3108	24.13	17	10.23
cssz-39b	Central and South America	282.3305	4.4864	24.13	6	5
cssz-39z	Central and South America	283.0603	4.1604	24.13	35	24.85
cssz-40a	Central and South America	282.1940	3.3863	35.28	17	10.23
cssz-40b	Central and South America	281.8427	3.6344	35.28	6	5
cssz-40y	Central and South America	282.7956	2.9613	35.28	35	53.52
cssz-40z	Central and South America	282.4948	3.1738	35.28	35	24.85
cssz-41a	Central and South America	281.6890	2.6611	34.27	17	10.23
cssz-41b	Central and South America	281.3336	2.9030	34.27	6	5
cssz-41z	Central and South America	281.9933	2.4539	34.27	35	24.85
cssz-42a	Central and South America	281.2266	1.9444	31.29	17	10.23
cssz-42b	Central and South America	280.8593	2.1675	31.29	6	5
cssz-42z	Central and South America	281.5411	1.7533	31.29	35	24.85
cssz-43a	Central and South America	280.7297	1.1593	33.3	17	10.23
cssz-43b	Central and South America	280.3706	1.3951	33.3	6	5
cssz-43z	Central and South America	281.0373	0.9573	33.3	35	24.85
cssz-44a	Central and South America	280.3018	0.4491	28.8	17	10.23
cssz-44b	Central and South America	279.9254	0.6560	28.8	6	5
cssz-45a	Central and South America	279.9083	-0.3259	26.91	10	8.49
cssz-45b	Central and South America	279.5139	-0.1257	26.91	4	5
cssz-46a	Central and South America	279.6461	-0.9975	15.76	10	8.49
cssz-46b	Central and South America	279.2203	-0.8774	15.76	4	5
cssz-47a	Central and South America	279.4972	-1.7407	6.9	10	8.49
cssz-47b	Central and South America	279.0579	-1.6876	6.9	4	5
cssz-48a	Central and South America	279.3695	-2.6622	8.96	10	8.49
cssz-48b	Central and South America	278.9321	-2.5933	8.96	4	5
cssz-48y	Central and South America	280.2444	-2.8000	8.96	10	25.85
cssz-48z	Central and South America	279.8070	-2.7311	8.96	10	17.17
cssz-49a	Central and South America	279.1852	-3.6070	13.15	10	8.49
cssz-49b	Central and South America	278.7536	-3.5064	13.15	4	5
cssz-49y	Central and South America	280.0486	-3.8082	13.15	10	25.85
cssz-49z	Central and South America	279.6169	-3.7076	13.15	10	17.17
cssz-50a	Central and South America	279.0652	-4.3635	4.78	10.33	9.64
cssz-50b	Central and South America	278.6235	-4.3267	4.78	5.33	5
cssz-51a	Central and South America	279.0349	-5.1773	359.4	10.67	10.81
cssz-51b	Central and South America	278.5915	-5.1817	359.4	6.67	5
cssz-52a	Central and South America	279.1047	-5.9196	349.8	11	11.96
cssz-52b	Central and South America	278.6685	-5.9981	349.8	8	5
cssz-53a	Central and South America	279.3044	-6.6242	339.2	10.25	11.74

continued on next page

Table B2: (continued)

Segment	Description	Longitude (°E)	Latitude (°N)	Strike (°)	Dip (°)	Depth (km)
cssz-53b	Central and South America	278.8884	-6.7811	339.2	7.75	5
cssz-53y	Central and South America	280.1024	-6.3232	339.2	19.25	37.12
cssz-53z	Central and South America	279.7035	-6.4737	339.2	19.25	20.64
cssz-54a	Central and South America	279.6256	-7.4907	340.8	9.5	11.53
cssz-54b	Central and South America	279.2036	-7.6365	340.8	7.5	5
cssz-54y	Central and South America	280.4267	-7.2137	340.8	20.5	37.29
cssz-54z	Central and South America	280.0262	-7.3522	340.8	20.5	19.78
cssz-55a	Central and South America	279.9348	-8.2452	335.4	8.75	11.74
cssz-55b	Central and South America	279.5269	-8.4301	335.4	7.75	5
cssz-55x	Central and South America	281.0837	-7.7238	335.4	21.75	56.4
cssz-55y	Central and South America	280.7009	-7.8976	335.4	21.75	37.88
cssz-55z	Central and South America	280.3180	-8.0714	335.4	21.75	19.35
cssz-56a	Central and South America	280.3172	-8.9958	331.6	8	11.09
cssz-56b	Central and South America	279.9209	-9.2072	331.6	7	5
cssz-56x	Central and South America	281.4212	-8.4063	331.6	23	57.13
cssz-56y	Central and South America	281.0534	-8.6028	331.6	23	37.59
cssz-56z	Central and South America	280.6854	-8.7993	331.6	23	18.05
cssz-57a	Central and South America	280.7492	-9.7356	328.7	8.6	10.75
cssz-57b	Central and South America	280.3640	-9.9663	328.7	6.6	5
cssz-57x	Central and South America	281.8205	-9.0933	328.7	23.4	57.94
cssz-57y	Central and South America	281.4636	-9.3074	328.7	23.4	38.08
cssz-57z	Central and South America	281.1065	-9.5215	328.7	23.4	18.22
cssz-58a	Central and South America	281.2275	-10.5350	330.5	9.2	10.4
cssz-58b	Central and South America	280.8348	-10.7532	330.5	6.2	5
cssz-58y	Central and South America	281.9548	-10.1306	330.5	23.8	38.57
cssz-58z	Central and South America	281.5913	-10.3328	330.5	23.8	18.39
cssz-59a	Central and South America	281.6735	-11.2430	326.2	9.8	10.05
cssz-59b	Central and South America	281.2982	-11.4890	326.2	5.8	5
cssz-59y	Central and South America	282.3675	-10.7876	326.2	24.2	39.06
cssz-59z	Central and South America	282.0206	-11.0153	326.2	24.2	18.56
cssz-60a	Central and South America	282.1864	-11.9946	326.5	10.4	9.71
cssz-60b	Central and South America	281.8096	-12.2384	326.5	5.4	5
cssz-60y	Central and South America	282.8821	-11.5438	326.5	24.6	39.55
cssz-60z	Central and South America	282.5344	-11.7692	326.5	24.6	18.73
cssz-61a	Central and South America	282.6944	-12.7263	325.5	11	9.36
cssz-61b	Central and South America	282.3218	-12.9762	325.5	5	5
cssz-61y	Central and South America	283.3814	-12.2649	325.5	25	40.03
cssz-61z	Central and South America	283.0381	-12.4956	325.5	25	18.9
cssz-62a	Central and South America	283.1980	-13.3556	319	11	9.79

continued on next page

Table B2: (continued)

Segment	Description	Longitude (°E)	Latitude (°N)	Strike (°)	Dip (°)	Depth (km)
cssz-62b	Central and South America	282.8560	-13.6451	319	5.5	5
cssz-62y	Central and South America	283.8178	-12.8300	319	27	42.03
cssz-62z	Central and South America	283.5081	-13.0928	319	27	19.33
cssz-63a	Central and South America	283.8032	-14.0147	317.9	11	10.23
cssz-63b	Central and South America	283.4661	-14.3106	317.9	6	5
cssz-63z	Central and South America	284.1032	-13.7511	317.9	29	19.77
cssz-64a	Central and South America	284.4144	-14.6482	315.7	13	11.96
cssz-64b	Central and South America	284.0905	-14.9540	315.7	8	5
cssz-65a	Central and South America	285.0493	-15.2554	313.2	15	13.68
cssz-65b	Central and South America	284.7411	-15.5715	313.2	10	5
cssz-66a	Central and South America	285.6954	-15.7816	307.7	14.5	13.68
cssz-66b	Central and South America	285.4190	-16.1258	307.7	10	5
cssz-67a	Central and South America	286.4127	-16.2781	304.3	14	13.68
cssz-67b	Central and South America	286.1566	-16.6381	304.3	10	5
cssz-67z	Central and South America	286.6552	-15.9365	304.3	23	25.78
cssz-68a	Central and South America	287.2481	-16.9016	311.8	14	13.68
cssz-68b	Central and South America	286.9442	-17.2264	311.8	10	5
cssz-68z	Central and South America	287.5291	-16.6007	311.8	26	25.78
cssz-69a	Central and South America	287.9724	-17.5502	314.9	14	13.68
cssz-69b	Central and South America	287.6496	-17.8590	314.9	10	5
cssz-69y	Central and South America	288.5530	-16.9934	314.9	29	50.02
cssz-69z	Central and South America	288.2629	-17.2718	314.9	29	25.78
cssz-70a	Central and South America	288.6731	-18.2747	320.4	14	13.25
cssz-70b	Central and South America	288.3193	-18.5527	320.4	9.5	5
cssz-70y	Central and South America	289.3032	-17.7785	320.4	30	50.35
cssz-70z	Central and South America	288.9884	-18.0266	320.4	30	25.35
cssz-71a	Central and South America	289.3089	-19.1854	333.2	14	12.82
cssz-71b	Central and South America	288.8968	-19.3820	333.2	9	5
cssz-71y	Central and South America	290.0357	-18.8382	333.2	31	50.67
cssz-71z	Central and South America	289.6725	-19.0118	333.2	31	24.92
cssz-72a	Central and South America	289.6857	-20.3117	352.4	14	12.54
cssz-72b	Central and South America	289.2250	-20.3694	352.4	8.67	5
cssz-72z	Central and South America	290.0882	-20.2613	352.4	32	24.63
cssz-73a	Central and South America	289.7731	-21.3061	358.9	14	12.24
cssz-73b	Central and South America	289.3053	-21.3142	358.9	8.33	5
cssz-73z	Central and South America	290.1768	-21.2991	358.9	33	24.34
cssz-74a	Central and South America	289.7610	-22.2671	3.06	14	11.96
cssz-74b	Central and South America	289.2909	-22.2438	3.06	8	5

continued on next page

Table B2: (continued)

Segment	Description	Longitude (°E)	Latitude (°N)	Strike (°)	Dip (°)	Depth (km)
cssz-75a	Central and South America	289.6982	-23.1903	4.83	14.09	11.96
cssz-75b	Central and South America	289.2261	-23.1536	4.83	8	5
cssz-76a	Central and South America	289.6237	-24.0831	4.67	14.18	11.96
cssz-76b	Central and South America	289.1484	-24.0476	4.67	8	5
cssz-77a	Central and South America	289.5538	-24.9729	4.3	14.27	11.96
cssz-77b	Central and South America	289.0750	-24.9403	4.3	8	5
cssz-78a	Central and South America	289.4904	-25.8621	3.86	14.36	11.96
cssz-78b	Central and South America	289.0081	-25.8328	3.86	8	5
cssz-79a	Central and South America	289.3491	-26.8644	11.34	14.45	11.96
cssz-79b	Central and South America	288.8712	-26.7789	11.34	8	5
cssz-80a	Central and South America	289.1231	-27.7826	14.16	14.54	11.96
cssz-80b	Central and South America	288.6469	-27.6762	14.16	8	5
cssz-81a	Central and South America	288.8943	-28.6409	13.19	14.63	11.96
cssz-81b	Central and South America	288.4124	-28.5417	13.19	8	5
cssz-82a	Central and South America	288.7113	-29.4680	9.68	14.72	11.96
cssz-82b	Central and South America	288.2196	-29.3950	9.68	8	5
cssz-83a	Central and South America	288.5944	-30.2923	5.36	14.81	11.96
cssz-83b	Central and South America	288.0938	-30.2517	5.36	8	5
cssz-84a	Central and South America	288.5223	-31.1639	3.8	14.9	11.96
cssz-84b	Central and South America	288.0163	-31.1351	3.8	8	5
cssz-85a	Central and South America	288.4748	-32.0416	2.55	15	11.96
cssz-85b	Central and South America	287.9635	-32.0223	2.55	8	5
cssz-86a	Central and South America	288.3901	-33.0041	7.01	15	11.96
cssz-86b	Central and South America	287.8768	-32.9512	7.01	8	5
cssz-87a	Central and South America	288.1050	-34.0583	19.4	15	11.96
cssz-87b	Central and South America	287.6115	-33.9142	19.4	8	5
cssz-88a	Central and South America	287.5309	-35.0437	32.81	15	11.96
cssz-88b	Central and South America	287.0862	-34.8086	32.81	8	5
cssz-88z	Central and South America	287.9308	-35.2545	32.81	30	24.9
cssz-89a	Central and South America	287.2380	-35.5993	14.52	16.67	11.96
cssz-89b	Central and South America	286.7261	-35.4914	14.52	8	5
cssz-89z	Central and South America	287.7014	-35.6968	14.52	30	26.3
cssz-90a	Central and South America	286.8442	-36.5645	22.64	18.33	11.96
cssz-90b	Central and South America	286.3548	-36.4004	22.64	8	5
cssz-90z	Central and South America	287.2916	-36.7142	22.64	30	27.68
cssz-91a	Central and South America	286.5925	-37.2488	10.9	20	11.96
cssz-91b	Central and South America	286.0721	-37.1690	10.9	8	5
cssz-91z	Central and South America	287.0726	-37.3224	10.9	30	29.06

continued on next page

Table B2: (continued)

Segment	Description	Longitude (°E)	Latitude (°N)	Strike (°)	Dip (°)	Depth (km)
cssz-92a	Central and South America	286.4254	-38.0945	8.23	20	11.96
cssz-92b	Central and South America	285.8948	-38.0341	8.23	8	5
cssz-92z	Central and South America	286.9303	-38.1520	8.23	26.67	29.06
cssz-93a	Central and South America	286.2047	-39.0535	13.46	20	11.96
cssz-93b	Central and South America	285.6765	-38.9553	13.46	8	5
cssz-93z	Central and South America	286.7216	-39.1495	13.46	23.33	29.06
cssz-94a	Central and South America	286.0772	-39.7883	3.4	20	11.96
cssz-94b	Central and South America	285.5290	-39.7633	3.4	8	5
cssz-94z	Central and South America	286.6255	-39.8133	3.4	20	29.06
cssz-95a	Central and South America	285.9426	-40.7760	9.84	20	11.96
cssz-95b	Central and South America	285.3937	-40.7039	9.84	8	5
cssz-95z	Central and South America	286.4921	-40.8481	9.84	20	29.06
cssz-96a	Central and South America	285.7839	-41.6303	7.6	20	11.96
cssz-96b	Central and South America	285.2245	-41.5745	7.6	8	5
cssz-96x	Central and South America	287.4652	-41.7977	7.6	20	63.26
cssz-96y	Central and South America	286.9043	-41.7419	7.6	20	46.16
cssz-96z	Central and South America	286.3439	-41.6861	7.6	20	29.06
cssz-97a	Central and South America	285.6695	-42.4882	5.3	20	11.96
cssz-97b	Central and South America	285.0998	-42.4492	5.3	8	5
cssz-97x	Central and South America	287.3809	-42.6052	5.3	20	63.26
cssz-97y	Central and South America	286.8101	-42.5662	5.3	20	46.16
cssz-97z	Central and South America	286.2396	-42.5272	5.3	20	29.06
cssz-98a	Central and South America	285.5035	-43.4553	10.53	20	11.96
cssz-98b	Central and South America	284.9322	-43.3782	10.53	8	5
cssz-98x	Central and South America	287.2218	-43.6866	10.53	20	63.26
cssz-98y	Central and South America	286.6483	-43.6095	10.53	20	46.16
cssz-98z	Central and South America	286.0755	-43.5324	10.53	20	29.06
cssz-99a	Central and South America	285.3700	-44.2595	4.86	20	11.96
cssz-99b	Central and South America	284.7830	-44.2237	4.86	8	5
cssz-99x	Central and South America	287.1332	-44.3669	4.86	20	63.26
cssz-99y	Central and South America	286.5451	-44.3311	4.86	20	46.16
cssz-99z	Central and South America	285.9574	-44.2953	4.86	20	29.06
cssz-100a	Central and South America	285.2713	-45.1664	5.68	20	11.96
cssz-100b	Central and South America	284.6758	-45.1246	5.68	8	5
cssz-100x	Central and South America	287.0603	-45.2918	5.68	20	63.26
cssz-100y	Central and South America	286.4635	-45.2500	5.68	20	46.16
cssz-100z	Central and South America	285.8672	-45.2082	5.68	20	29.06
cssz-101a	Central and South America	285.3080	-45.8607	352.6	20	9.36

continued on next page

Table B2: (continued)

Segment	Description	Longitude (°E)	Latitude (°N)	Strike (°)	Dip (°)	Depth (km)
cssz-101b	Central and South America	284.7067	-45.9152	352.6	5	5
cssz-101y	Central and South America	286.5089	-45.7517	352.6	20	43.56
cssz-101z	Central and South America	285.9088	-45.8062	352.6	20	26.46
cssz-102a	Central and South America	285.2028	-47.1185	17.72	5	9.36
cssz-102b	Central and South America	284.5772	-46.9823	17.72	5	5
cssz-102y	Central and South America	286.4588	-47.3909	17.72	5	18.07
cssz-102z	Central and South America	285.8300	-47.2547	17.72	5	13.72
cssz-103a	Central and South America	284.7075	-48.0396	23.37	7.5	11.53
cssz-103b	Central and South America	284.0972	-47.8630	23.37	7.5	5
cssz-103x	Central and South America	286.5511	-48.5694	23.37	7.5	31.11
cssz-103y	Central and South America	285.9344	-48.3928	23.37	7.5	24.58
cssz-103z	Central and South America	285.3199	-48.2162	23.37	7.5	18.05
cssz-104a	Central and South America	284.3440	-48.7597	14.87	10	13.68
cssz-104b	Central and South America	283.6962	-48.6462	14.87	10	5
cssz-104x	Central and South America	286.2962	-49.1002	14.87	10	39.73
cssz-104y	Central and South America	285.6440	-48.9867	14.87	10	31.05
cssz-104z	Central and South America	284.9933	-48.8732	14.87	10	22.36
cssz-105a	Central and South America	284.2312	-49.4198	0.25	9.67	13.4
cssz-105b	Central and South America	283.5518	-49.4179	0.25	9.67	5
cssz-105x	Central and South America	286.2718	-49.4255	0.25	9.67	38.59
cssz-105y	Central and South America	285.5908	-49.4236	0.25	9.67	30.2
cssz-105z	Central and South America	284.9114	-49.4217	0.25	9.67	21.8
cssz-106a	Central and South America	284.3730	-50.1117	347.5	9.25	13.04
cssz-106b	Central and South America	283.6974	-50.2077	347.5	9.25	5
cssz-106x	Central and South America	286.3916	-49.8238	347.5	9.25	37.15
cssz-106y	Central and South America	285.7201	-49.9198	347.5	9.25	29.11
cssz-106z	Central and South America	285.0472	-50.0157	347.5	9.25	21.07
cssz-107a	Central and South America	284.7130	-50.9714	346.5	9	12.82
cssz-107b	Central and South America	284.0273	-51.0751	346.5	9	5
cssz-107x	Central and South America	286.7611	-50.6603	346.5	9	36.29
cssz-107y	Central and South America	286.0799	-50.7640	346.5	9	28.47
cssz-107z	Central and South America	285.3972	-50.8677	346.5	9	20.64
cssz-108a	Central and South America	285.0378	-51.9370	352	8.67	12.54
cssz-108b	Central and South America	284.3241	-51.9987	352	8.67	5
cssz-108x	Central and South America	287.1729	-51.7519	352	8.67	35.15
cssz-108y	Central and South America	286.4622	-51.8136	352	8.67	27.61
cssz-108z	Central and South America	285.7505	-51.8753	352	8.67	20.07
cssz-109a	Central and South America	285.2635	-52.8439	353.1	8.33	12.24
cssz-109b	Central and South America	284.5326	-52.8974	353.1	8.33	5

continued on next page

Table B2: (continued)

Segment	Description	Longitude (°E)	Latitude (°N)	Strike (°)	Dip (°)	Depth (km)
cssz-109x	Central and South America	287.4508	-52.6834	353.1	8.33	33.97
cssz-109y	Central and South America	286.7226	-52.7369	353.1	8.33	26.73
cssz-109z	Central and South America	285.9935	-52.7904	353.1	8.33	19.49
cssz-110a	Central and South America	285.5705	-53.4139	334.2	8	11.96
cssz-110b	Central and South America	284.8972	-53.6076	334.2	8	5
cssz-110x	Central and South America	287.5724	-52.8328	334.2	8	32.83
cssz-110y	Central and South America	286.9081	-53.0265	334.2	8	25.88
cssz-110z	Central and South America	286.2408	-53.2202	334.2	8	18.92
cssz-111a	Central and South America	286.1627	-53.8749	313.8	8	11.96
cssz-111b	Central and South America	285.6382	-54.1958	313.8	8	5
cssz-111x	Central and South America	287.7124	-52.9122	313.8	8	32.83
cssz-111y	Central and South America	287.1997	-53.2331	313.8	8	25.88
cssz-111z	Central and South America	286.6832	-53.5540	313.8	8	18.92
cssz-112a	Central and South America	287.3287	-54.5394	316.4	8	11.96
cssz-112b	Central and South America	286.7715	-54.8462	316.4	8	5
cssz-112x	Central and South America	288.9756	-53.6190	316.4	8	32.83
cssz-112y	Central and South America	288.4307	-53.9258	316.4	8	25.88
cssz-112z	Central and South America	287.8817	-54.2326	316.4	8	18.92
cssz-113a	Central and South America	288.3409	-55.0480	307.6	8	11.96
cssz-113b	Central and South America	287.8647	-55.4002	307.6	8	5
cssz-113x	Central and South America	289.7450	-53.9914	307.6	8	32.83
cssz-113y	Central and South America	289.2810	-54.3436	307.6	8	25.88
cssz-113z	Central and South America	288.8130	-54.6958	307.6	8	18.92
cssz-114a	Central and South America	289.5342	-55.5026	301.5	8	11.96
cssz-114b	Central and South America	289.1221	-55.8819	301.5	8	5
cssz-114x	Central and South America	290.7472	-54.3647	301.5	8	32.83
cssz-114y	Central and South America	290.3467	-54.7440	301.5	8	25.88
cssz-114z	Central and South America	289.9424	-55.1233	301.5	8	18.92
cssz-115a	Central and South America	290.7682	-55.8485	292.7	8	11.96
cssz-115b	Central and South America	290.4608	-56.2588	292.7	8	5
cssz-115x	Central and South America	291.6714	-54.6176	292.7	8	32.83
cssz-115y	Central and South America	291.3734	-55.0279	292.7	8	25.88
cssz-115z	Central and South America	291.0724	-55.4382	292.7	8	18.92

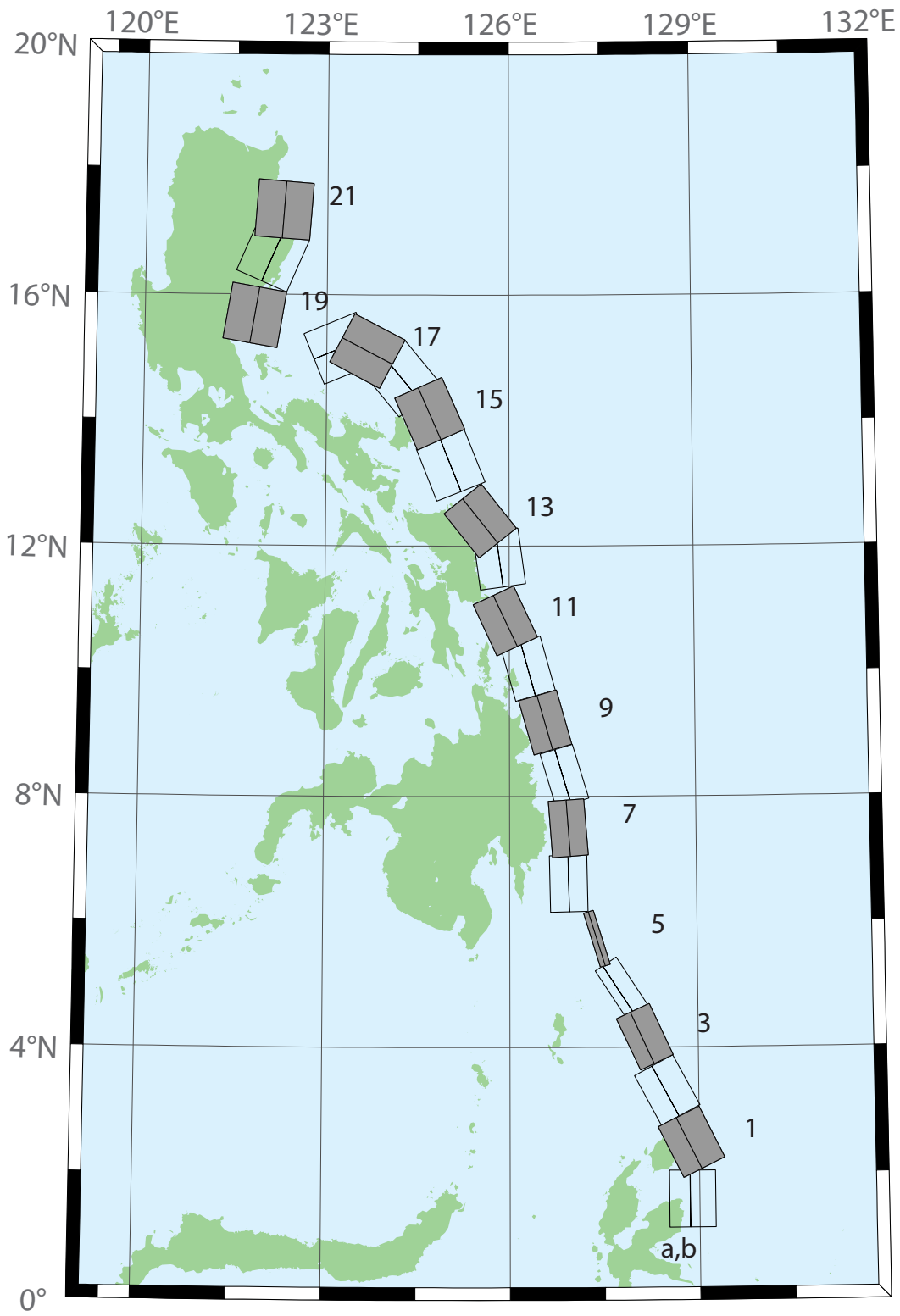


Figure B3: Eastern Philippines Subduction Zone unit sources.

Table B3: Earthquake parameters for Eastern Philippines Subduction Zone unit sources.

Segment	Description	Longitude (°E)	Latitude (°N)	Strike (°)	Dip (°)	Depth (km)
epsz-0a	Eastern Philippines	128.5264	1.5930	180	44	26.92
epsz-0b	Eastern Philippines	128.8496	1.5930	180	26	5
epsz-1a	Eastern Philippines	128.5521	2.3289	153.6	44.2	27.62
epsz-1b	Eastern Philippines	128.8408	2.4720	153.6	26.9	5
epsz-2a	Eastern Philippines	128.1943	3.1508	151.9	45.9	32.44
epsz-2b	Eastern Philippines	128.4706	3.2979	151.9	32.8	5.35
epsz-3a	Eastern Philippines	127.8899	4.0428	155.2	57.3	40.22
epsz-3b	Eastern Philippines	128.1108	4.1445	155.2	42.7	6.31
epsz-4a	Eastern Philippines	127.6120	4.8371	146.8	71.4	48.25
epsz-4b	Eastern Philippines	127.7324	4.9155	146.8	54.8	7.39
epsz-5a	Eastern Philippines	127.3173	5.7040	162.9	79.9	57.4
epsz-5b	Eastern Philippines	127.3930	5.7272	162.9	79.4	8.25
epsz-6a	Eastern Philippines	126.6488	6.6027	178.9	48.6	45.09
epsz-6b	Eastern Philippines	126.9478	6.6085	178.9	48.6	7.58
epsz-7a	Eastern Philippines	126.6578	7.4711	175.8	50.7	45.52
epsz-7b	Eastern Philippines	126.9439	7.4921	175.8	50.7	6.83
epsz-8a	Eastern Philippines	126.6227	8.2456	163.3	56.7	45.6
epsz-8b	Eastern Philippines	126.8614	8.3164	163.3	48.9	7.92
epsz-9a	Eastern Philippines	126.2751	9.0961	164.1	47	43.59
epsz-9b	Eastern Philippines	126.5735	9.1801	164.1	44.9	8.3
epsz-10a	Eastern Philippines	125.9798	9.9559	164.5	43.1	42.25
epsz-10b	Eastern Philippines	126.3007	10.0438	164.5	43.1	8.09
epsz-11a	Eastern Philippines	125.6079	10.6557	155	37.8	38.29
epsz-11b	Eastern Philippines	125.9353	10.8059	155	37.8	7.64
epsz-12a	Eastern Philippines	125.4697	11.7452	172.1	36	37.01
epsz-12b	Eastern Philippines	125.8374	11.7949	172.1	36	7.62
epsz-13a	Eastern Philippines	125.2238	12.1670	141.5	32.4	33.87
epsz-13b	Eastern Philippines	125.5278	12.4029	141.5	32.4	7.08
epsz-14a	Eastern Philippines	124.6476	13.1365	158.2	23	25.92
epsz-14b	Eastern Philippines	125.0421	13.2898	158.2	23	6.38
epsz-15a	Eastern Philippines	124.3107	13.9453	156.1	24.1	26.51
epsz-15b	Eastern Philippines	124.6973	14.1113	156.1	24.1	6.09
epsz-16a	Eastern Philippines	123.8998	14.4025	140.3	19.5	21.69
epsz-16b	Eastern Philippines	124.2366	14.6728	140.3	19.5	5
epsz-17a	Eastern Philippines	123.4604	14.7222	117.6	15.3	18.19
epsz-17b	Eastern Philippines	123.6682	15.1062	117.6	15.3	5
epsz-18a	Eastern Philippines	123.3946	14.7462	67.4	15	17.94
epsz-18b	Eastern Philippines	123.2219	15.1467	67.4	15	5
epsz-19a	Eastern Philippines	121.3638	15.7400	189.6	15	17.94
epsz-19b	Eastern Philippines	121.8082	15.6674	189.6	15	5
epsz-20a	Eastern Philippines	121.6833	16.7930	203.3	15	17.94
epsz-20b	Eastern Philippines	122.0994	16.6216	203.3	15	5
epsz-21a	Eastern Philippines	121.8279	17.3742	184.2	15	17.94
epsz-21b	Eastern Philippines	122.2814	17.3425	184.2	15	5

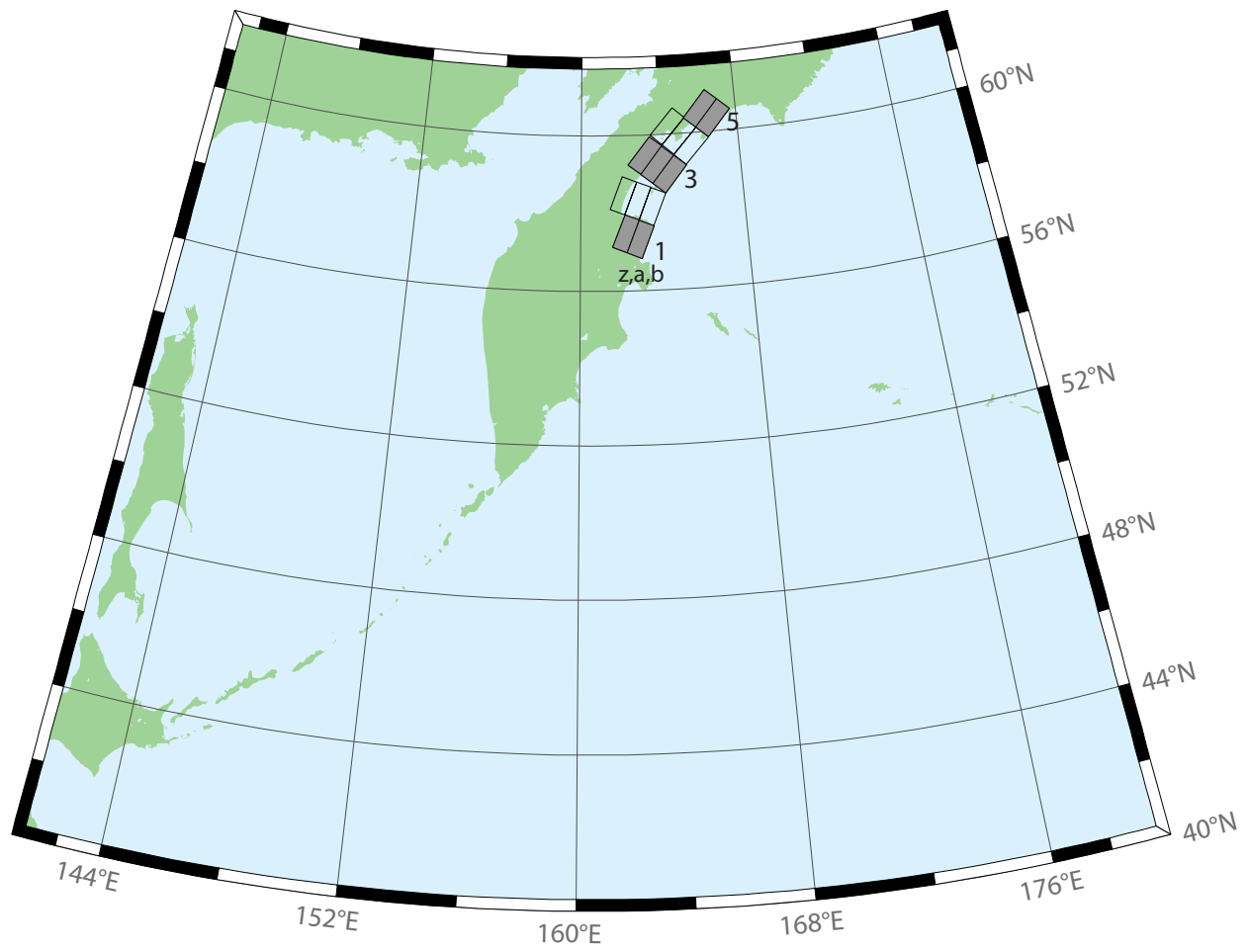


Figure B4: Kamchatka–Bering Subduction Zone unit sources.

Table B4: Earthquake parameters for Kamchatka–Bering Subduction Zone unit sources.

Segment	Description	Longitude (°E)	Latitude (°N)	Strike (°)	Dip (°)	Depth (km)
kbsz-1a	Kamchatka-Bering	161.8374	57.5485	201.5	29	26.13
kbsz-1b	Kamchatka-Bering	162.5162	57.4030	202.1	25	5
kbsz-2a	Kamchatka-Bering	162.4410	58.3816	201.7	29	26.13
kbsz-2b	Kamchatka-Bering	163.1344	58.2343	202.3	25	5
kbsz-2z	Kamchatka-Bering	161.7418	58.5249	201.1	29	50.37
kbsz-3a	Kamchatka-Bering	163.5174	59.3493	218.9	29	26.13
kbsz-3b	Kamchatka-Bering	164.1109	59.1001	219.4	25	5
kbsz-3z	Kamchatka-Bering	162.9150	59.5958	218.4	29	50.37
kbsz-4a	Kamchatka-Bering	164.7070	60.0632	222.2	29	26.13
kbsz-4b	Kamchatka-Bering	165.2833	59.7968	222.7	25	5
kbsz-4z	Kamchatka-Bering	164.1212	60.3270	221.7	29	50.37
kbsz-5a	Kamchatka-Bering	165.8652	60.7261	220.5	29	26.13
kbsz-5b	Kamchatka-Bering	166.4692	60.4683	221	25	5

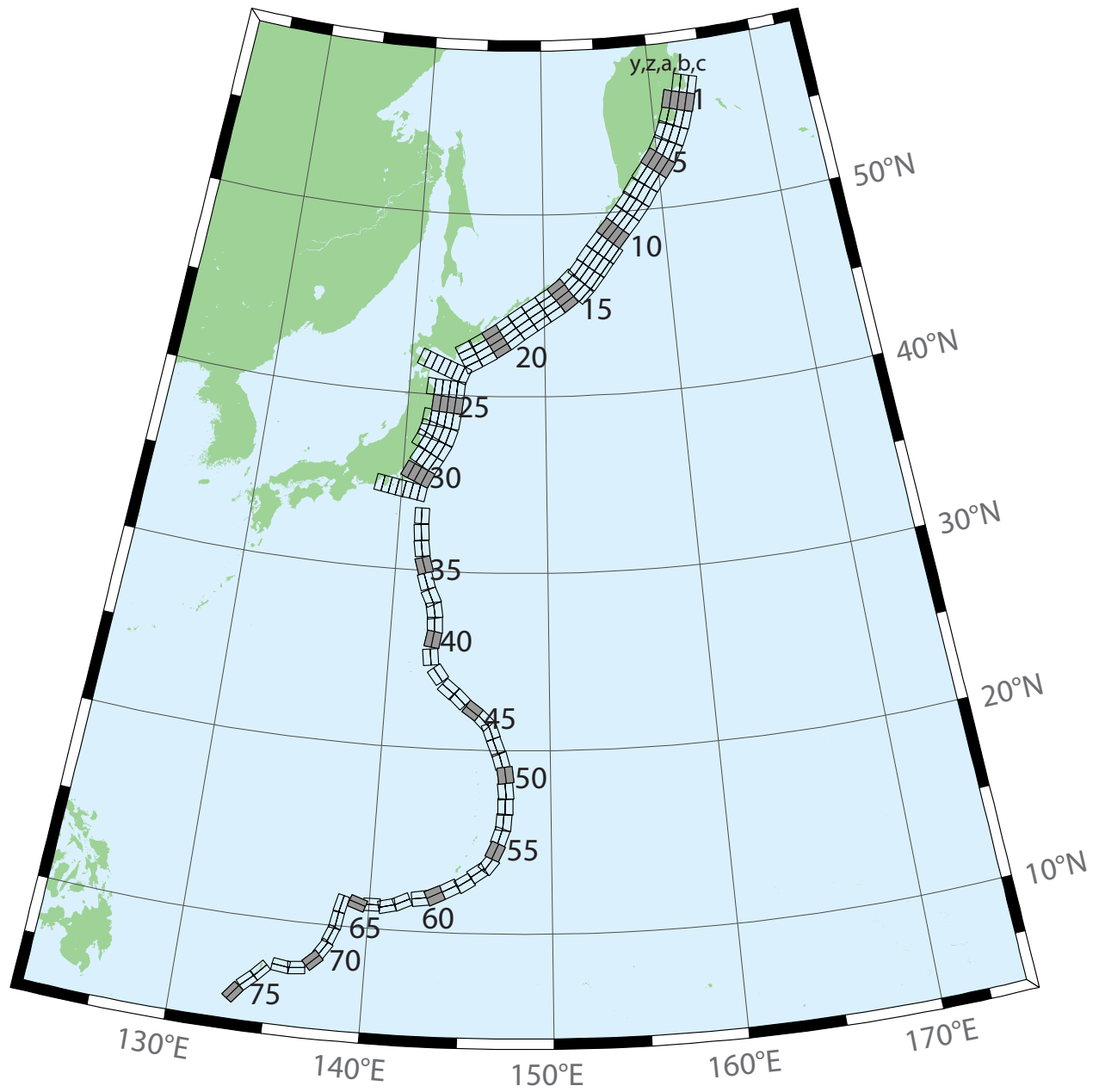


Figure B5: Kamchatka–Kuril–Japan–Izu–Mariana–Yap Subduction Zone unit sources.

Table B5: Earthquake parameters for Kamchatka-Kuril-Japan-Izu-Mariana-Yap Subduction Zone unit sources.

Segment	Description	Longitude (°E)	Latitude (°N)	Strike (°)	Dip (°)	Depth (km)
kisz-0a	Kamchatka-Kuril-Japan-Izu-Mariana-Yap	162.8200	56.3667	194.4	29	26.13
kisz-0b	Kamchatka-Kuril-Japan-Izu-Mariana-Yap	163.5057	56.2677	195	25	5
kisz-0z	Kamchatka-Kuril-Japan-Izu-Mariana-Yap	162.1309	56.4618	193.8	29	50.37
kisz-1a	Kamchatka-Kuril-Japan-Izu-Mariana-Yap	162.4318	55.5017	195	29	26.13
kisz-1b	Kamchatka-Kuril-Japan-Izu-Mariana-Yap	163.1000	55.4000	195	25	5
kisz-1y	Kamchatka-Kuril-Japan-Izu-Mariana-Yap	161.0884	55.7050	195	29	74.61
kisz-1z	Kamchatka-Kuril-Japan-Izu-Mariana-Yap	161.7610	55.6033	195	29	50.37
kisz-2a	Kamchatka-Kuril-Japan-Izu-Mariana-Yap	161.9883	54.6784	200	29	26.13
kisz-2b	Kamchatka-Kuril-Japan-Izu-Mariana-Yap	162.6247	54.5440	200	25	5
kisz-2y	Kamchatka-Kuril-Japan-Izu-Mariana-Yap	160.7072	54.9471	200	29	74.61
kisz-2z	Kamchatka-Kuril-Japan-Izu-Mariana-Yap	161.3488	54.8127	200	29	50.37
kisz-3a	Kamchatka-Kuril-Japan-Izu-Mariana-Yap	161.4385	53.8714	204	29	26.13
kisz-3b	Kamchatka-Kuril-Japan-Izu-Mariana-Yap	162.0449	53.7116	204	25	5
kisz-3y	Kamchatka-Kuril-Japan-Izu-Mariana-Yap	160.2164	54.1910	204	29	74.61
kisz-3z	Kamchatka-Kuril-Japan-Izu-Mariana-Yap	160.8286	54.0312	204	29	50.37
kisz-4a	Kamchatka-Kuril-Japan-Izu-Mariana-Yap	160.7926	53.1087	210	29	26.13
kisz-4b	Kamchatka-Kuril-Japan-Izu-Mariana-Yap	161.3568	52.9123	210	25	5
kisz-4y	Kamchatka-Kuril-Japan-Izu-Mariana-Yap	159.6539	53.5015	210	29	74.61
kisz-4z	Kamchatka-Kuril-Japan-Izu-Mariana-Yap	160.2246	53.3051	210	29	50.37
kisz-5a	Kamchatka-Kuril-Japan-Izu-Mariana-Yap	160.0211	52.4113	218	29	26.13
kisz-5b	Kamchatka-Kuril-Japan-Izu-Mariana-Yap	160.5258	52.1694	218	25	5
kisz-5y	Kamchatka-Kuril-Japan-Izu-Mariana-Yap	159.0005	52.8950	218	29	74.61
kisz-5z	Kamchatka-Kuril-Japan-Izu-Mariana-Yap	159.5122	52.6531	218	29	50.37
kisz-6a	Kamchatka-Kuril-Japan-Izu-Mariana-Yap	159.1272	51.7034	218	29	26.13
kisz-6b	Kamchatka-Kuril-Japan-Izu-Mariana-Yap	159.6241	51.4615	218	25	5
kisz-6y	Kamchatka-Kuril-Japan-Izu-Mariana-Yap	158.1228	52.1871	218	29	74.61
kisz-6z	Kamchatka-Kuril-Japan-Izu-Mariana-Yap	158.6263	51.9452	218	29	50.37
kisz-7a	Kamchatka-Kuril-Japan-Izu-Mariana-Yap	158.2625	50.9549	214	29	26.13
kisz-7b	Kamchatka-Kuril-Japan-Izu-Mariana-Yap	158.7771	50.7352	214	25	5
kisz-7y	Kamchatka-Kuril-Japan-Izu-Mariana-Yap	157.2236	51.3942	214	29	74.61
kisz-7z	Kamchatka-Kuril-Japan-Izu-Mariana-Yap	157.7443	51.1745	214	29	50.37
kisz-8a	Kamchatka-Kuril-Japan-Izu-Mariana-Yap	157.4712	50.2459	218	31	27.7
kisz-8b	Kamchatka-Kuril-Japan-Izu-Mariana-Yap	157.9433	50.0089	218	27	5
kisz-8y	Kamchatka-Kuril-Japan-Izu-Mariana-Yap	156.5176	50.7199	218	31	79.2
kisz-8z	Kamchatka-Kuril-Japan-Izu-Mariana-Yap	156.9956	50.4829	218	31	53.45
kisz-9a	Kamchatka-Kuril-Japan-Izu-Mariana-Yap	156.6114	49.5583	220	31	27.7
kisz-9b	Kamchatka-Kuril-Japan-Izu-Mariana-Yap	157.0638	49.3109	220	27	5
kisz-9y	Kamchatka-Kuril-Japan-Izu-Mariana-Yap	155.6974	50.0533	220	31	79.2
kisz-9z	Kamchatka-Kuril-Japan-Izu-Mariana-Yap	156.1556	49.8058	220	31	53.45

continued on next page

Table B5: (continued)

Segment	Description	Longitude (°E)	Latitude (°N)	Strike (°)	Dip (°)	Depth (km)
kisz-10a	Kamchatka-Kuril-Japan-Izu-Mariana-Yap	155.7294	48.8804	221	31	27.7
kisz-10b	Kamchatka-Kuril-Japan-Izu-Mariana-Yap	156.1690	48.6278	221	27	5
kisz-10y	Kamchatka-Kuril-Japan-Izu-Mariana-Yap	154.8413	49.3856	221	31	79.2
kisz-10z	Kamchatka-Kuril-Japan-Izu-Mariana-Yap	155.2865	49.1330	221	31	53.45
kisz-11a	Kamchatka-Kuril-Japan-Izu-Mariana-Yap	154.8489	48.1821	219	31	27.7
kisz-11b	Kamchatka-Kuril-Japan-Izu-Mariana-Yap	155.2955	47.9398	219	27	5
kisz-11y	Kamchatka-Kuril-Japan-Izu-Mariana-Yap	153.9472	48.6667	219	31	79.2
kisz-11z	Kamchatka-Kuril-Japan-Izu-Mariana-Yap	154.3991	48.4244	219	31	53.45
kisz-11c	Kamchatka-Kuril-Japan-Izu-Mariana-Yap	156.0358	47.5374	39	57.89	4.602
kisz-12a	Kamchatka-Kuril-Japan-Izu-Mariana-Yap	153.9994	47.4729	217	31	27.7
kisz-12b	Kamchatka-Kuril-Japan-Izu-Mariana-Yap	154.4701	47.2320	217	27	5
kisz-12y	Kamchatka-Kuril-Japan-Izu-Mariana-Yap	153.0856	47.9363	217	31	79.2
kisz-12z	Kamchatka-Kuril-Japan-Izu-Mariana-Yap	153.5435	47.7046	217	31	53.45
kisz-12c	Kamchatka-Kuril-Japan-Izu-Mariana-Yap	155.2208	46.8473	37	57.89	4.602
kisz-13a	Kamchatka-Kuril-Japan-Izu-Mariana-Yap	153.2239	46.7564	218	31	27.7
kisz-13b	Kamchatka-Kuril-Japan-Izu-Mariana-Yap	153.6648	46.5194	218	27	5
kisz-13y	Kamchatka-Kuril-Japan-Izu-Mariana-Yap	152.3343	47.2304	218	31	79.2
kisz-13z	Kamchatka-Kuril-Japan-Izu-Mariana-Yap	152.7801	46.9934	218	31	53.45
kisz-13c	Kamchatka-Kuril-Japan-Izu-Mariana-Yap	154.3957	46.1257	38	57.89	4.602
kisz-14a	Kamchatka-Kuril-Japan-Izu-Mariana-Yap	152.3657	46.1514	225	23	24.54
kisz-14b	Kamchatka-Kuril-Japan-Izu-Mariana-Yap	152.7855	45.8591	225	23	5
kisz-14y	Kamchatka-Kuril-Japan-Izu-Mariana-Yap	151.5172	46.7362	225	23	63.62
kisz-14z	Kamchatka-Kuril-Japan-Izu-Mariana-Yap	151.9426	46.4438	225	23	44.08
kisz-14c	Kamchatka-Kuril-Japan-Izu-Mariana-Yap	153.4468	45.3976	45	57.89	4.602
kisz-15a	Kamchatka-Kuril-Japan-Izu-Mariana-Yap	151.4663	45.5963	233	25	23.73
kisz-15b	Kamchatka-Kuril-Japan-Izu-Mariana-Yap	151.8144	45.2712	233	22	5
kisz-15y	Kamchatka-Kuril-Japan-Izu-Mariana-Yap	150.7619	46.2465	233	25	65.99
kisz-15z	Kamchatka-Kuril-Japan-Izu-Mariana-Yap	151.1151	45.9214	233	25	44.86
kisz-16a	Kamchatka-Kuril-Japan-Izu-Mariana-Yap	150.4572	45.0977	237	25	23.73
kisz-16b	Kamchatka-Kuril-Japan-Izu-Mariana-Yap	150.7694	44.7563	237	22	5
kisz-16y	Kamchatka-Kuril-Japan-Izu-Mariana-Yap	149.8253	45.7804	237	25	65.99
kisz-16z	Kamchatka-Kuril-Japan-Izu-Mariana-Yap	150.1422	45.4390	237	25	44.86
kisz-17a	Kamchatka-Kuril-Japan-Izu-Mariana-Yap	149.3989	44.6084	237	25	23.73
kisz-17b	Kamchatka-Kuril-Japan-Izu-Mariana-Yap	149.7085	44.2670	237	22	5
kisz-17y	Kamchatka-Kuril-Japan-Izu-Mariana-Yap	148.7723	45.2912	237	25	65.99
kisz-17z	Kamchatka-Kuril-Japan-Izu-Mariana-Yap	149.0865	44.9498	237	25	44.86
kisz-18a	Kamchatka-Kuril-Japan-Izu-Mariana-Yap	148.3454	44.0982	235	25	23.73
kisz-18b	Kamchatka-Kuril-Japan-Izu-Mariana-Yap	148.6687	43.7647	235	22	5
kisz-18y	Kamchatka-Kuril-Japan-Izu-Mariana-Yap	147.6915	44.7651	235	25	65.99

continued on next page

Table B5: (continued)

Segment	Description	Longitude (°E)	Latitude (°N)	Strike (°)	Dip (°)	Depth (km)
kisz-18z	Kamchatka-Kuril-Japan-Izu-Mariana-Yap	148.0194	44.4316	235	25	44.86
kisz-19a	Kamchatka-Kuril-Japan-Izu-Mariana-Yap	147.3262	43.5619	233	25	23.73
kisz-19b	Kamchatka-Kuril-Japan-Izu-Mariana-Yap	147.6625	43.2368	233	22	5
kisz-19y	Kamchatka-Kuril-Japan-Izu-Mariana-Yap	146.6463	44.2121	233	25	65.99
kisz-19z	Kamchatka-Kuril-Japan-Izu-Mariana-Yap	146.9872	43.8870	233	25	44.86
kisz-20a	Kamchatka-Kuril-Japan-Izu-Mariana-Yap	146.3513	43.0633	237	25	23.73
kisz-20b	Kamchatka-Kuril-Japan-Izu-Mariana-Yap	146.6531	42.7219	237	22	5
kisz-20y	Kamchatka-Kuril-Japan-Izu-Mariana-Yap	145.7410	43.7461	237	25	65.99
kisz-20z	Kamchatka-Kuril-Japan-Izu-Mariana-Yap	146.0470	43.4047	237	25	44.86
kisz-21a	Kamchatka-Kuril-Japan-Izu-Mariana-Yap	145.3331	42.5948	239	25	23.73
kisz-21b	Kamchatka-Kuril-Japan-Izu-Mariana-Yap	145.6163	42.2459	239	22	5
kisz-21y	Kamchatka-Kuril-Japan-Izu-Mariana-Yap	144.7603	43.2927	239	25	65.99
kisz-21z	Kamchatka-Kuril-Japan-Izu-Mariana-Yap	145.0475	42.9438	239	25	44.86
kisz-22a	Kamchatka-Kuril-Japan-Izu-Mariana-Yap	144.3041	42.1631	242	25	23.73
kisz-22b	Kamchatka-Kuril-Japan-Izu-Mariana-Yap	144.5605	41.8037	242	22	5
kisz-22y	Kamchatka-Kuril-Japan-Izu-Mariana-Yap	143.7854	42.8819	242	25	65.99
kisz-22z	Kamchatka-Kuril-Japan-Izu-Mariana-Yap	144.0455	42.5225	242	25	44.86
kisz-23a	Kamchatka-Kuril-Japan-Izu-Mariana-Yap	143.2863	41.3335	202	21	21.28
kisz-23b	Kamchatka-Kuril-Japan-Izu-Mariana-Yap	143.8028	41.1764	202	19	5
kisz-23v	Kamchatka-Kuril-Japan-Izu-Mariana-Yap	140.6816	42.1189	202	21	110.9
kisz-23w	Kamchatka-Kuril-Japan-Izu-Mariana-Yap	141.2050	41.9618	202	21	92.95
kisz-23x	Kamchatka-Kuril-Japan-Izu-Mariana-Yap	141.7273	41.8047	202	21	75.04
kisz-23y	Kamchatka-Kuril-Japan-Izu-Mariana-Yap	142.2482	41.6476	202	21	57.12
kisz-23z	Kamchatka-Kuril-Japan-Izu-Mariana-Yap	142.7679	41.4905	202	21	39.2
kisz-24a	Kamchatka-Kuril-Japan-Izu-Mariana-Yap	142.9795	40.3490	185	21	21.28
kisz-24b	Kamchatka-Kuril-Japan-Izu-Mariana-Yap	143.5273	40.3125	185	19	5
kisz-24x	Kamchatka-Kuril-Japan-Izu-Mariana-Yap	141.3339	40.4587	185	21	75.04
kisz-24y	Kamchatka-Kuril-Japan-Izu-Mariana-Yap	141.8827	40.4221	185	21	57.12
kisz-24z	Kamchatka-Kuril-Japan-Izu-Mariana-Yap	142.4312	40.3856	185	21	39.2
kisz-25a	Kamchatka-Kuril-Japan-Izu-Mariana-Yap	142.8839	39.4541	185	21	21.28
kisz-25b	Kamchatka-Kuril-Japan-Izu-Mariana-Yap	143.4246	39.4176	185	19	5
kisz-25y	Kamchatka-Kuril-Japan-Izu-Mariana-Yap	141.8012	39.5272	185	21	57.12
kisz-25z	Kamchatka-Kuril-Japan-Izu-Mariana-Yap	142.3426	39.4907	185	21	39.2
kisz-26a	Kamchatka-Kuril-Japan-Izu-Mariana-Yap	142.7622	38.5837	188	21	21.28
kisz-26b	Kamchatka-Kuril-Japan-Izu-Mariana-Yap	143.2930	38.5254	188	19	5
kisz-26x	Kamchatka-Kuril-Japan-Izu-Mariana-Yap	141.1667	38.7588	188	21	75.04
kisz-26y	Kamchatka-Kuril-Japan-Izu-Mariana-Yap	141.6990	38.7004	188	21	57.12
kisz-26z	Kamchatka-Kuril-Japan-Izu-Mariana-Yap	142.2308	38.6421	188	21	39.2
kisz-27a	Kamchatka-Kuril-Japan-Izu-Mariana-Yap	142.5320	37.7830	198	21	21.28

continued on next page

Table B5: (continued)

Segment	Description	Longitude (°E)	Latitude (°N)	Strike (°)	Dip (°)	Depth (km)
kisz-27b	Kamchatka-Kuril-Japan-Izu-Mariana-Yap	143.0357	37.6534	198	19	5
kisz-27x	Kamchatka-Kuril-Japan-Izu-Mariana-Yap	141.0142	38.1717	198	21	75.04
kisz-27y	Kamchatka-Kuril-Japan-Izu-Mariana-Yap	141.5210	38.0421	198	21	57.12
kisz-27z	Kamchatka-Kuril-Japan-Izu-Mariana-Yap	142.0269	37.9126	198	21	39.2
kisz-28a	Kamchatka-Kuril-Japan-Izu-Mariana-Yap	142.1315	37.0265	208	21	21.28
kisz-28b	Kamchatka-Kuril-Japan-Izu-Mariana-Yap	142.5941	36.8297	208	19	5
kisz-28x	Kamchatka-Kuril-Japan-Izu-Mariana-Yap	140.7348	37.6171	208	21	75.04
kisz-28y	Kamchatka-Kuril-Japan-Izu-Mariana-Yap	141.2016	37.4202	208	21	57.12
kisz-28z	Kamchatka-Kuril-Japan-Izu-Mariana-Yap	141.6671	37.2234	208	21	39.2
kisz-29a	Kamchatka-Kuril-Japan-Izu-Mariana-Yap	141.5970	36.2640	211	21	21.28
kisz-29b	Kamchatka-Kuril-Japan-Izu-Mariana-Yap	142.0416	36.0481	211	19	5
kisz-29y	Kamchatka-Kuril-Japan-Izu-Mariana-Yap	140.7029	36.6960	211	21	57.12
kisz-29z	Kamchatka-Kuril-Japan-Izu-Mariana-Yap	141.1506	36.4800	211	21	39.2
kisz-30a	Kamchatka-Kuril-Japan-Izu-Mariana-Yap	141.0553	35.4332	205	21	21.28
kisz-30b	Kamchatka-Kuril-Japan-Izu-Mariana-Yap	141.5207	35.2560	205	19	5
kisz-30y	Kamchatka-Kuril-Japan-Izu-Mariana-Yap	140.1204	35.7876	205	21	57.12
kisz-30z	Kamchatka-Kuril-Japan-Izu-Mariana-Yap	140.5883	35.6104	205	21	39.2
kisz-31a	Kamchatka-Kuril-Japan-Izu-Mariana-Yap	140.6956	34.4789	190	22	22.1
kisz-31b	Kamchatka-Kuril-Japan-Izu-Mariana-Yap	141.1927	34.4066	190	20	5
kisz-31v	Kamchatka-Kuril-Japan-Izu-Mariana-Yap	138.2025	34.8405	190	22	115.8
kisz-31w	Kamchatka-Kuril-Japan-Izu-Mariana-Yap	138.7021	34.7682	190	22	97.02
kisz-31x	Kamchatka-Kuril-Japan-Izu-Mariana-Yap	139.2012	34.6958	190	22	78.29
kisz-31y	Kamchatka-Kuril-Japan-Izu-Mariana-Yap	139.6997	34.6235	190	22	59.56
kisz-31z	Kamchatka-Kuril-Japan-Izu-Mariana-Yap	140.1979	34.5512	190	22	40.83
kisz-32a	Kamchatka-Kuril-Japan-Izu-Mariana-Yap	141.0551	33.0921	180	32	23.48
kisz-32b	Kamchatka-Kuril-Japan-Izu-Mariana-Yap	141.5098	33.0921	180	21.69	5
kisz-33a	Kamchatka-Kuril-Japan-Izu-Mariana-Yap	141.0924	32.1047	173.8	27.65	20.67
kisz-33b	Kamchatka-Kuril-Japan-Izu-Mariana-Yap	141.5596	32.1473	173.8	18.27	5
kisz-34a	Kamchatka-Kuril-Japan-Izu-Mariana-Yap	141.1869	31.1851	172.1	25	18.26
kisz-34b	Kamchatka-Kuril-Japan-Izu-Mariana-Yap	141.6585	31.2408	172.1	15.38	5
kisz-35a	Kamchatka-Kuril-Japan-Izu-Mariana-Yap	141.4154	30.1707	163	25	17.12
kisz-35b	Kamchatka-Kuril-Japan-Izu-Mariana-Yap	141.8662	30.2899	163	14.03	5
kisz-36a	Kamchatka-Kuril-Japan-Izu-Mariana-Yap	141.6261	29.2740	161.7	25.73	18.71
kisz-36b	Kamchatka-Kuril-Japan-Izu-Mariana-Yap	142.0670	29.4012	161.7	15.91	5
kisz-37a	Kamchatka-Kuril-Japan-Izu-Mariana-Yap	142.0120	28.3322	154.7	20	14.54
kisz-37b	Kamchatka-Kuril-Japan-Izu-Mariana-Yap	142.4463	28.5124	154.7	11	5
kisz-38a	Kamchatka-Kuril-Japan-Izu-Mariana-Yap	142.2254	27.6946	170.3	20	14.54
kisz-38b	Kamchatka-Kuril-Japan-Izu-Mariana-Yap	142.6955	27.7659	170.3	11	5
kisz-39a	Kamchatka-Kuril-Japan-Izu-Mariana-Yap	142.3085	26.9127	177.2	24.23	17.42

continued on next page

Table B5: (continued)

Segment	Description	Longitude (°E)	Latitude (°N)	Strike (°)	Dip (°)	Depth (km)
kisz-39b	Kamchatka-Kuril-Japan-Izu-Mariana-Yap	142.7674	26.9325	177.2	14.38	5
kisz-40a	Kamchatka-Kuril-Japan-Izu-Mariana-Yap	142.2673	26.1923	189.4	26.49	22.26
kisz-40b	Kamchatka-Kuril-Japan-Izu-Mariana-Yap	142.7090	26.1264	189.4	20.2	5
kisz-41a	Kamchatka-Kuril-Japan-Izu-Mariana-Yap	142.1595	25.0729	173.7	22.07	19.08
kisz-41b	Kamchatka-Kuril-Japan-Izu-Mariana-Yap	142.6165	25.1184	173.7	16.36	5
kisz-42a	Kamchatka-Kuril-Japan-Izu-Mariana-Yap	142.7641	23.8947	143.5	21.54	18.4
kisz-42b	Kamchatka-Kuril-Japan-Izu-Mariana-Yap	143.1321	24.1432	143.5	15.54	5
kisz-43a	Kamchatka-Kuril-Japan-Izu-Mariana-Yap	143.5281	23.0423	129.2	23.02	18.77
kisz-43b	Kamchatka-Kuril-Japan-Izu-Mariana-Yap	143.8128	23.3626	129.2	15.99	5
kisz-44a	Kamchatka-Kuril-Japan-Izu-Mariana-Yap	144.2230	22.5240	134.6	28.24	18.56
kisz-44b	Kamchatka-Kuril-Japan-Izu-Mariana-Yap	144.5246	22.8056	134.6	15.74	5
kisz-45a	Kamchatka-Kuril-Japan-Izu-Mariana-Yap	145.0895	21.8866	125.8	36.73	22.79
kisz-45b	Kamchatka-Kuril-Japan-Izu-Mariana-Yap	145.3171	22.1785	125.8	20.84	5
kisz-46a	Kamchatka-Kuril-Japan-Izu-Mariana-Yap	145.6972	21.3783	135.9	30.75	20.63
kisz-46b	Kamchatka-Kuril-Japan-Izu-Mariana-Yap	145.9954	21.6469	135.9	18.22	5
kisz-47a	Kamchatka-Kuril-Japan-Izu-Mariana-Yap	146.0406	20.9341	160.1	29.87	19.62
kisz-47b	Kamchatka-Kuril-Japan-Izu-Mariana-Yap	146.4330	21.0669	160.1	17	5
kisz-48a	Kamchatka-Kuril-Japan-Izu-Mariana-Yap	146.3836	20.0690	158	32.75	19.68
kisz-48b	Kamchatka-Kuril-Japan-Izu-Mariana-Yap	146.7567	20.2108	158	17.07	5
kisz-49a	Kamchatka-Kuril-Japan-Izu-Mariana-Yap	146.6689	19.3123	164.5	25.07	21.41
kisz-49b	Kamchatka-Kuril-Japan-Izu-Mariana-Yap	147.0846	19.4212	164.5	19.16	5
kisz-50a	Kamchatka-Kuril-Japan-Izu-Mariana-Yap	146.9297	18.5663	172.1	22	22.1
kisz-50b	Kamchatka-Kuril-Japan-Izu-Mariana-Yap	147.3650	18.6238	172.1	20	5
kisz-51a	Kamchatka-Kuril-Japan-Izu-Mariana-Yap	146.9495	17.7148	175.1	22.06	22.04
kisz-51b	Kamchatka-Kuril-Japan-Izu-Mariana-Yap	147.3850	17.7503	175.1	19.93	5
kisz-52a	Kamchatka-Kuril-Japan-Izu-Mariana-Yap	146.9447	16.8869	180	25.51	18.61
kisz-52b	Kamchatka-Kuril-Japan-Izu-Mariana-Yap	147.3683	16.8869	180	15.79	5
kisz-53a	Kamchatka-Kuril-Japan-Izu-Mariana-Yap	146.8626	16.0669	185.2	27.39	18.41
kisz-53b	Kamchatka-Kuril-Japan-Izu-Mariana-Yap	147.2758	16.0309	185.2	15.56	5
kisz-54a	Kamchatka-Kuril-Japan-Izu-Mariana-Yap	146.7068	15.3883	199.1	28.12	20.91
kisz-54b	Kamchatka-Kuril-Japan-Izu-Mariana-Yap	147.0949	15.2590	199.1	18.56	5
kisz-55a	Kamchatka-Kuril-Japan-Izu-Mariana-Yap	146.4717	14.6025	204.3	29.6	26.27
kisz-55b	Kamchatka-Kuril-Japan-Izu-Mariana-Yap	146.8391	14.4415	204.3	25.18	5
kisz-56a	Kamchatka-Kuril-Japan-Izu-Mariana-Yap	146.1678	13.9485	217.4	32.04	26.79
kisz-56b	Kamchatka-Kuril-Japan-Izu-Mariana-Yap	146.4789	13.7170	217.4	25.84	5
kisz-57a	Kamchatka-Kuril-Japan-Izu-Mariana-Yap	145.6515	13.5576	235.8	37	24.54
kisz-57b	Kamchatka-Kuril-Japan-Izu-Mariana-Yap	145.8586	13.2609	235.8	23	5
kisz-58a	Kamchatka-Kuril-Japan-Izu-Mariana-Yap	144.9648	12.9990	237.8	37.72	24.54
kisz-58b	Kamchatka-Kuril-Japan-Izu-Mariana-Yap	145.1589	12.6984	237.8	23	5

continued on next page

Table B5: (continued)

Segment	Description	Longitude (°E)	Latitude (°N)	Strike (°)	Dip (°)	Depth (km)
kisz-59a	Kamchatka-Kuril-Japan-Izu-Mariana-Yap	144.1799	12.6914	242.9	34.33	22.31
kisz-59b	Kamchatka-Kuril-Japan-Izu-Mariana-Yap	144.3531	12.3613	242.9	20.25	5
kisz-60a	Kamchatka-Kuril-Japan-Izu-Mariana-Yap	143.3687	12.3280	244.9	30.9	20.62
kisz-60b	Kamchatka-Kuril-Japan-Izu-Mariana-Yap	143.5355	11.9788	244.9	18.2	5
kisz-61a	Kamchatka-Kuril-Japan-Izu-Mariana-Yap	142.7051	12.1507	261.8	35.41	25.51
kisz-61b	Kamchatka-Kuril-Japan-Izu-Mariana-Yap	142.7582	11.7883	261.8	24.22	5
kisz-62a	Kamchatka-Kuril-Japan-Izu-Mariana-Yap	141.6301	11.8447	245.7	39.86	34.35
kisz-62b	Kamchatka-Kuril-Japan-Izu-Mariana-Yap	141.7750	11.5305	245.7	35.94	5
kisz-63a	Kamchatka-Kuril-Japan-Izu-Mariana-Yap	140.8923	11.5740	256.2	42	38.46
kisz-63b	Kamchatka-Kuril-Japan-Izu-Mariana-Yap	140.9735	11.2498	256.2	42	5
kisz-64a	Kamchatka-Kuril-Japan-Izu-Mariana-Yap	140.1387	11.6028	269.6	42.48	38.77
kisz-64b	Kamchatka-Kuril-Japan-Izu-Mariana-Yap	140.1410	11.2716	269.6	42.48	5
kisz-65a	Kamchatka-Kuril-Japan-Izu-Mariana-Yap	139.4595	11.5883	288.7	44.16	39.83
kisz-65b	Kamchatka-Kuril-Japan-Izu-Mariana-Yap	139.3541	11.2831	288.7	44.16	5
kisz-66a	Kamchatka-Kuril-Japan-Izu-Mariana-Yap	138.1823	11.2648	193.1	45	40.36
kisz-66b	Kamchatka-Kuril-Japan-Izu-Mariana-Yap	138.4977	11.1929	193.1	45	5
kisz-67a	Kamchatka-Kuril-Japan-Izu-Mariana-Yap	137.9923	10.3398	189.8	45	40.36
kisz-67b	Kamchatka-Kuril-Japan-Izu-Mariana-Yap	138.3104	10.2856	189.8	45	5
kisz-68a	Kamchatka-Kuril-Japan-Izu-Mariana-Yap	137.7607	9.6136	201.7	45	40.36
kisz-68b	Kamchatka-Kuril-Japan-Izu-Mariana-Yap	138.0599	9.4963	201.7	45	5
kisz-69a	Kamchatka-Kuril-Japan-Izu-Mariana-Yap	137.4537	8.8996	213.5	45	40.36
kisz-69b	Kamchatka-Kuril-Japan-Izu-Mariana-Yap	137.7215	8.7241	213.5	45	5
kisz-70a	Kamchatka-Kuril-Japan-Izu-Mariana-Yap	137.0191	8.2872	226.5	45	40.36
kisz-70b	Kamchatka-Kuril-Japan-Izu-Mariana-Yap	137.2400	8.0569	226.5	45	5
kisz-71a	Kamchatka-Kuril-Japan-Izu-Mariana-Yap	136.3863	7.9078	263.9	45	40.36
kisz-71b	Kamchatka-Kuril-Japan-Izu-Mariana-Yap	136.4202	7.5920	263.9	45	5
kisz-72a	Kamchatka-Kuril-Japan-Izu-Mariana-Yap	135.6310	7.9130	276.9	45	40.36
kisz-72b	Kamchatka-Kuril-Japan-Izu-Mariana-Yap	135.5926	7.5977	276.9	45	5
kisz-73a	Kamchatka-Kuril-Japan-Izu-Mariana-Yap	134.3296	7.4541	224	45	40.36
kisz-73b	Kamchatka-Kuril-Japan-Izu-Mariana-Yap	134.5600	7.2335	224	45	5
kisz-74a	Kamchatka-Kuril-Japan-Izu-Mariana-Yap	133.7125	6.8621	228.1	45	40.36
kisz-74b	Kamchatka-Kuril-Japan-Izu-Mariana-Yap	133.9263	6.6258	228.1	45	5
kisz-75a	Kamchatka-Kuril-Japan-Izu-Mariana-Yap	133.0224	6.1221	217.7	45	40.36
kisz-75b	Kamchatka-Kuril-Japan-Izu-Mariana-Yap	133.2751	5.9280	217.7	45	5

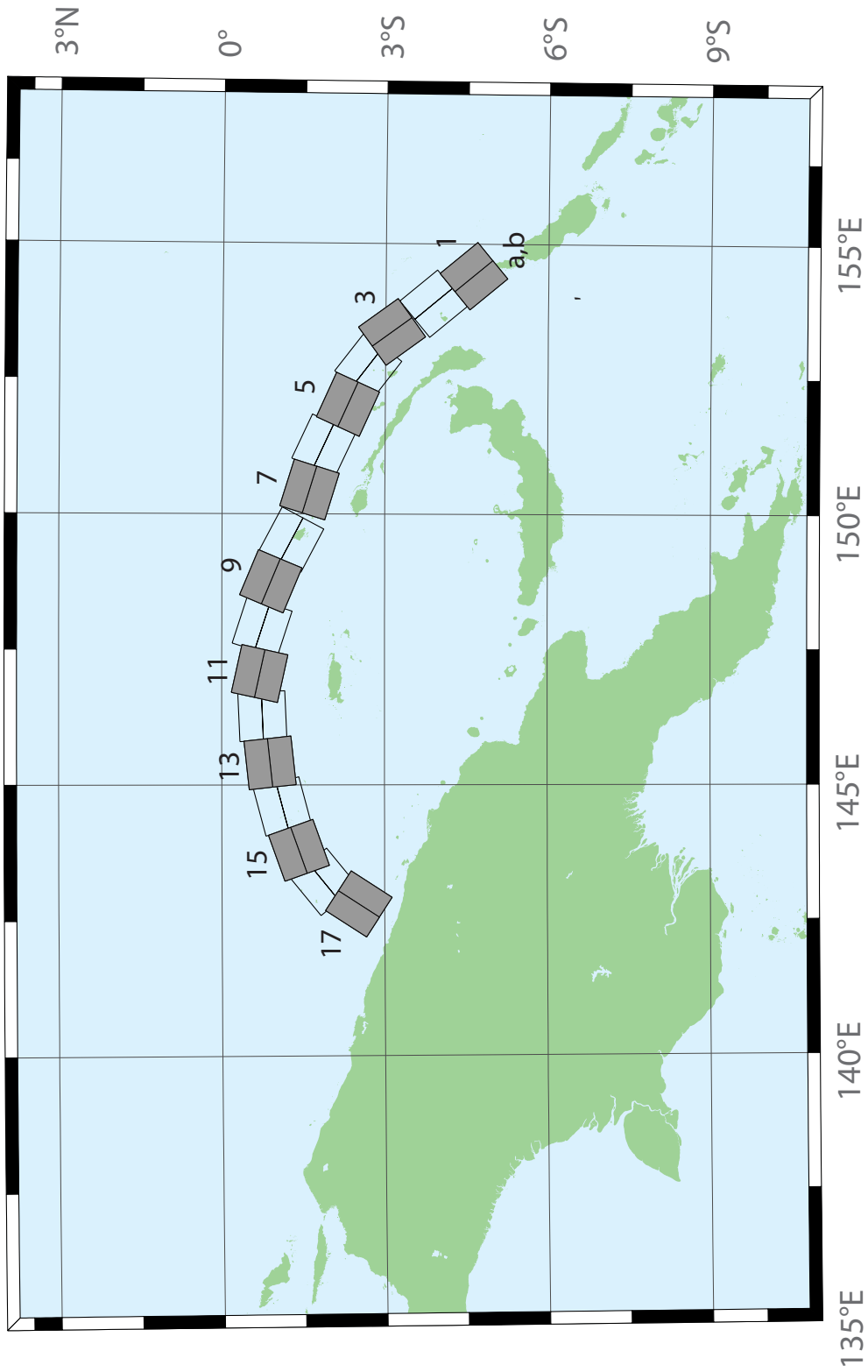


Figure B6: Manus–Oceanic Convergent Boundary Subduction Zone unit sources.

Table B6: Earthquake parameters for Manus–Oceanic Convergent Boundary Subduction Zone unit sources.

Segment	Description	Longitude (°E)	Latitude (°N)	Strike (°)	Dip (°)	Depth (km)
mosz-1a	Manus-Oceanic Convergent Boundary	154.0737	-4.8960	140.2	15	15.88
mosz-1b	Manus-Oceanic Convergent Boundary	154.4082	-4.6185	140.2	15	2.94
mosz-2a	Manus-Oceanic Convergent Boundary	153.5589	-4.1575	140.2	15	15.91
mosz-2b	Manus-Oceanic Convergent Boundary	153.8931	-3.8800	140.2	15	2.97
mosz-3a	Manus-Oceanic Convergent Boundary	153.0151	-3.3716	143.9	15	16.64
mosz-3b	Manus-Oceanic Convergent Boundary	153.3662	-3.1160	143.9	15	3.7
mosz-4a	Manus-Oceanic Convergent Boundary	152.4667	-3.0241	127.7	15	17.32
mosz-4b	Manus-Oceanic Convergent Boundary	152.7321	-2.6806	127.7	15	4.38
mosz-5a	Manus-Oceanic Convergent Boundary	151.8447	-2.7066	114.3	15	17.57
mosz-5b	Manus-Oceanic Convergent Boundary	152.0235	-2.3112	114.3	15	4.63
mosz-6a	Manus-Oceanic Convergent Boundary	151.0679	-2.2550	115	15	17.66
mosz-6b	Manus-Oceanic Convergent Boundary	151.2513	-1.8618	115	15	4.72
mosz-7a	Manus-Oceanic Convergent Boundary	150.3210	-2.0236	107.2	15	17.73
mosz-7b	Manus-Oceanic Convergent Boundary	150.4493	-1.6092	107.2	15	4.79
mosz-8a	Manus-Oceanic Convergent Boundary	149.3226	-1.6666	117.8	15	17.83
mosz-8b	Manus-Oceanic Convergent Boundary	149.5251	-1.2829	117.8	15	4.89
mosz-9a	Manus-Oceanic Convergent Boundary	148.5865	-1.3017	112.7	15	17.84
mosz-9b	Manus-Oceanic Convergent Boundary	148.7540	-0.9015	112.7	15	4.9
mosz-10a	Manus-Oceanic Convergent Boundary	147.7760	-1.1560	108	15	17.78
mosz-10b	Manus-Oceanic Convergent Boundary	147.9102	-0.7434	108	15	4.84
mosz-11a	Manus-Oceanic Convergent Boundary	146.9596	-1.1226	102.5	15	17.54
mosz-11b	Manus-Oceanic Convergent Boundary	147.0531	-0.6990	102.5	15	4.6
mosz-12a	Manus-Oceanic Convergent Boundary	146.2858	-1.1820	87.48	15	17.29
mosz-12b	Manus-Oceanic Convergent Boundary	146.2667	-0.7486	87.48	15	4.35
mosz-13a	Manus-Oceanic Convergent Boundary	145.4540	-1.3214	83.75	15	17.34
mosz-13b	Manus-Oceanic Convergent Boundary	145.4068	-0.8901	83.75	15	4.4
mosz-14a	Manus-Oceanic Convergent Boundary	144.7151	-1.5346	75.09	15	17.21
mosz-14b	Manus-Oceanic Convergent Boundary	144.6035	-1.1154	75.09	15	4.27
mosz-15a	Manus-Oceanic Convergent Boundary	143.9394	-1.8278	70.43	15	16.52
mosz-15b	Manus-Oceanic Convergent Boundary	143.7940	-1.4190	70.43	15	3.58
mosz-16a	Manus-Oceanic Convergent Boundary	143.4850	-2.2118	50.79	15	15.86
mosz-16b	Manus-Oceanic Convergent Boundary	143.2106	-1.8756	50.79	15	2.92
mosz-17a	Manus-Oceanic Convergent Boundary	143.1655	-2.7580	33	15	16.64
mosz-17b	Manus-Oceanic Convergent Boundary	142.8013	-2.5217	33	15	3.7

Table B7: Earthquake parameters for New Guinea Subduction Zone unit sources.

Segment	Description	Longitude (°E)	Latitude (°N)	Strike (°)	Dip (°)	Depth (km)
ngsz-1a	New Guinea	143.6063	-4.3804	120	29	25.64
ngsz-1b	New Guinea	143.8032	-4.0402	120	29	1.4
ngsz-2a	New Guinea	142.9310	-3.9263	114	27.63	20.1
ngsz-2b	New Guinea	143.0932	-3.5628	114	21.72	1.6
ngsz-3a	New Guinea	142.1076	-3.5632	114	20.06	18.73
ngsz-3b	New Guinea	142.2795	-3.1778	114	15.94	5
ngsz-4a	New Guinea	141.2681	-3.2376	114	21	17.76
ngsz-4b	New Guinea	141.4389	-2.8545	114	14.79	5
ngsz-5a	New Guinea	140.4592	-2.8429	114	21.26	16.14
ngsz-5b	New Guinea	140.6296	-2.4605	114	12.87	5
ngsz-6a	New Guinea	139.6288	-2.4960	114	22.72	15.4
ngsz-6b	New Guinea	139.7974	-2.1175	114	12	5
ngsz-7a	New Guinea	138.8074	-2.1312	114	21.39	15.4
ngsz-7b	New Guinea	138.9776	-1.7491	114	12	5
ngsz-8a	New Guinea	138.0185	-1.7353	113.1	18.79	15.14
ngsz-8b	New Guinea	138.1853	-1.3441	113.1	11.7	5
ngsz-9a	New Guinea	137.1805	-1.5037	111	15.24	13.23
ngsz-9b	New Guinea	137.3358	-1.0991	111	9.47	5
ngsz-10a	New Guinea	136.3418	-1.1774	111	13.51	11.09
ngsz-10b	New Guinea	136.4983	-0.7697	111	7	5
ngsz-11a	New Guinea	135.4984	-0.8641	111	11.38	12.49
ngsz-11b	New Guinea	135.6562	-0.4530	111	8.62	5
ngsz-12a	New Guinea	134.6759	-0.5216	110.5	10	13.68
ngsz-12b	New Guinea	134.8307	-0.1072	110.5	10	5
ngsz-13a	New Guinea	133.3065	-1.0298	99.5	10	13.68
ngsz-13b	New Guinea	133.3795	-0.5935	99.5	10	5
ngsz-14a	New Guinea	132.4048	-0.8816	99.5	10	13.68
ngsz-14b	New Guinea	132.4778	-0.4453	99.5	10	5
ngsz-15a	New Guinea	131.5141	-0.7353	99.5	10	13.68
ngsz-15b	New Guinea	131.5871	-0.2990	99.5	10	5

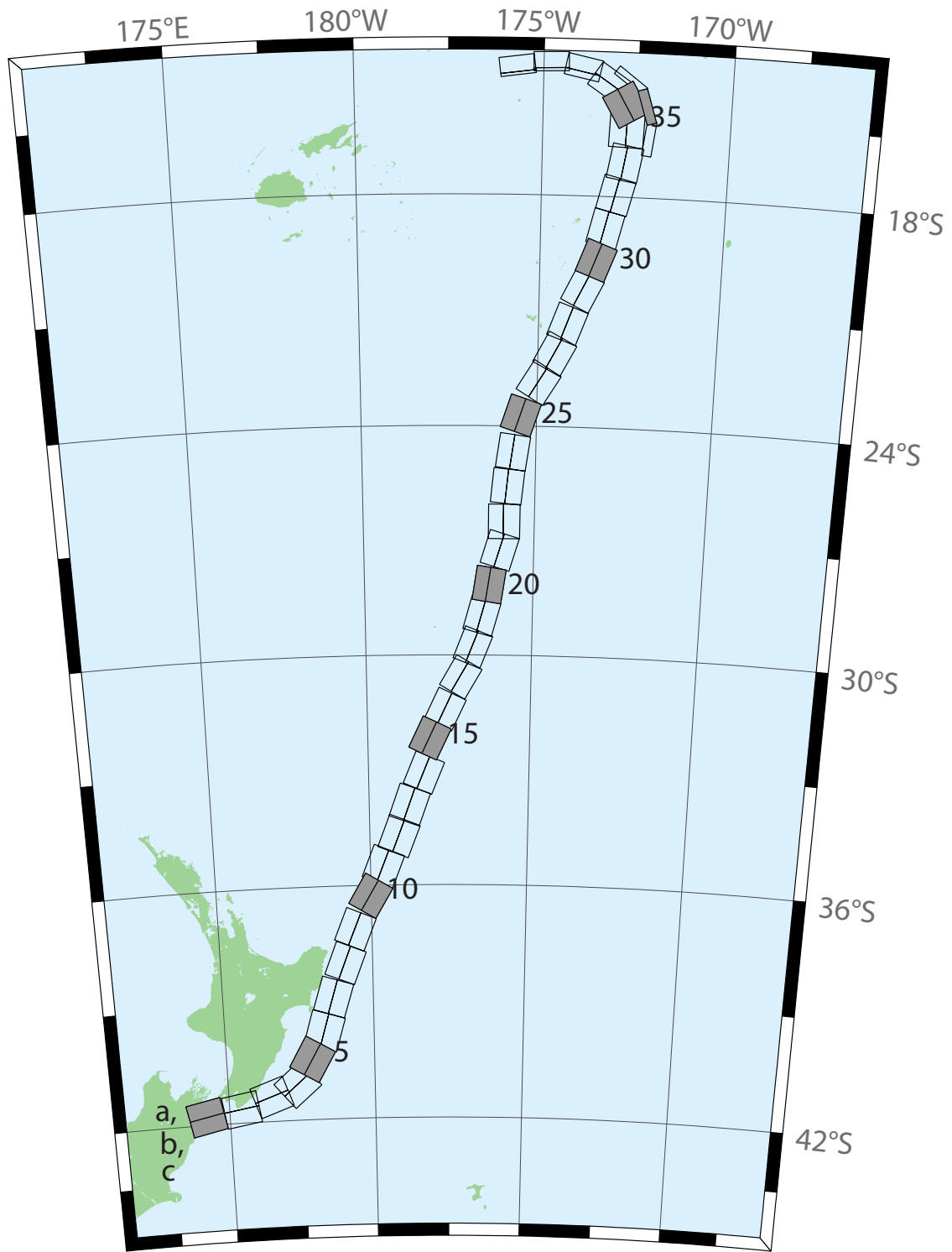


Figure B8: New Zealand–Kermadec–Tonga Subduction Zone unit sources.

Table B8: Earthquake parameters for New Zealand–Kermadec–Tonga Subduction Zone unit sources.

Segment	Description	Longitude (°E)	Latitude (°N)	Strike (°)	Dip (°)	Depth (km)
ntsz-1a	New Zealand–Kermadec–Tonga	174.0985	-41.3951	258.6	24	25.34
ntsz-1b	New Zealand–Kermadec–Tonga	174.2076	-41.7973	258.6	24	5
ntsz-2a	New Zealand–Kermadec–Tonga	175.3289	-41.2592	260.6	29.38	23.17
ntsz-2b	New Zealand–Kermadec–Tonga	175.4142	-41.6454	260.6	21.31	5
ntsz-3a	New Zealand–Kermadec–Tonga	176.2855	-40.9950	250.7	29.54	21.74
ntsz-3b	New Zealand–Kermadec–Tonga	176.4580	-41.3637	250.7	19.56	5
ntsz-4a	New Zealand–Kermadec–Tonga	177.0023	-40.7679	229.4	24.43	18.87
ntsz-4b	New Zealand–Kermadec–Tonga	177.3552	-41.0785	229.4	16.1	5
ntsz-5a	New Zealand–Kermadec–Tonga	177.4114	-40.2396	210	18.8	19.29
ntsz-5b	New Zealand–Kermadec–Tonga	177.8951	-40.4525	210	16.61	5
ntsz-6a	New Zealand–Kermadec–Tonga	177.8036	-39.6085	196.7	18.17	15.8
ntsz-6b	New Zealand–Kermadec–Tonga	178.3352	-39.7310	196.7	12.48	5
ntsz-7a	New Zealand–Kermadec–Tonga	178.1676	-38.7480	197	28.1	17.85
ntsz-7b	New Zealand–Kermadec–Tonga	178.6541	-38.8640	197	14.89	5
ntsz-8a	New Zealand–Kermadec–Tonga	178.6263	-37.8501	201.4	31.47	18.78
ntsz-8b	New Zealand–Kermadec–Tonga	179.0788	-37.9899	201.4	16	5
ntsz-9a	New Zealand–Kermadec–Tonga	178.9833	-36.9770	202.2	29.58	20.02
ntsz-9b	New Zealand–Kermadec–Tonga	179.4369	-37.1245	202.2	17.48	5
ntsz-10a	New Zealand–Kermadec–Tonga	179.5534	-36.0655	210.6	32.1	20.72
ntsz-10b	New Zealand–Kermadec–Tonga	179.9595	-36.2593	210.6	18.32	5
ntsz-11a	New Zealand–Kermadec–Tonga	179.9267	-35.3538	201.7	25	16.09
ntsz-11b	New Zealand–Kermadec–Tonga	180.3915	-35.5040	201.7	12.81	5
ntsz-12a	New Zealand–Kermadec–Tonga	180.4433	-34.5759	201.2	25	15.46
ntsz-12b	New Zealand–Kermadec–Tonga	180.9051	-34.7230	201.2	12.08	5
ntsz-13a	New Zealand–Kermadec–Tonga	180.7990	-33.7707	199.8	25.87	19.06
ntsz-13b	New Zealand–Kermadec–Tonga	181.2573	-33.9073	199.8	16.33	5
ntsz-14a	New Zealand–Kermadec–Tonga	181.2828	-32.9288	202.4	31.28	22.73
ntsz-14b	New Zealand–Kermadec–Tonga	181.7063	-33.0751	202.4	20.77	5
ntsz-15a	New Zealand–Kermadec–Tonga	181.4918	-32.0035	205.4	32.33	22.64
ntsz-15b	New Zealand–Kermadec–Tonga	181.8967	-32.1665	205.4	20.66	5
ntsz-16a	New Zealand–Kermadec–Tonga	181.9781	-31.2535	205.5	34.29	23.59
ntsz-16b	New Zealand–Kermadec–Tonga	182.3706	-31.4131	205.5	21.83	5
ntsz-17a	New Zealand–Kermadec–Tonga	182.4819	-30.3859	210.3	37.6	25.58
ntsz-17b	New Zealand–Kermadec–Tonga	182.8387	-30.5655	210.3	24.3	5
ntsz-18a	New Zealand–Kermadec–Tonga	182.8176	-29.6545	201.6	37.65	26.13
ntsz-18b	New Zealand–Kermadec–Tonga	183.1985	-29.7856	201.6	25	5
ntsz-19a	New Zealand–Kermadec–Tonga	183.0622	-28.8739	195.7	34.41	26.13
ntsz-19b	New Zealand–Kermadec–Tonga	183.4700	-28.9742	195.7	25	5
ntsz-20a	New Zealand–Kermadec–Tonga	183.2724	-28.0967	188.8	38	26.13
ntsz-20b	New Zealand–Kermadec–Tonga	183.6691	-28.1508	188.8	25	5

continued on next page

Table B8: (continued)

Segment	Description	Longitude (°E)	Latitude (°N)	Strike (°)	Dip (°)	Depth (km)
ntsz-21a	New Zealand–Kermadec–Tonga	183.5747	-27.1402	197.1	32.29	24.83
ntsz-21b	New Zealand–Kermadec–Tonga	183.9829	-27.2518	197.1	23.37	5
ntsz-22a	New Zealand–Kermadec–Tonga	183.6608	-26.4975	180	29.56	18.63
ntsz-22b	New Zealand–Kermadec–Tonga	184.0974	-26.4975	180	15.82	5
ntsz-23a	New Zealand–Kermadec–Tonga	183.7599	-25.5371	185.8	32.42	20.56
ntsz-23b	New Zealand–Kermadec–Tonga	184.1781	-25.5752	185.8	18.13	5
ntsz-24a	New Zealand–Kermadec–Tonga	183.9139	-24.6201	188.2	33.31	23.73
ntsz-24b	New Zealand–Kermadec–Tonga	184.3228	-24.6734	188.2	22	5
ntsz-25a	New Zealand–Kermadec–Tonga	184.1266	-23.5922	198.5	29.34	19.64
ntsz-25b	New Zealand–Kermadec–Tonga	184.5322	-23.7163	198.5	17.03	5
ntsz-26a	New Zealand–Kermadec–Tonga	184.6613	-22.6460	211.7	30.26	19.43
ntsz-26b	New Zealand–Kermadec–Tonga	185.0196	-22.8497	211.7	16.78	5
ntsz-27a	New Zealand–Kermadec–Tonga	185.0879	-21.9139	207.9	31.73	20.67
ntsz-27b	New Zealand–Kermadec–Tonga	185.4522	-22.0928	207.9	18.27	5
ntsz-28a	New Zealand–Kermadec–Tonga	185.4037	-21.1758	200.5	32.44	21.76
ntsz-28b	New Zealand–Kermadec–Tonga	185.7849	-21.3084	200.5	19.58	5
ntsz-29a	New Zealand–Kermadec–Tonga	185.8087	-20.2629	206.4	32.47	20.4
ntsz-29b	New Zealand–Kermadec–Tonga	186.1710	-20.4312	206.4	17.94	5
ntsz-30a	New Zealand–Kermadec–Tonga	186.1499	-19.5087	200.9	32.98	22.46
ntsz-30b	New Zealand–Kermadec–Tonga	186.5236	-19.6432	200.9	20.44	5
ntsz-31a	New Zealand–Kermadec–Tonga	186.3538	-18.7332	193.9	34.41	21.19
ntsz-31b	New Zealand–Kermadec–Tonga	186.7339	-18.8221	193.9	18.89	5
ntsz-32a	New Zealand–Kermadec–Tonga	186.5949	-17.8587	194.1	30	19.12
ntsz-32b	New Zealand–Kermadec–Tonga	186.9914	-17.9536	194.1	16.4	5
ntsz-33a	New Zealand–Kermadec–Tonga	186.8172	-17.0581	190	33.15	23.34
ntsz-33b	New Zealand–Kermadec–Tonga	187.2047	-17.1237	190	21.52	5
ntsz-34a	New Zealand–Kermadec–Tonga	186.7814	-16.2598	182.1	15	13.41
ntsz-34b	New Zealand–Kermadec–Tonga	187.2330	-16.2759	182.1	9.68	5
ntsz-34c	New Zealand–Kermadec–Tonga	187.9697	-16.4956	7.62	57.06	6.571
ntsz-35a	New Zealand–Kermadec–Tonga	186.8000	-15.8563	149.8	15	12.17
ntsz-35b	New Zealand–Kermadec–Tonga	187.1896	-15.6384	149.8	8.24	5
ntsz-35c	New Zealand–Kermadec–Tonga	187.8776	-15.6325	342.4	57.06	6.571
ntsz-36a	New Zealand–Kermadec–Tonga	186.5406	-15.3862	123.9	40.44	36.72
ntsz-36b	New Zealand–Kermadec–Tonga	186.7381	-15.1025	123.9	39.38	5
ntsz-36c	New Zealand–Kermadec–Tonga	187.3791	-14.9234	307	57.06	6.571
ntsz-37a	New Zealand–Kermadec–Tonga	185.9883	-14.9861	102	68.94	30.99
ntsz-37b	New Zealand–Kermadec–Tonga	186.0229	-14.8282	102	31.32	5
ntsz-38a	New Zealand–Kermadec–Tonga	185.2067	-14.8259	88.4	80	26.13
ntsz-38b	New Zealand–Kermadec–Tonga	185.2044	-14.7479	88.4	25	5
ntsz-39a	New Zealand–Kermadec–Tonga	184.3412	-14.9409	82.55	80	26.13
ntsz-39b	New Zealand–Kermadec–Tonga	184.3307	-14.8636	82.55	25	5

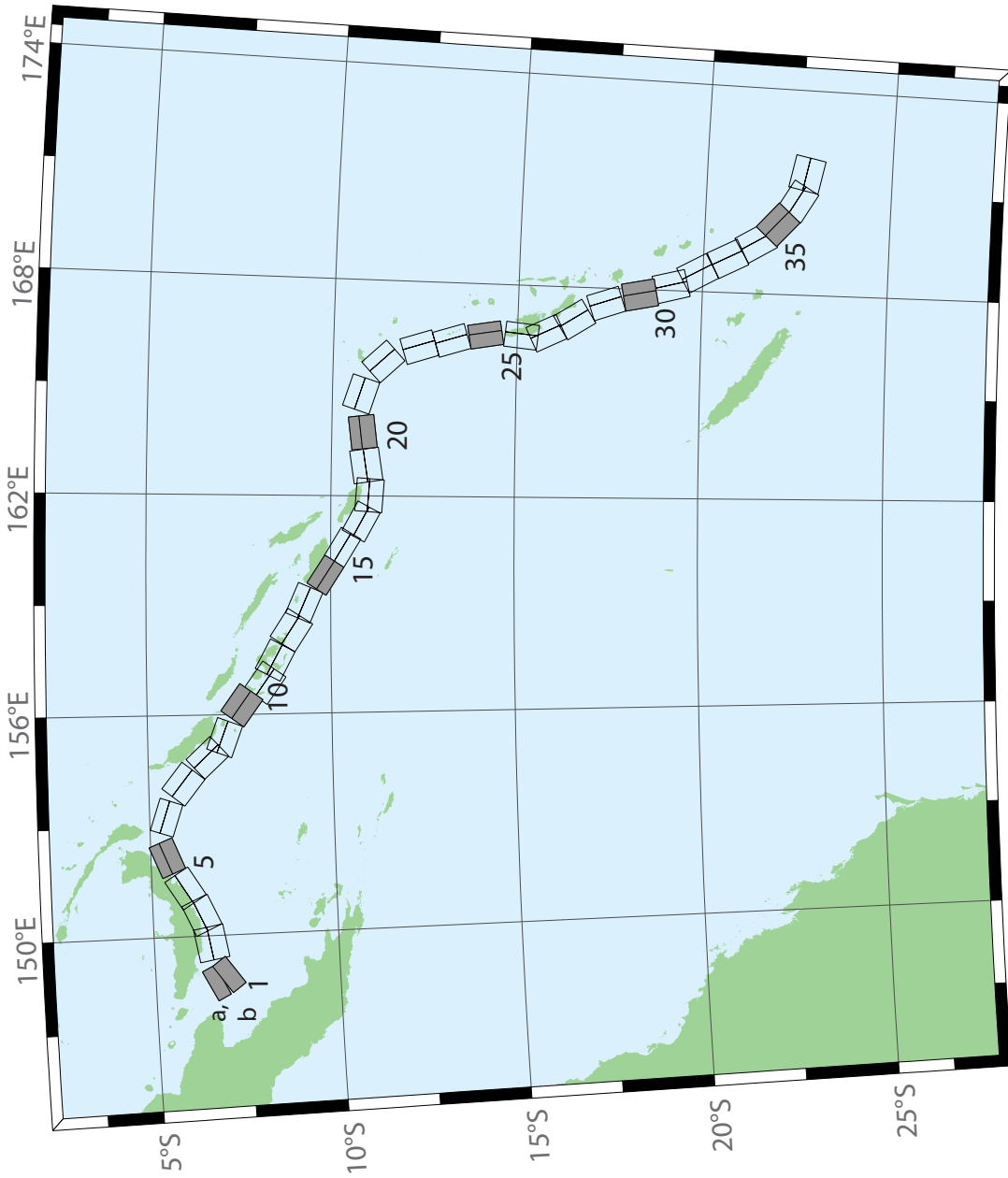


Figure B9: New Britain-Solomons-Vanuatu Subduction Zone unit sources.

Table B9: Earthquake parameters for New Britain–Solomons–Vanuatu Subduction Zone unit sources.

Segment	Description	Longitude (°E)	Latitude (°N)	Strike (°)	Dip (°)	Depth (km)
nvsz-1a	New Britain–Solomons–Vanuatu	148.6217	-6.4616	243.2	32.34	15.69
nvsz-1b	New Britain–Solomons–Vanuatu	148.7943	-6.8002	234.2	12.34	5
nvsz-2a	New Britain–Solomons–Vanuatu	149.7218	-6.1459	260.1	35.1	16.36
nvsz-2b	New Britain–Solomons–Vanuatu	149.7856	-6.5079	260.1	13.13	5
nvsz-3a	New Britain–Solomons–Vanuatu	150.4075	-5.9659	245.7	42.35	18.59
nvsz-3b	New Britain–Solomons–Vanuatu	150.5450	-6.2684	245.7	15.77	5
nvsz-4a	New Britain–Solomons–Vanuatu	151.1095	-5.5820	238.2	42.41	23.63
nvsz-4b	New Britain–Solomons–Vanuatu	151.2851	-5.8639	238.2	21.88	5
nvsz-5a	New Britain–Solomons–Vanuatu	152.0205	-5.1305	247.7	49.22	32.39
nvsz-5b	New Britain–Solomons–Vanuatu	152.1322	-5.4020	247.7	33.22	5
nvsz-6a	New Britain–Solomons–Vanuatu	153.3450	-5.1558	288.6	53.53	33.59
nvsz-6b	New Britain–Solomons–Vanuatu	153.2595	-5.4089	288.6	34.87	5
nvsz-7a	New Britain–Solomons–Vanuatu	154.3814	-5.6308	308.3	39.72	19.18
nvsz-7b	New Britain–Solomons–Vanuatu	154.1658	-5.9017	308.3	16.48	5
nvsz-8a	New Britain–Solomons–Vanuatu	155.1097	-6.3511	317.2	45.33	22.92
nvsz-8b	New Britain–Solomons–Vanuatu	154.8764	-6.5656	317.2	21	5
nvsz-9a	New Britain–Solomons–Vanuatu	155.5027	-6.7430	290.5	48.75	22.92
nvsz-9b	New Britain–Solomons–Vanuatu	155.3981	-7.0204	290.5	21	5
nvsz-10a	New Britain–Solomons–Vanuatu	156.4742	-7.2515	305.9	36.88	27.62
nvsz-10b	New Britain–Solomons–Vanuatu	156.2619	-7.5427	305.9	26.9	5
nvsz-11a	New Britain–Solomons–Vanuatu	157.0830	-7.8830	305.4	32.97	29.72
nvsz-11b	New Britain–Solomons–Vanuatu	156.8627	-8.1903	305.4	29.63	5
nvsz-12a	New Britain–Solomons–Vanuatu	157.6537	-8.1483	297.9	37.53	28.57
nvsz-12b	New Britain–Solomons–Vanuatu	157.4850	-8.4630	297.9	28.13	5
nvsz-13a	New Britain–Solomons–Vanuatu	158.5089	-8.5953	302.7	33.62	23.02
nvsz-13b	New Britain–Solomons–Vanuatu	158.3042	-8.9099	302.7	21.12	5
nvsz-14a	New Britain–Solomons–Vanuatu	159.1872	-8.9516	293.3	38.44	34.06
nvsz-14b	New Britain–Solomons–Vanuatu	159.0461	-9.2747	293.3	35.54	5
nvsz-15a	New Britain–Solomons–Vanuatu	159.9736	-9.5993	302.8	46.69	41.38
nvsz-15b	New Britain–Solomons–Vanuatu	159.8044	-9.8584	302.8	46.69	5
nvsz-16a	New Britain–Solomons–Vanuatu	160.7343	-10.0574	301	46.05	41
nvsz-16b	New Britain–Solomons–Vanuatu	160.5712	-10.3246	301	46.05	5
nvsz-17a	New Britain–Solomons–Vanuatu	161.4562	-10.5241	298.4	40.12	37.22
nvsz-17b	New Britain–Solomons–Vanuatu	161.2900	-10.8263	298.4	40.12	5
nvsz-18a	New Britain–Solomons–Vanuatu	162.0467	-10.6823	274.1	40.33	29.03
nvsz-18b	New Britain–Solomons–Vanuatu	162.0219	-11.0238	274.1	28.72	5
nvsz-19a	New Britain–Solomons–Vanuatu	162.7818	-10.5645	261.3	34.25	24.14
nvsz-19b	New Britain–Solomons–Vanuatu	162.8392	-10.9315	261.3	22.51	5
nvsz-20a	New Britain–Solomons–Vanuatu	163.7222	-10.5014	262.9	50.35	26.3

continued on next page

Table B9: (continued)

Segment	Description	Longitude (°E)	Latitude (°N)	Strike (°)	Dip (°)	Depth (km)
nvsz-20b	New Britain–Solomons–Vanuatu	163.7581	-10.7858	262.9	25.22	5
nvsz-21a	New Britain–Solomons–Vanuatu	164.9445	-10.4183	287.9	40.31	23.3
nvsz-21b	New Britain–Solomons–Vanuatu	164.8374	-10.7442	287.9	21.47	5
nvsz-22a	New Britain–Solomons–Vanuatu	166.0261	-11.1069	317.1	42.39	20.78
nvsz-22b	New Britain–Solomons–Vanuatu	165.7783	-11.3328	317.1	18.4	5
nvsz-23a	New Britain–Solomons–Vanuatu	166.5179	-12.2260	342.4	47.95	22.43
nvsz-23b	New Britain–Solomons–Vanuatu	166.2244	-12.3171	342.4	20.4	5
nvsz-24a	New Britain–Solomons–Vanuatu	166.7236	-13.1065	342.6	47.13	28.52
nvsz-24b	New Britain–Solomons–Vanuatu	166.4241	-13.1979	342.6	28.06	5
nvsz-25a	New Britain–Solomons–Vanuatu	166.8914	-14.0785	350.3	54.1	31.16
nvsz-25b	New Britain–Solomons–Vanuatu	166.6237	-14.1230	350.3	31.55	5
nvsz-26a	New Britain–Solomons–Vanuatu	166.9200	-15.1450	365.6	50.46	29.05
nvsz-26b	New Britain–Solomons–Vanuatu	166.6252	-15.1170	365.6	28.75	5
nvsz-27a	New Britain–Solomons–Vanuatu	167.0053	-15.6308	334.2	44.74	25.46
nvsz-27b	New Britain–Solomons–Vanuatu	166.7068	-15.7695	334.2	24.15	5
nvsz-28a	New Britain–Solomons–Vanuatu	167.4074	-16.3455	327.5	41.53	22.44
nvsz-28b	New Britain–Solomons–Vanuatu	167.1117	-16.5264	327.5	20.42	5
nvsz-29a	New Britain–Solomons–Vanuatu	167.9145	-17.2807	341.2	49.1	24.12
nvsz-29b	New Britain–Solomons–Vanuatu	167.6229	-17.3757	341.2	22.48	5
nvsz-30a	New Britain–Solomons–Vanuatu	168.2220	-18.2353	348.6	44.19	23.99
nvsz-30b	New Britain–Solomons–Vanuatu	167.8895	-18.2991	348.6	22.32	5
nvsz-31a	New Britain–Solomons–Vanuatu	168.5022	-19.0510	345.6	42.2	22.26
nvsz-31b	New Britain–Solomons–Vanuatu	168.1611	-19.1338	345.6	20.2	5
nvsz-32a	New Britain–Solomons–Vanuatu	168.8775	-19.6724	331.1	42.03	21.68
nvsz-32b	New Britain–Solomons–Vanuatu	168.5671	-19.8338	331.1	19.49	5
nvsz-33a	New Britain–Solomons–Vanuatu	169.3422	-20.4892	332.9	40.25	22.4
nvsz-33b	New Britain–Solomons–Vanuatu	169.0161	-20.6453	332.9	20.37	5
nvsz-34a	New Britain–Solomons–Vanuatu	169.8304	-21.2121	329.1	39	22.73
nvsz-34b	New Britain–Solomons–Vanuatu	169.5086	-21.3911	329.1	20.77	5
nvsz-35a	New Britain–Solomons–Vanuatu	170.3119	-21.6945	311.9	39	22.13
nvsz-35b	New Britain–Solomons–Vanuatu	170.0606	-21.9543	311.9	20.03	5
nvsz-36a	New Britain–Solomons–Vanuatu	170.9487	-22.1585	300.4	39.42	23.5
nvsz-36b	New Britain–Solomons–Vanuatu	170.7585	-22.4577	300.4	21.71	5
nvsz-37a	New Britain–Solomons–Vanuatu	171.6335	-22.3087	281.3	30	22.1
nvsz-37b	New Britain–Solomons–Vanuatu	171.5512	-22.6902	281.3	20	5

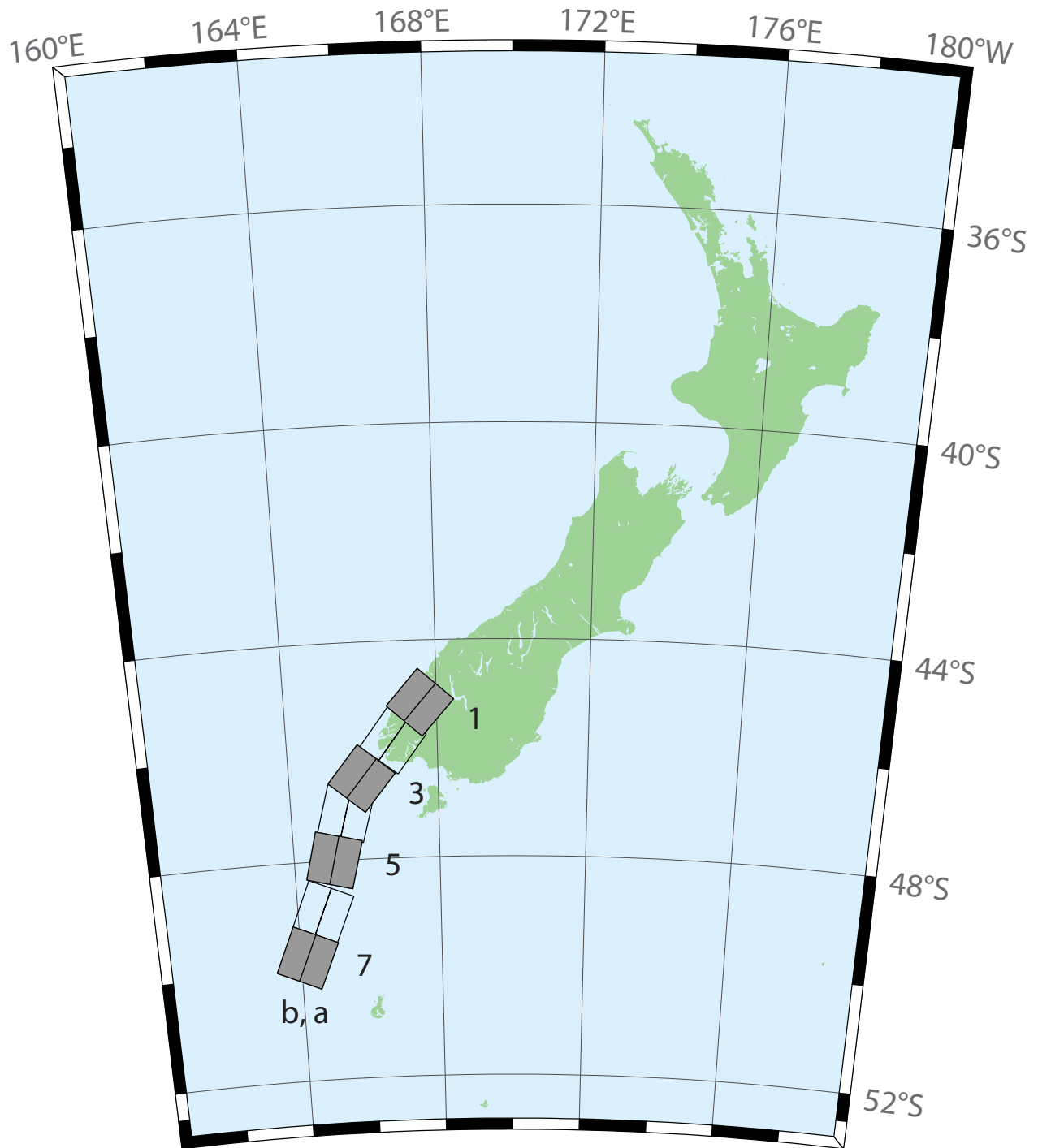


Figure B10: New Zealand–Puysegur Subduction Zone unit sources.

Table B10: Earthquake parameters for New Zealand–Puysegur Subduction Zone unit sources.

Segment	Description	Longitude (°E)	Latitude (°N)	Strike (°)	Dip (°)	Depth (km)
nzzs-1a	New Zealand–Puysegur	168.0294	-45.4368	41.5	15	17.94
nzzs-1b	New Zealand–Puysegur	167.5675	-45.1493	41.5	15	5
nzzs-2a	New Zealand–Puysegur	167.3256	-46.0984	37.14	15	17.94
nzzs-2b	New Zealand–Puysegur	166.8280	-45.8365	37.14	15	5
nzzs-3a	New Zealand–Puysegur	166.4351	-46.7897	39.53	15	17.94
nzzs-3b	New Zealand–Puysegur	165.9476	-46.5136	39.53	15	5
nzzs-4a	New Zealand–Puysegur	166.0968	-47.2583	15.38	15	17.94
nzzs-4b	New Zealand–Puysegur	165.4810	-47.1432	15.38	15	5
nzzs-5a	New Zealand–Puysegur	165.7270	-48.0951	13.94	15	17.94
nzzs-5b	New Zealand–Puysegur	165.0971	-47.9906	13.94	15	5
nzzs-6a	New Zealand–Puysegur	165.3168	-49.0829	22.71	15	17.94
nzzs-6b	New Zealand–Puysegur	164.7067	-48.9154	22.71	15	5
nzzs-7a	New Zealand–Puysegur	164.8017	-49.9193	23.25	15	17.94
nzzs-7b	New Zealand–Puysegur	164.1836	-49.7480	23.25	15	5

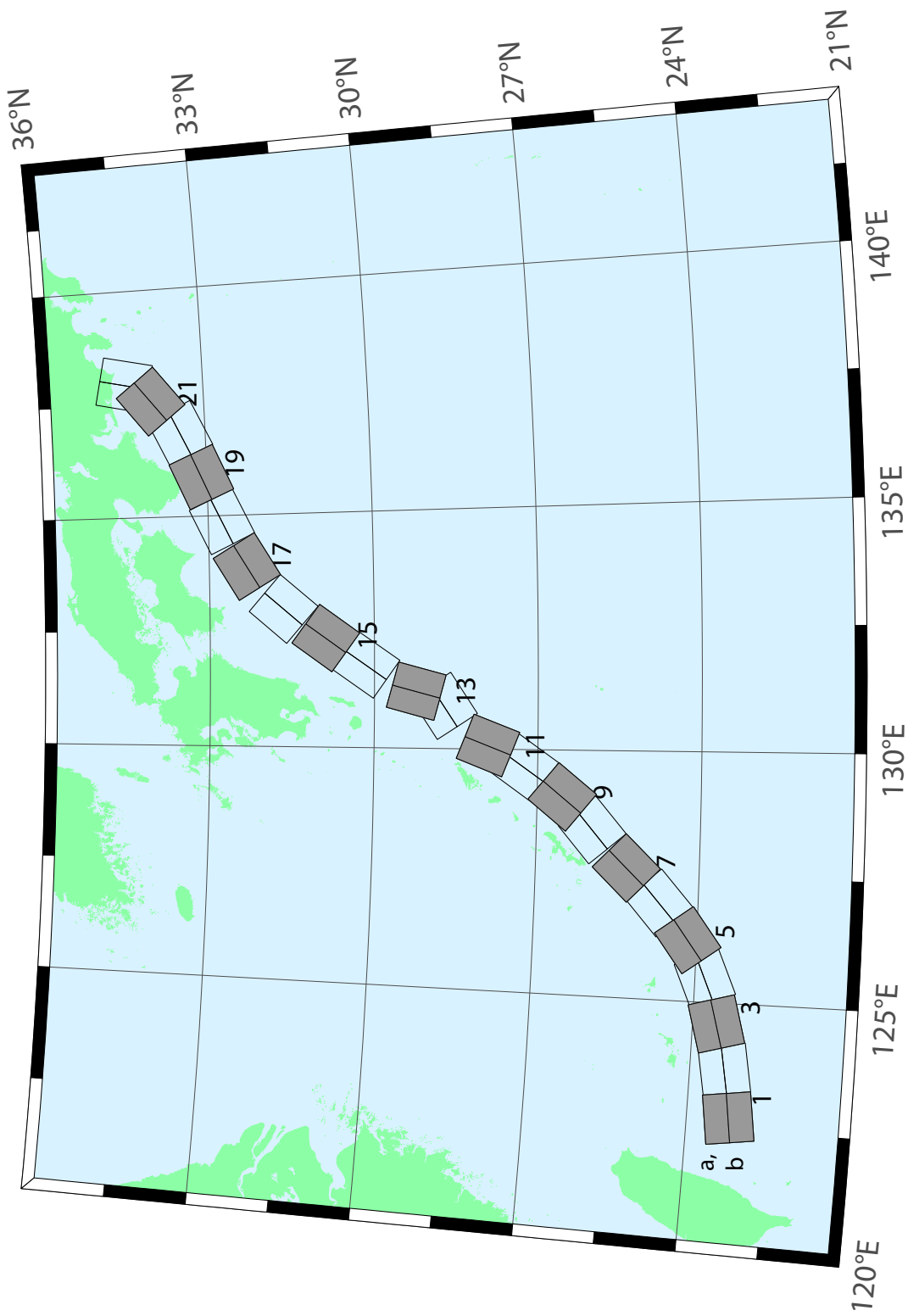


Figure B11: Ryukyu-Kyushu-Nankai Subduction Zone unit sources.

Table B11: Earthquake parameters for Ryukyu–Kyushu–Nankai Subduction Zone unit sources.

Segment	Description	Longitude (°E)	Latitude (°N)	Strike (°)	Dip (°)	Depth (km)
rnsz-1a	Ryukyu–Kyushu–Nankai	122.6672	23.6696	262	14	11.88
rnsz-1b	Ryukyu–Kyushu–Nankai	122.7332	23.2380	262	10	3.2
rnsz-2a	Ryukyu–Kyushu–Nankai	123.5939	23.7929	259.9	18.11	12.28
rnsz-2b	Ryukyu–Kyushu–Nankai	123.6751	23.3725	259.9	10	3.6
rnsz-3a	Ryukyu–Kyushu–Nankai	124.4604	23.9777	254.6	19.27	14.65
rnsz-3b	Ryukyu–Kyushu–Nankai	124.5830	23.5689	254.6	12.18	4.1
rnsz-4a	Ryukyu–Kyushu–Nankai	125.2720	24.2102	246.8	18	20.38
rnsz-4b	Ryukyu–Kyushu–Nankai	125.4563	23.8177	246.8	16	6.6
rnsz-5a	Ryukyu–Kyushu–Nankai	125.9465	24.5085	233.6	18	20.21
rnsz-5b	Ryukyu–Kyushu–Nankai	126.2241	24.1645	233.6	16	6.43
rnsz-6a	Ryukyu–Kyushu–Nankai	126.6349	25.0402	228.7	17.16	19.55
rnsz-6b	Ryukyu–Kyushu–Nankai	126.9465	24.7176	228.7	15.16	6.47
rnsz-7a	Ryukyu–Kyushu–Nankai	127.2867	25.6343	224	15.85	17.98
rnsz-7b	Ryukyu–Kyushu–Nankai	127.6303	25.3339	224	13.56	6.26
rnsz-8a	Ryukyu–Kyushu–Nankai	128.0725	26.3146	229.7	14.55	14.31
rnsz-8b	Ryukyu–Kyushu–Nankai	128.3854	25.9831	229.7	9.64	5.94
rnsz-9a	Ryukyu–Kyushu–Nankai	128.6642	26.8177	219.2	15.4	12.62
rnsz-9b	Ryukyu–Kyushu–Nankai	129.0391	26.5438	219.2	8	5.66
rnsz-10a	Ryukyu–Kyushu–Nankai	129.2286	27.4879	215.2	17	12.55
rnsz-10b	Ryukyu–Kyushu–Nankai	129.6233	27.2402	215.2	8.16	5.45
rnsz-11a	Ryukyu–Kyushu–Nankai	129.6169	28.0741	201.3	17	12.91
rnsz-11b	Ryukyu–Kyushu–Nankai	130.0698	27.9181	201.3	8.8	5.26
rnsz-12a	Ryukyu–Kyushu–Nankai	130.6175	29.0900	236.7	16.42	13.05
rnsz-12b	Ryukyu–Kyushu–Nankai	130.8873	28.7299	236.7	9.57	4.74
rnsz-13a	Ryukyu–Kyushu–Nankai	130.7223	29.3465	195.2	20.25	15.89
rnsz-13b	Ryukyu–Kyushu–Nankai	131.1884	29.2362	195.2	12.98	4.66
rnsz-14a	Ryukyu–Kyushu–Nankai	131.3467	30.3899	215.1	22.16	19.73
rnsz-14b	Ryukyu–Kyushu–Nankai	131.7402	30.1507	215.1	17.48	4.71
rnsz-15a	Ryukyu–Kyushu–Nankai	131.9149	31.1450	216	15.11	16.12
rnsz-15b	Ryukyu–Kyushu–Nankai	132.3235	30.8899	216	13.46	4.48
rnsz-16a	Ryukyu–Kyushu–Nankai	132.5628	31.9468	220.9	10.81	10.88
rnsz-16b	Ryukyu–Kyushu–Nankai	132.9546	31.6579	220.9	7.19	4.62
rnsz-17a	Ryukyu–Kyushu–Nankai	133.6125	32.6956	239	10.14	12.01
rnsz-17b	Ryukyu–Kyushu–Nankai	133.8823	32.3168	239	8.41	4.7
rnsz-18a	Ryukyu–Kyushu–Nankai	134.6416	33.1488	244.7	10.99	14.21
rnsz-18b	Ryukyu–Kyushu–Nankai	134.8656	32.7502	244.5	10.97	4.7
rnsz-19a	Ryukyu–Kyushu–Nankai	135.6450	33.5008	246.5	14.49	14.72
rnsz-19b	Ryukyu–Kyushu–Nankai	135.8523	33.1021	246.5	11.87	4.44
rnsz-20a	Ryukyu–Kyushu–Nankai	136.5962	33.8506	244.8	15	14.38
rnsz-20b	Ryukyu–Kyushu–Nankai	136.8179	33.4581	244.8	12	3.98
rnsz-21a	Ryukyu–Kyushu–Nankai	137.2252	34.3094	231.9	15	15.4
rnsz-21b	Ryukyu–Kyushu–Nankai	137.5480	33.9680	231.9	12	5
rnsz-22a	Ryukyu–Kyushu–Nankai	137.4161	34.5249	192.3	15	15.4
rnsz-22b	Ryukyu–Kyushu–Nankai	137.9301	34.4327	192.3	12	5

Appendix C.

Synthetic Testing: Arena Cove, California*

C1. Purpose

Forecast models are tested with synthetic tsunami events covering a range of tsunami source locations and magnitudes ranging from mega-tsunami events to micro-tsunami events. Testing is also done with selected historical tsunami events when available.

The purpose of forecast model testing is three-fold. The first objective is to assure that the results obtained with NOAA's tsunami forecast system, which has been released to the Tsunami Warning Centers for operational use, are consistent with those obtained by the researcher during the development of the forecast model. The second objective is to test the forecast model for consistency, accuracy, time efficiency, and quality of results over a range of possible tsunami locations and magnitudes. The third objective is to identify bugs and issues in need of resolution by the researcher who developed the forecast model or by the forecast software development team before the next version release to NOAA's two Tsunami Warning Centers.

Local hardware and software applications are used with tools familiar to the researcher(s) to run the Method of Splitting Tsunami (MOST) model during the forecast model development. The test results presented in this report lend confidence that the model performs as developed and produces the same results when initiated within the forecast application in an operational setting as those produced by the researcher during the forecast model development. The test results assure those who rely on the tsunami forecast model for Arena Cove, California, that consistent results are produced irrespective of system.

C2. Testing procedure

The general procedure for forecast model testing is to run a set of synthetic tsunami scenarios and a selected set of historical tsunami events through the forecast system application, and compare the results with those obtained by the researcher during the forecast model development (as presented in the Tsunami Forecast Model Report). Specific steps taken to test the model include:

1. Identification of testing scenarios, including the standard set of synthetic events, appropriate historical events, and customized synthetic scenarios that may have been used by the researcher(s) in the development of the forecast model.
2. Creation of new events to represent customized synthetic scenarios used by the researcher(s) in the development of the forecast model, if any.
3. Submission of test model runs with the forecast system, and export of the results from A, B, and C grids, along with time series.

* Authors: Mick Spillane, Lindsey Wright

4. Recording applicable metadata, including the specific version of the forecast system used for testing.
5. Examination of forecast system model results for instabilities in both time series and plot results.
6. Comparison of forecast model results obtained through the forecast system with those obtained during the forecast model development.
7. Summarization of results with specific mention of quality, consistency, and time efficiency.
8. Reporting of issues identified to modeler and forecast software development team.
9. Retesting the forecast models in the forecast system when reported issues have been addressed or explained.

Synthetic model runs were tested on a DELL PowerEdge R510 computer equipped with two Xeon E5670 processors at 2.93 GHz, each with 12 MBytes of cache and 32 GB memory. The processors are hex core and support hyperthreading, resulting in the computer performing as a 24 processor core machine. Additionally, the testing computer supports 10 Gigabit Ethernet for fast network connections. This computer configuration is similar or the same as the configurations of the computers installed at the Tsunami Warning Centers so the compute times should only vary slightly.

C3. Results

The Arena Cove forecast model was tested with NOAA's tsunami forecast system, SIFT. Test results from the forecast system and comparisons with the results obtained during the forecast model development are shown numerically in **Table C1** and graphically in **Figures C1–C6** as described below. The results show that the forecast model is stable and robust, with consistent and high-quality results across geographically distributed tsunami sources and mega-tsunami event magnitudes. The model run time (wall-clock time) for all six cases was under 19 min for 8 hr of simulation, and under 10 min for 4.0 hr, thereby satisfying the criterion of 10 min run time per 4 hr of simulation time for operational efficiency.

A suite of five synthetic events and one historical case were run on the Arena Cove forecast model. The modeled scenarios were stable for all cases tested, with no instabilities or ringing. Results show that the largest modeled height (see **Table C1**) was 295.03 cm, originating from the Cascadia source ACSZ 56–65. Amplitudes greater than 100 cm were recorded for four of the five mega-tsunami scenarios; the smallest signal of 47.67 cm originated from the far-field South American source CSSZ 89–98. Direct comparisons of output from the forecast tool with results of both the historical event (2011 Tohoku, alternately referred to as 2011 Honshu) and available development synthetic events demonstrated that the wave patterns were similar in shape, pattern, and amplitude. Where available, the figure captions in this appendix point to the relevant figures of the main report. Where time series in the main text were not available, the extrema reported in **Table C1** were obtained from the output files saved during model development

Table C1: Maximum and minimum amplitudes (cm) at the Arena Cove, California, warning point for synthetic and historical events tested using SIFT 3.2 and obtained during development.

Scenarios	Source Zone	Tsunami Source	α [m]	Maxima (cm)		Minima (cm)	
				SIFT	Development	SIFT	Development
Mega-tsunami Scenarios							
KISZ 1-10	Kamchatka-Kuril-Japan-Izu-Mariana-Yap	A1-10, B1-10	25	250.055	250.055	-368.491	-315.426
KISZ 22-31	Kamchatka-Kuril-Japan-Izu-Mariana-Yap	A22-31, B22-31	25	266.764	266.764	-198.325	-198.325
ACSZ 56-65	Aleutian-Alaska-Cascadia	A56-65, B56-65	25	295.027	292.952	-226.995	-231.452
CSSZ 89-98	Central and South America	A89-98, B89-98	25	47.673	47.673	-47.978	-47.978
NTSZ 30-39	New Zealand-Kermadec-Tonga	A30-39, B30-39	25	175.210	175.210	-179.082	-179.082
Historical Event							
2011 Tohoku	Kamchatka-Kuril-Japan-Izu-Mariana-Yap	4.66 b24 + 12.23 b25 + 26.31 a26 +21.27 b26 + 22.75 a27 + 4.98 b27		147.809	147.957	-133.476	-133.518

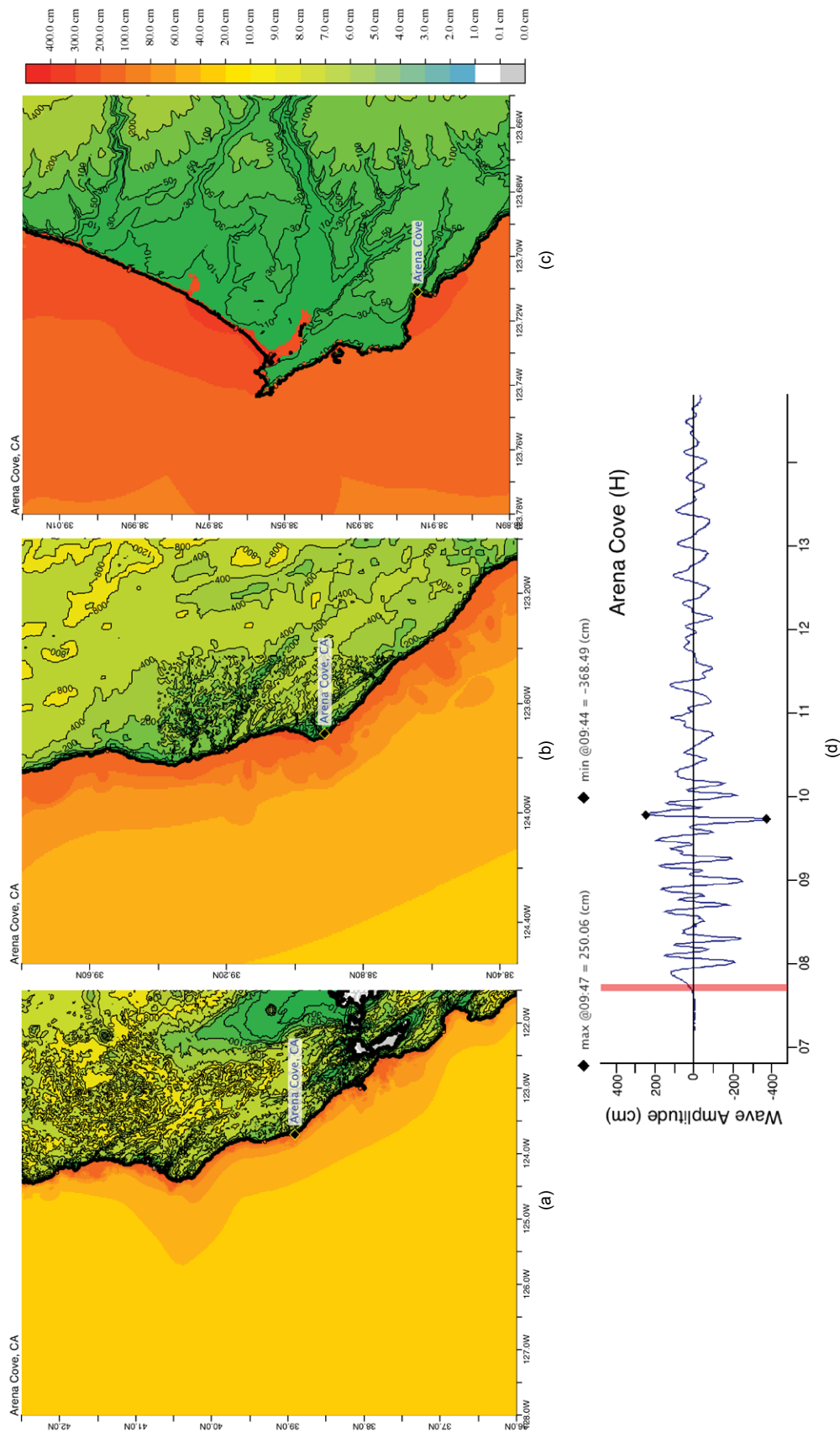


Figure C1: Response of the Arena Cove forecast model to synthetic scenario KISZ 1–10 ($\alpha=25$). Maximum sea surface elevation for (a) A grid, (b) B grid, and (c) C grid. Sea surface elevation time series at the C-grid warning point (d). Panel (d) can be compared with the equivalent values obtained during model development, displayed in **Figure 12**.

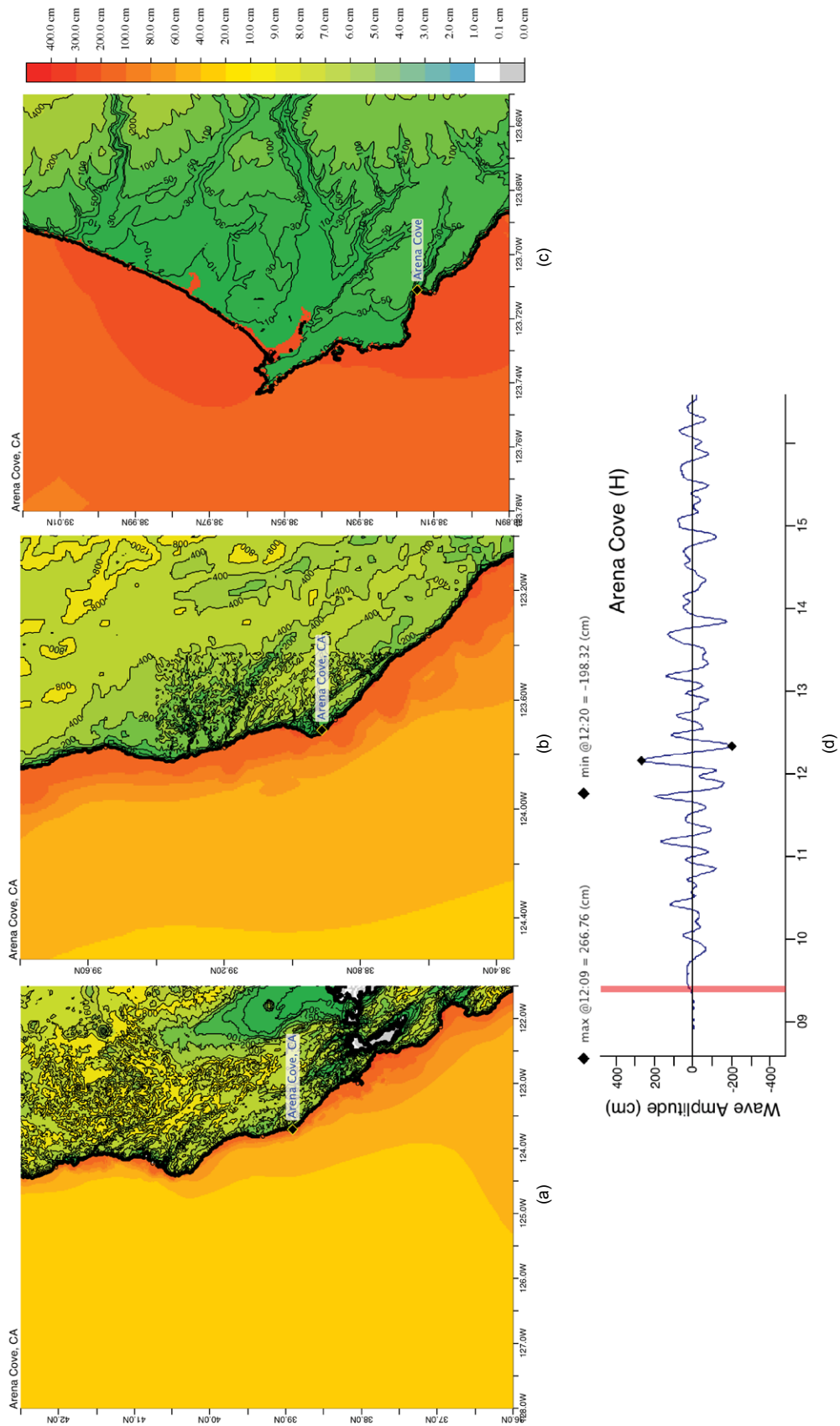


Figure C2: Response of the Arena Cove forecast model to synthetic scenario KISZ 22–31 ($\alpha=25$). Maximum sea surface elevation for (a) A grid, (b) B grid, and (c) C grid. Sea surface elevation time series at the C-grid warning point (d). For extrema computed during model development, see **Table C1**.

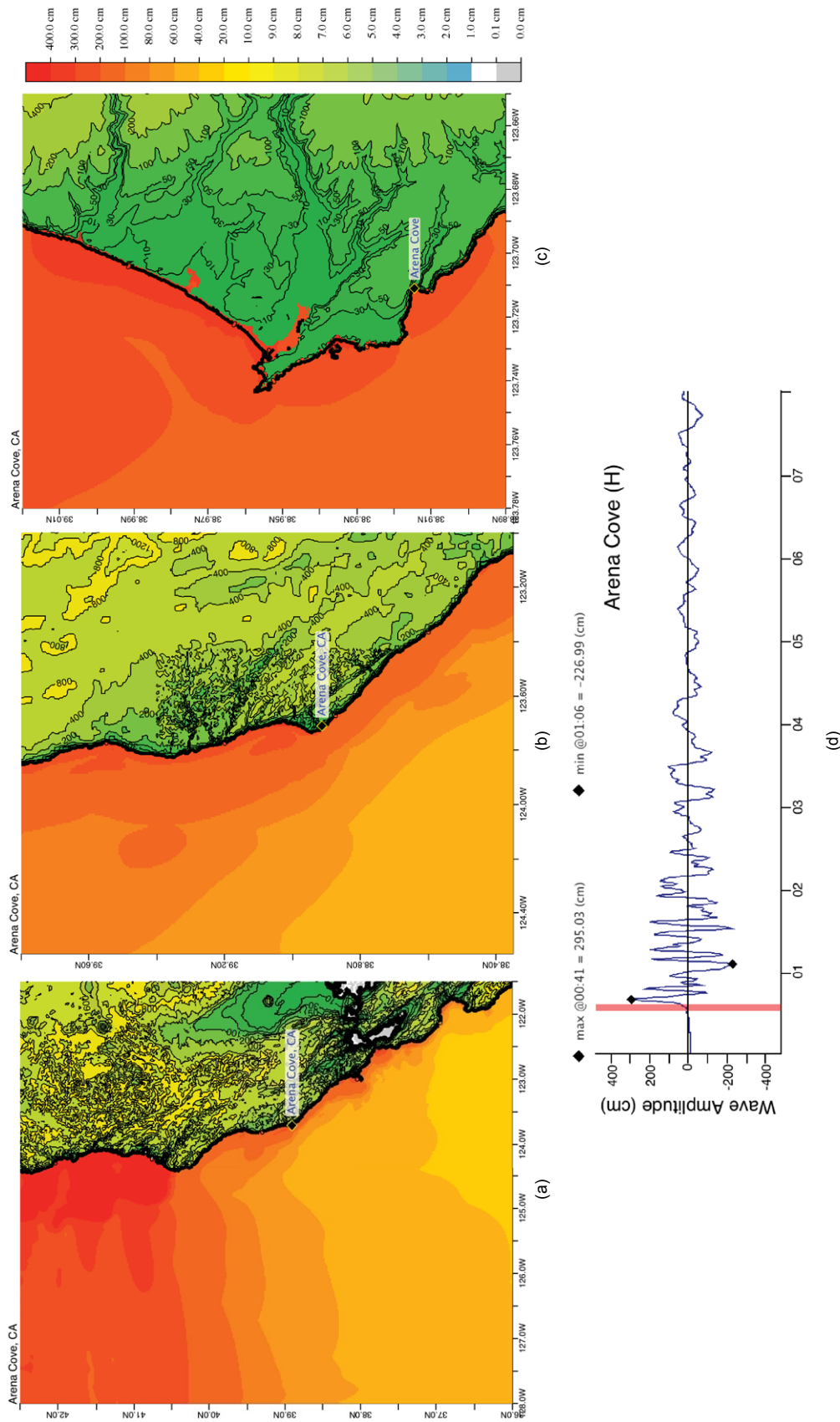


Figure C3: Response of the Arena Cove forecast model to synthetic scenario ACSZ 56–65 ($\alpha=25$). Maximum sea surface elevation for (a) A grid, (b) B grid, and (c) C grid. Sea surface elevation time series at the C-grid warning point (d). Panel (d) can be compared with the equivalent results, obtained during model development, displayed in **Figure 11**.

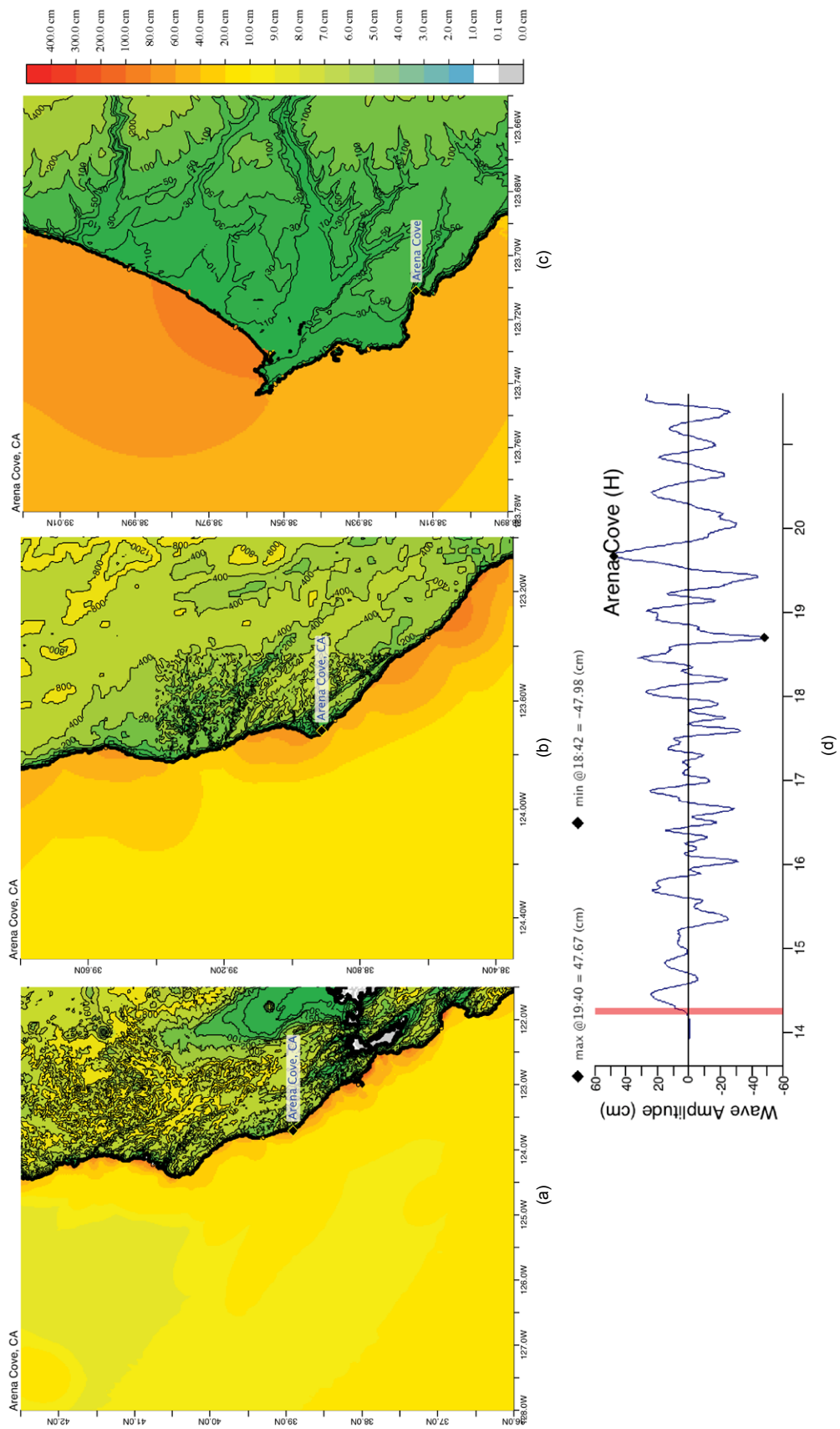


Figure C4: Response of the Arena Cove forecast model to synthetic scenario CSSZ 89–98 ($\alpha=25$). Maximum sea surface elevation for (a) A grid, (b) B grid, and (c) C grid. Sea surface elevation time series at the C-grid warning point (d). For extrema computed during model development, see **Table C1**.

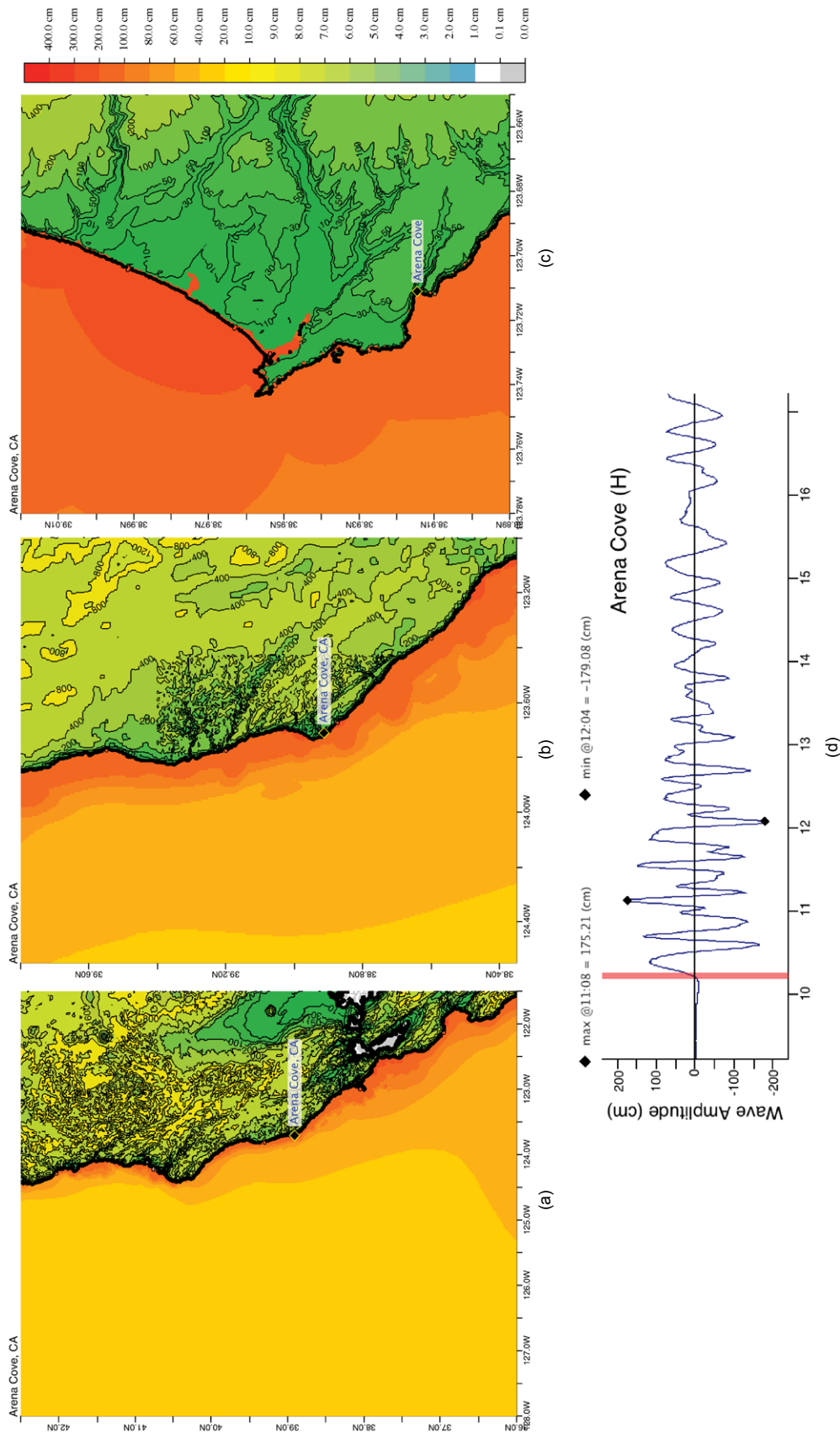


Figure C5: Response of the Arena Cove forecast model to synthetic scenario NTSZ 30–39 ($\alpha=25$). Maximum sea surface elevation for (a) A grid, (b) B grid, (c) C grid. Sea surface elevation time series at the C-grid warning point (d). Panel (d) can be compared with the equivalent results, obtained during model development, displayed in **Figure 13**.

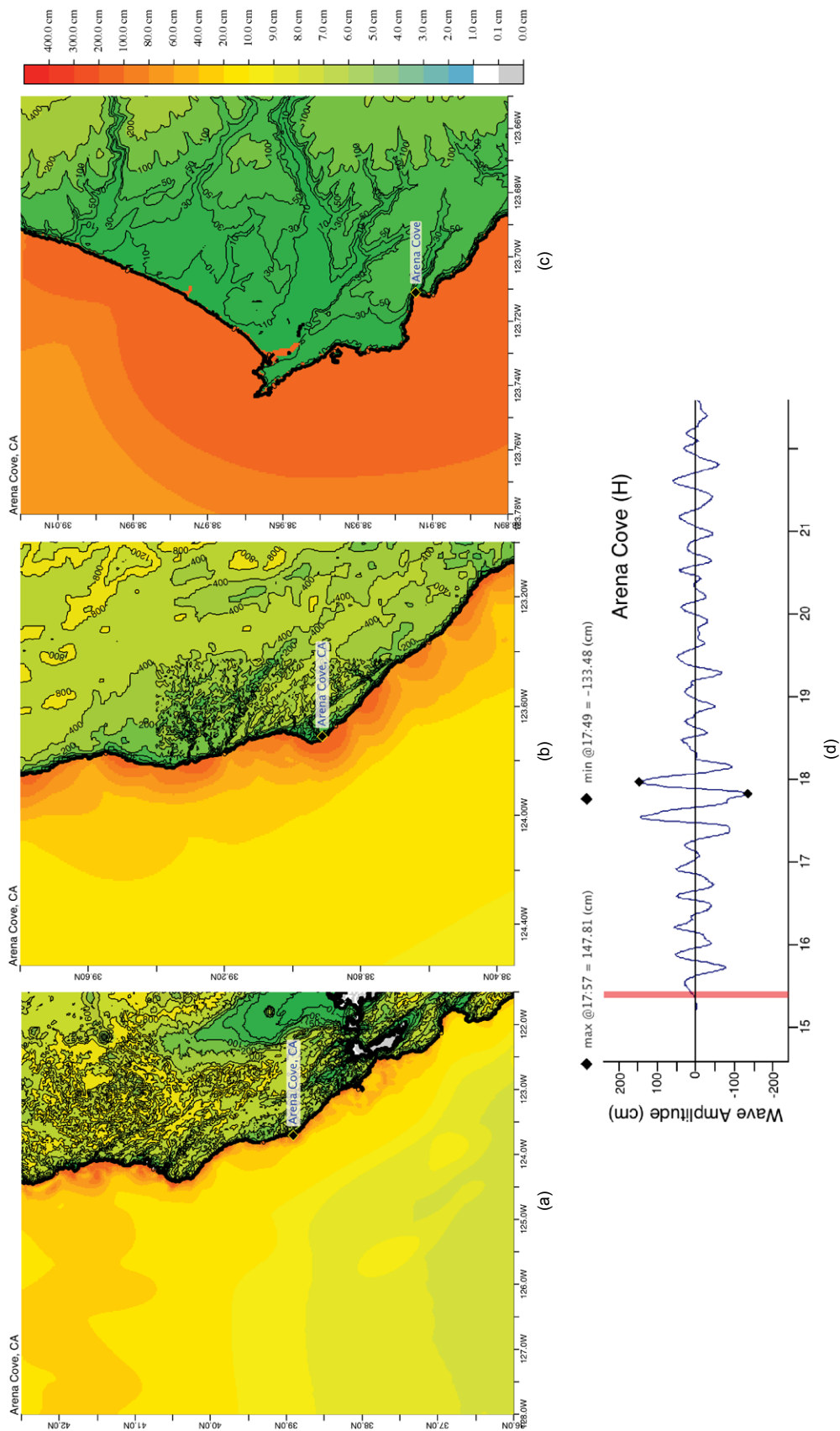


Figure C6: Response of the Arena Cove forecast model to the 11 March 2011 Tohoku tsunami. Maximum sea surface elevation for (a) A-grid, (b) B-grid, and (c) C-grid. Sea surface elevation time series at the C-grid warning point (d). Panel (d) can be compared with the equivalent results, obtained during model development, displayed in **Figure 27**.

Glossary

Arrival time The time when the first tsunami wave is observed at a particular location, typically given in local and/or universal time, but also commonly noted in minutes or hours relative to the time of the earthquake.

Bathymetry The measurement of water depth of an undisturbed body of water.

Cascadia Subduction Zone Fault that extends from Cape Mendocino in Northern California northward to mid-Vancouver Island, Canada. The fault marks the convergence boundary where the Juan de Fuca tectonic plate is being subducted under the margin of the North America plate.

Current speed The scalar rate of water motion measured as distance/time.

Current velocity Movement of water expressed as a vector quantity. Velocity is the distance of movement per time coupled with direction of motion.

Deep-ocean Assessment and Reporting of Tsunamis (DART[®]) Tsunami detection and transmission system that measures the pressure of an overlying column of water and detects the passage of a tsunami.

Digital Elevation Model (DEM) A digital representation of bathymetry or topography based on regional survey data or satellite imagery. Data are arrays of regularly spaced elevations referenced to a map projection of the geographic coordinate system.

Epicenter The point on the surface of the earth that is directly above the focus of an earthquake.

Far-field Region outside of the source of a tsunami where no direct observations of the tsunami-generating event are evident, except for the tsunami waves themselves.

Focus The point beneath the surface of the earth where a rupture or energy release occurs due to a buildup of stress or the movement of Earth's tectonic plates relative to one another.

Inundation The horizontal inland extent of land that a tsunami penetrates, generally measured perpendicularly to a shoreline.

Marigram Tide gauge recording of wave level as a function of time at a particular location. The instrument used for recording is termed a marigraph.

Method of Splitting Tsunami (MOST) A suite of numerical simulation codes used to provide estimates of the three processes of tsunami evolution: tsunami generation, propagation, and inundation.

Moment magnitude (M_w) The magnitude of an earthquake on a logarithmic scale in terms of the energy released. Moment magnitude is based on the size and characteristics of a fault rupture as determined from long-period seismic waves.

Near-field Region of primary tsunami impact near the source of a tsunami. The near-field is defined as the region where non-tsunami effects of the tsunami-generating event have been observed, such as earth shaking from the earthquake, visible or measured ground deformation, or other direct (non-tsunami) evidences of the source of the tsunami wave.

Propagation database A basin-wide database of precomputed water elevations and flow velocities at uniformly spaced grid points throughout the world oceans. Values are computed from tsunamis generated by earthquakes with a fault rupture at any one of discrete 100×50 km unit sources along worldwide subduction zones.

Runup Vertical difference between the elevation of tsunami inundation and the sea level at the time of a tsunami. Runup is the elevation of the highest point of land inundated by a tsunami as measured relative to a stated datum, such as mean sea level.

Short-term Inundation Forecasting for Tsunamis (SIFT) A tsunami forecast system that integrates tsunami observations in deep ocean with numerical models to provide an estimate of tsunami wave arrival and amplitude at specific coastal locations while a tsunami propagates across an ocean basin.

Subduction zone A submarine region of the earth's crust at which two or more tectonic plates converge to cause one plate to sink under another, overriding plate. Subduction zones are regions of high seismic activity.

Synthetic event Hypothetical events based on computer simulations or theory of possible or even likely future scenarios.

Tele-tsunami or distant tsunami or far-field tsunami Most commonly, a tsunami originating from a source greater than 1000 km away from a particular location. In some contexts, a tele-tsunami is one that propagates through deep ocean before reaching a particular location without regard to distance separation.

Tidal wave Term frequently used incorrectly as a synonym for tsunami. A tsunami is unrelated to the predictable periodic rise and fall of sea level due to the gravitational attractions of the moon and sun; see **Tide**, below.

Tide The predictable rise and fall of a body of water (ocean, sea, bay, etc.) due to the gravitational attractions of the moon and sun.

Tide gauge An instrument for measuring the rise and fall of a column of water over time at a particular location.

Travel time The time it takes for a tsunami to travel from the generating source to a particular location.

Tsunamieter An oceanographic instrument used to detect and measure tsunamis in the deep ocean. Tsunami measurements are typically transmitted acoustically to a surface buoy that in turn relays them in real time to ground stations via satellite.

Tsunami A Japanese term that literally translates to “harbor wave.” Tsunamis are a series of long-period shallow water waves that are generated by the sudden displacement of water due to subsea disturbances such as earthquakes, submarine landslides, or volcanic eruptions. Less commonly, meteoric impact to the ocean or meteorological forcing can generate a tsunami.

Tsunami hazard assessment A systematic investigation of seismically active regions of the world oceans to determine their potential tsunami impact at a particular location. Numerical models are typically used to characterize tsunami generation, propagation, and inundation, and to quantify the risk posed to a particular community from tsunamis generated in each source region investigated.

Tsunami propagation The directional movement of a tsunami wave outward from the source of generation. The speed at which a tsunami propagates depends on the depth of the water column in which the wave is traveling. Tsunamis travel at a speed of 700 km/hr (450 mi/hr) over the average depth of 4000 m in the open deep Pacific Ocean.

Tsunami magnitude A number that characterizes the strength of a tsunami based on the tsunami wave amplitudes. Several different tsunami magnitude determination methods have been proposed.

Tsunami source Location of tsunami origin, most typically an underwater earthquake epicenter. Tsunamis are also generated by submarine landslides, underwater volcanic eruptions, or, less commonly, by meteoric impact of the ocean.

Wall-clock time The time that passes on a common clock or watch between the start and end of a model run, as distinguished from the time needed by a CPU or computer processor to complete the run, typically less than wall-clock time.

Wave amplitude The maximum vertical rise or drop of a column of water as measured from wave crest (peak) or trough to a defined mean water level state.

Wave crest or peak The highest part of a wave or maximum rise above a defined mean water level state, such as mean lower low water.

Wave height The vertical difference between the highest part of a specific wave (crest) and its corresponding lowest point (trough).

Wavelength The horizontal distance between two successive wave crests or troughs.

Wave period The length of time between the passage of two successive wave crests or troughs as measured at a fixed location.

Wave trough The lowest part of a wave or the maximum drop below a defined mean water level state, such as mean lower low water.

PMEL Tsunami Forecast Series Locations

Adak, AK
Apra Harbor, Guam
Arecibo, Puerto Rico
Arena Cove, CA — **Vol. 10**
Atka, AK
Atlantic City, NJ
Bar Harbor, ME
Cape Hatteras, NC
Charlotte Amalie, U.S. Virgin Islands
Chignik, AK
Christiansted, U.S. Virgin Islands
Cordova, AK
Craig, AK
Crescent City, CA — **Vol. 2**
Daytona Beach, FL
Elfin Cove, AK
Eureka, CA
Fajardo, PR
Florence, OR
Garibaldi, OR
Haleiwa, HI
Hilo, HI — **Vol. 1**
Homer, AK
Honolulu, HI
Kahului, HI
Kailua-Kona, HI
Kawaihae, HI
Keauhou, HI
Key West, FL
Kihei, HI
King Cove, AK
Kodiak, AK — **Vol. 4**
Lahaina, HI
La Push, WA
Los Angeles, CA
Mayaguez, PR
Midway Atoll — **Vol. 7**
Montauk, NY
Monterey, CA
Morehead City, NC
Myrtle Beach, SC
Nantucket, MA — **Vol. 8**
Nawiliwili, HI
Neah Bay, WA
Newport, OR — **Vol. 5**
Nikolski, AK
Ocean City, MD
Pago Pago, American Samoa
Palm Beach, FL
Pearl Harbor, HI
Point Reyes, CA — **Vol. 6**
Ponce, PR
Port Alexander, AK
Port Angeles, WA
Port Orford, OR
Port San Luis, CA
Port Townsend, WA
Portland, ME
San Diego, CA
San Francisco, CA — **Vol. 3**
San Juan, Puerto Rico
Sand Point, AK
Santa Barbara, CA
Santa Monica, CA — **Vol. 9**
Savannah, GA
Seaside, OR
Seward, AK
Shemya, AK
Sitka, AK
Toke Point, WA
Unalaska, AK
Virginia Beach, VA
Wake Island, U.S. Territory
Westport, WA
Yakutat, AK

